Fakultät für Medizin

Lehrstuhl für molekulare Allergologie

Transitional T Cell Phenotypes in Allergen-specific Immunotherapy

Shu-Hung Wang

Vollständiger Abdruck der von der Fakultät für Medizin der Technischen Universität München zur Erlangung des akademischen Grades eines

Doctor of Philosophy (Ph.D.)

genehmigten Dissertation.

Vorsitzender: Prof. Dr. Marc Schmidt-Supprian

Betreuer: Prof. Dr. Carsten Schmidt-Weber

Prüfer der Dissertation:

1. Prof. Dr. Dietmar Zehn

2. Priv.-Doz. Dr. Caspar Ohnmacht

Die Dissertation wurde am 10.12.2020 bei der Fakultät für Medizin der Technischen Universität München eingereicht und durch die Fakultät für Medizin am 02.03.2021 angenommen.

Table of Contents

List of Figures

List of Tables

List of abbreviations

AA	Allergic asthma
AAI	Allergic airway inflammation
AIT	Allergen-specific immunotherapy
APC	Antigen presenting cell
AR	Allergic rhinitis
BAL	Bronchoalveolar lavage
BALF	Bronchoalveolar lavage fluid
CCL	CC motif chemokine ligand
CCR	CC motif chemokine receptor
CD	Cluster of differentiation
CRTH2	Chemoattractant receptor-homologous molecule expressed on T_H2 cells
CTLA-4	Cytotoxic T-lymphocyte-associated antigen 4
CXCL	CXC motif chemokine ligand
DEG	Differentially expressed gene
FACS	Fluorescence-activated cell sorting
FSC	Forward scatter
GO	Gene ontology
GSEA	Gene Set Enrichment Analysis
IFN-γ	Interferon gamma
IgE	Immunoglobulin E
IgG	Immunoglobulin G
IL	Interleukin
ILC2	Group 2 innate lymphoid cell
ITIM	Immunoreceptor tyrosine-based inhibitory motif
ITSM	Immunoreceptor tyrosine-based switch motif
KLRG1	Killer cell lectin-like receptor G1
LAG-3	Lymphocyte activation gene 3
LCMV	Lymphocytic choriomeningitis virus
MACS	Magnetic activated cell sorting

MFI	Mean fluorescence intensity
MHC	Major histocompatibility complex
OVA	Ovalbumin
PB	Peripheral blood
PBMC	Peripheral blood mononuclear cell
PBS	Phosphate-buffered saline
PD-1	Programmed cell death protein 1
PI3K	Phosphatidylinositol-3-kinase
PIP3	Phosphatidylinositol triphosphate
PKCθ	Protein kinase C theta
PTEN	Phosphatase and tensin homolog
RORγt	Retineic-acid-receptor-related orphan nuclear receptor gamma
SEM	Standard error of mean
SH2/3	Src homology region 2/3
SHP	SH2 domain-containing tyrosine phosphatases
sIgE	Specific Immunoglobulin E
SSC	Side scatter
TCF-1	T cell factor 1
TCR	T cell receptor
T_H17	T helper 17 cell
T_H2	T helper 2 cell
TIM-3	T cell immunoglobulin and mucin domain-containing protein 3
TNF-α	Tumor necrosis factor alpha
Tr17	IL-17$^+$ Treg
Treg	Regulatory T cell
UAD	United airway disease

1 Introduction

1.1 Allergic rhinitis, asthma and allergen-specific immunotherapy

1.1.1 Allergic rhinitis and allergic asthma

Allergic rhinitis (AR) is a common atopic disease, affecting people worldwide with a prevalence up to 30% (Mims, 2014; Tohidinik, Mallah, & Takkouche, 2019). Patients with AR manifest symptoms such as sneezing, nasal pruritus, nasal congestion, and rhinorrhea and have a confirmed sensitization to one or several aeroallergens (Bousquet et al., 2008). Although its etiology remains unclear, studies have shown that it is associated with both genetic and environmental factors (Kappen, Durham, Veen, & Shamji, 2017; Meng, Wang, & Zhang, 2019). Genetic factors could render individuals more susceptible to AR, such as single nucleotide polymorphisms and epigenetic modifications (Meng et al., 2019). Epigenetic regulation is of particular interest, given its potential role as a biomarker for treatment response and as a therapeutic target for allergic inflammation (North et al., 2018). On the other hand, environmental factors such as air pollution and flight of aeroallergens are directly involved in the pathogenesis of AR (Meng et al., 2019; X. D. Wang et al., 2016). While air pollutants aggravate AR exacerbation and raise the risk of sensitization, exposure of sensitized individuals to aeroallergens results in an allergic milieu, involving innate and adaptive immune cells (Meng et al., 2019). Environmental factors can also influence epigenetic modifications, further reinforcing its role in the pathogenesis of AR (Kappen et al., 2017; Meng et al., 2019; North et al., 2018).

Asthma is a heterogeneous inflammatory disorder of the airways characterized by recurrent episodes of reversible bronchial obstruction. In recent decades, the prevalence of asthma has grown markedly worldwide, particularly in industrialized countries (Martinez & Vercelli, 2013; Romanet-Manent et al., 2002). Allergic asthma (AA) has a distinct genetic component and an early onset in life as opposed to non-allergic asthma (Martinez & Vercelli, 2013; Romanet-Manent et al., 2002). In addition, AA is often associated with other atopic diseases, with a typical progression classically known as the atopic march, which describes the development of allergic diseases from atopic dermatitis in infancy to IgE-mediated food allergy, AA, and AR in later childhood (**Figure 1.1**) (Hill & Spergel, 2018; Tham & Leung, 2019). Major environmental risk

factors for AA include air pollution, respiratory viral infections, and urban lifestyles with excessive hygiene (Martinez & Vercelli, 2013; Pividori, Schoettler, Nicolae, Ober, & Im, 2019; Radermecker et al., 2019; Romanet-Manent et al., 2002).

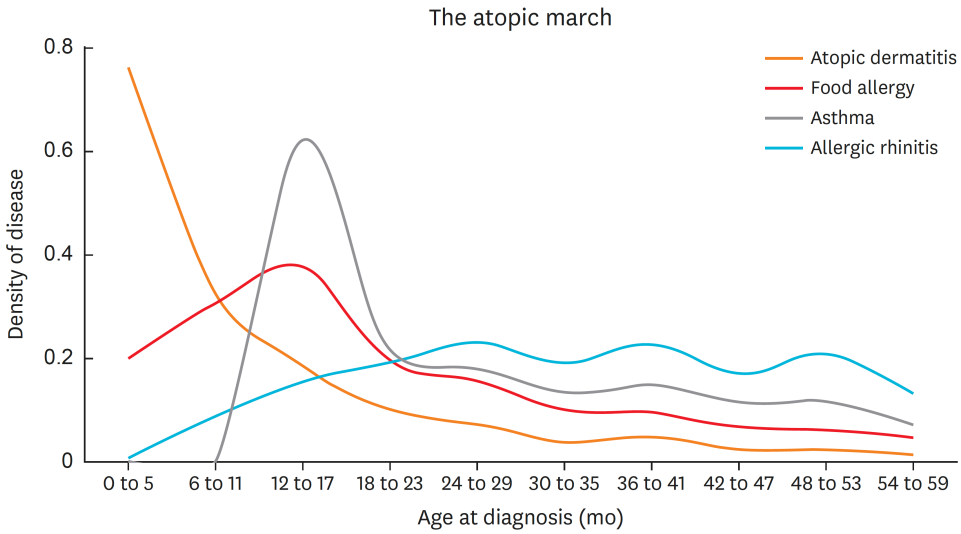

Figure 1.1 The atopic march

Shown is the age at diagnosis of common atopic diseases. Adapted and reprinted by permission from Allergy, Asthma & Immunology Research, Mechanisms by Which Atopic Dermatitis Predisposes to Food Allergy and the Atopic March, Tham and Leung, 2018.

For both AR and AA, proallergic T_H2 cells play a crucial role in the inflammatory response to allergens (Martinez & Vercelli, 2013; Meng et al., 2019; Romanet-Manent et al., 2002). A Japanese research group showed that upon allergen stimulation memory T_H2 cells derived from allergic patients produced significantly more type-2 cytokines (IL-4, IL-5, IL-9, IL-13) and had elevated reactivity to IL-33 compared to those from non-allergic individuals (Iinuma et al., 2018). Type-2 cytokines promote T_H2 cell differentiation, IgE class switching and eosinophilia (Martinez & Vercelli, 2013; Meng et al., 2019; Romanet-Manent et al., 2002). Importantly, IgE can bind to mast cells and basophils via their high-affinity receptors FcεRI, and cross-linking of the cell-bound IgE by allergens can then trigger the release of the inflammatory mediators, eliciting an immediate allergic reaction (Deo, Mistry, Kakade, & Niphadkar, 2010; Qiu et al., 2020). In addition to T_H2 cells, group 2 innate lymphoid cells (ILC2) also produce abundant type-2 cytokines, which help augment and maintain allergic inflammation (Shamji & Durham, 2017). Indeed, allergic patients were noted to have an increased number of ILC2 during pollen flight (Shamji & Durham, 2017).

The concept of united airways disease (UAD) considers the respiratory system as a single entity, given that upper and lower respiratory tracts share many similarities in terms of histology, pathophysiology, and mucosal immunity (Ciprandi et al., 2012; Giavina-Bianchi, Aun, Takejima, Kalil, & Agondi, 2016). AR patients frequently manifest bronchial hyperreactivity and are predisposed to develop asthma, while asthmatic patients usually manifest symptoms of rhinitis (Giavina-Bianchi et al., 2016; Tohidinik et al., 2019). Hence, the Allergic Rhinitis and Its Impact on Asthma (ARIA) initiative has addressed these observations and proposed a guideline to manage AR patients with or without asthma in an integrated manner (Brozek et al., 2017).

1.1.2 Allergen-specific immunotherapy

Allergen avoidance and pharmacotherapy can effectively alleviate symptoms and control the inflammatory process for AR with and without asthma (Jacobsen, Wahn, & Bilo, 2012; Kappen et al., 2017; Meng et al., 2019). However, although pharmacotherapy is deemed as first-line treatment, some patients respond poorly (Kappen et al., 2017; Meng et al., 2019). In such individuals, allergen-specific immunotherapy (AIT) is of particular importance. Successful AIT may induce immunologic tolerance to the allergen, reduce the medical need and improve the quality of life of the allergic patients (Kappen et al., 2017; Martinez & Vercelli, 2013; Meng et al., 2019; Y. S. Shin et al., 2019). Indeed, AIT is effective against AR caused by inhalant allergens, including grass and tree pollens, house dust mites, and animal dander (Moote, Kim, & Ellis, 2018; Y. S. Shin et al., 2019). Furthermore, AIT can change the natural course of AR and prevent disease progression to asthma (Jacobsen et al., 2012). Both sublingual and subcutaneous immunotherapies have been shown to be disease-modifying with long-term clinical benefits after termination of treatment (Durham et al., 2012; Jutel et al., 2005). By contrast, a meta-analysis of 98 studies on AIT for allergic asthma showed that patients, upon completion of AIT, had lower symptom and medication scores, but AIT did not improve asthma control and exacerbations (Dhami et al., 2017).

In practice, AIT consists of up-dosing and maintenance phases. In the up-dosing phase, allergen extracts are administered in gradually increasing doses over three to six months until the top dose is reached. During the maintenance phase, patients

receive the treatment every 4–8 weeks and the treatment is generally continued for three to five years (Burks et al., 2013; Cox et al., 2011).

To date, however, there is no validated biomarker that can predict the clinical response to AIT. In this regard, a European Academy of Allergy and Clinical Immunology (EAACI) taskforce has reviewed all candidate biomarkers and considered the sIgE/tIgE ratio and IgE-facilitated antigen binding (IgE-FAB) as potential surrogate markers for the clinical outcome (Shamji et al., 2017). Both markers reflect the importance of IgE in the pathogenesis of allergic inflammation as described earlier and have the advantage of being serum-based. On the other hand, AIT has also been shown to modulate T_H2 response and induce regulatory T cells (Tregs) and regulatory B cells (Bregs). Hence, understanding the cellular responses of different immune subsets during AIT can help us gain better insight into the mechanisms of AIT, and provide another dimension to evaluate the clinical response to AIT. The following sections will focus specifically on the dynamics of T cell subsets during AIT.

1.2 Dynamic change of different T cell subsets during allergen-specific immunotherapy

1.2.1 Decreases in the number of T_H2 cells

In a placebo-controlled study of sublingual immunotherapy, allergen-reactive memory T_H2 cells significantly decreased in patients receiving active treatment, suggesting that these proallergic T_H2 cells were targeted and could serve as biomarkers for treatment efficacy (Ihara et al., 2018). In particular, a proallergic subset among allergen-specific T_H2 cells was characterized by the surface expression of CRTH2, CD161, and CD49d and lack of expression of CD27 and CD45RB (Wambre et al., 2017; Wambre et al., 2012). This terminally differentiated T_H2 cell subset was preferentially depleted after successful AIT, in parallel to clinical improvement (Wambre et al., 2017; Wambre et al., 2012). In line with these observations, one study reported that AIT-treated patients had a decrease in type-2 cytokine levels in nasal fluid after nasal allergen challenge (Scadding et al., 2015).

1.2.2 Regulatory T cells and Tr17 cells

Tregs were induced after AIT (Francis, Till, & Durham, 2003; Zissler et al., 2018). Time-course analysis revealed that the IL-10-producing capacity of Tregs grew during the up-dosing phase, preceding the rise in serum IgG_4 levels (Francis et al., 2008; Zissler et al., 2018). Importantly, IL-10 has been shown to restrict differentiation and survival of T_H2 cells and suppress the production of type-2 cytokines by ILC2 (Coomes et al., 2017; Ogasawara et al., 2018). On a side note, Bregs and $CD27^+$ allergen-specific $CD4^+$ T cells represent an alternative source of IL-10, which could be elicited after AIT (van de Veen et al., 2013; Wambre et al., 2012).

Interestingly, in contrast to $IL\text{-}10^+$ Tregs, the frequency of $IL\text{-}17^+CCR6^+Foxp3^+$ T cells (denoted as Tr17) declined during up-dosing, followed by an increase to pretreatment levels (Zissler et al., 2018). However, its role in tolerance induction after AIT remains yet to be defined. Some consider Tr17 cells transitory, given that Tregs could trans-differentiate into T_H17 cells in an inflammatory milieu and vice versa (Gagliani et al., 2015; Komatsu et al., 2014; Massoud et al., 2016; Valmori, Raffin, Raimbaud, & Ayyoub, 2010). Meanwhile, Tr17 cells were shown to pertain in human tonsil and other pathological conditions such as cancer and autoimmune disease (Chellappa et al., 2015; Kim et al., 2017; Voo et al., 2009). Although Tr17 cells displayed immunosuppressive activity and appeared to restrict autoimmunity, IL-17 might exacerbate allergic inflammation and serve as a therapeutic target (Allen, Sutherland, & Ruckerl, 2015; Gu, Wang, & Cao, 2017; Massoud et al., 2016)

1.3 T cell exhaustion of Proallergic T_H2 cells during allergen-specific immunotherapy

1.3.1 T cell activation and signaling

Antigen-presenting cells (APCs) take up antigens and present the digested antigenic peptide to T cells via peptide-major histocompatibility complex (pMHC) complexes (Saito, 2013). Engagement of the T-cell receptors (TCRs) brings signal protein kinases close to the TCR-CD3 complex and initiates a phosphorylation cascade, which results in phospholipid hydrolysis and generation of two second messengers: Inositol 1,4,5-

triphosphate (IP3) and diacylglycerol (DAG). IP3 and DAG then transduce signals in downstream signaling pathways, leading to T cell activation, proliferation, and cytokine production (**Figure 1.2**) (Saito, 2013).

When IP3 binds to its receptors, it depletes the calcium storage in the endoplasmic reticulum, thereby triggering an influx of extracellular calcium, a process called store-operated calcium entry (Feske, 2007). Increased calcium input activates calcineurin, which can then dephosphorylate NFAT, inducing its nuclear translocation (Feske, 2007). Meanwhile, membrane-bound DAG phosphorylates RAS guanyl-releasing protein, which in turn activates the mitogen-activated protein kinase cascade (Rincon, Flavell, & Davis, 2001). In parallel, DAG also activates protein kinase C-theta (PKCθ), as it translocates to the center of the immunological synapse through its association with CD28 cytoplasmic tail; this process enables PKCθ to actively regulate the NF-κB pathway (Isakov & Altman, 2012).

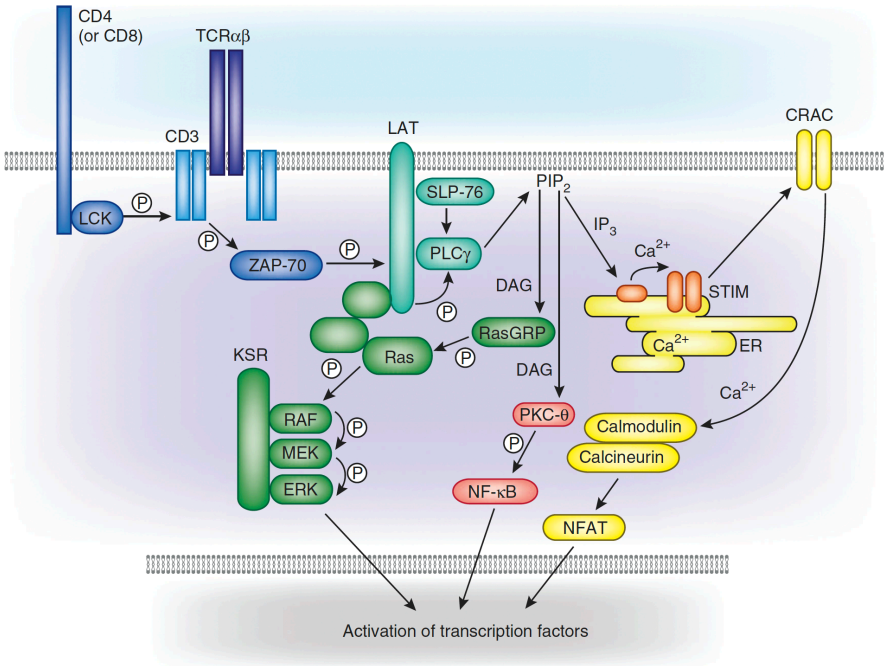

Figure 1.2 TCR signaling pathways

T-cell receptors (TCRs) engagement results in phospholipid hydrolysis and generation of Inositol 1,4,5-triphosphate (IP3) and diacylglycerol (DAG). While IP3 transduces the signal through calcium-calcineurin pathway (*yellow*), DAG activates mitogen-activated protein kinase cascade (*green*) and PKCθ, which in turn activates NF-κB (*red*). Adapted and reprinted by permission from Springer Nature, Nature Immunology, How the TCR balances sensitivity and specificity for the recognition of self and pathogens, Morris & Allen, 2012.

1.3.2 Regulatory process of T cell activation

In conjunction with TCR-pMHC interaction, a number of cell-surface molecules interact with their ligands on APCs, whereby the downstream signaling can potentiate or dampen T cell activation – thus, named co-stimulatory or co-inhibitory receptors (Fife & Bluestone, 2008; Sharpe & Freeman, 2002).

CD28 is a key co-stimulatory receptor constitutively expressed on T cells and may interact with either CD80 or CD86 expressed on activated APCs. CD28 activates phosphatidylinositol-3-kinase (PI3K) and downstream AKT pathway, thereby promoting IL-2 production, T cell proliferation and survival (Sharpe & Freeman, 2002). TCR engagement without CD28 co-stimulation may lead to anergy or clonal deletion (Schwartz, 2003).

In contrast to CD28, there are co-inhibitory receptors that suppress T cell activation, such as cytotoxic T-lymphocyte-associated antigen 4 (CTLA-4) and programmed cell death 1 (PD-1). Interestingly, expression of CTLA-4 and PD-1 is amplified by CD28 engagement upon antigen stimulation, implying a sophisticated balance between the positive and negative regulation (Fife & Bluestone, 2008; Francisco, Sage, & Sharpe, 2010).

CTLA-4 outcompetes CD28 with higher affinity for the same ligands CD80/CD86 on APCs and thus limits the stimulatory effects of CD28 signaling, preventing overactivation of the T cell response (Yokosuka et al., 2010). Moreover, CTLA-4 blocks AKT phosphorylation via activation of protein phosphatase 2 (**Figure 1.3)** (Fife & Bluestone, 2008; Sugiura et al., 2019). In addition to the cell-intrinsic mechanism, CTLA-4 also impairs CD28 costimulation through trans-endocytosis of CD80/CD86, followed by degradation (Qureshi et al., 2011).

Following ligation by PD-L1/PD-L2, PD-1 recruits Src homology region 2 domain-containing tyrosine phosphatases (SHPs) via immunoreceptor tyrosine-based switch motif (ITSM) in its cytoplasmic tail (Chemnitz, Parry, Nichols, June, & Riley, 2004; Francisco et al., 2010). SHPs then dephosphorylate proximal protein kinases to hamper TCR signaling and inhibit the PI3K/AKT pathway. In parallel, SHPs augment expression of phosphatase and tensin homolog (PTEN), which converts phosphatidylinositol triphosphate (PIP3) into PIP2 and thus blocks AKT activation

(Figure 1.3). Consequently, PD-1 signaling may attenuate proliferation, survival, protein synthesis, and IL-2 production in T cells (Chemnitz et al., 2004; Francisco et al., 2010).

CTLA-4- and PD-1-mediated inhibition target different signaling molecules, suggesting that they are not functionally redundant (Fife & Bluestone, 2008; Francisco et al., 2010). Besides, CTLA-4 is believed to function mainly in the T cell activation phase, whereas PD-1 mostly during the effector phase (Fife & Bluestone, 2008; Sugiura et al., 2019). Importantly, PD-1 ligation appeared to suppress gene expression induced by T cell activation to a greater extent than CTLA-4 ligation (Parry et al., 2005).

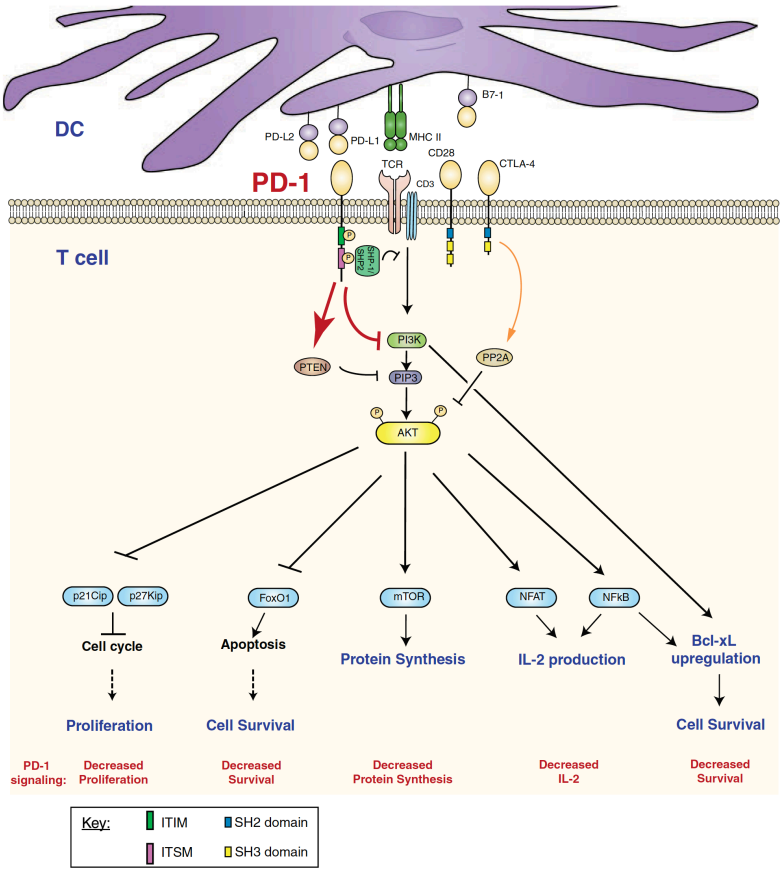

Figure 1.3 PD-1 signaling

Ligation of PD-1 results in tyrosine phosphorylation of its cytoplasmic domains. Phosphorylated ITSM recruits SHP-1/SHP-2, which in turn dephosphorylate proximal signaling molecules and augment PTEN expression, thereby limiting activation of the PI3K and AKT pathways. Consequently, PD-1 signaling may attenuate T-cell proliferation, survival, protein synthesis, and IL-2 production. ITIM, Immunoreceptor tyrosine-based inhibitory motif; ITSM, immunoreceptor tyrosine-based switch motif; SH2, Src homology region 2; SHP, SH2 domain-containing tyrosine phosphatases; PTEN, Phosphatase and tensin homolog; PIP3, phosphatidylinositol triphosphate; PP2A, protein phosphatase 2. Adapted and reprinted by permission from John Wiley and Sons, Immunological Reviews, The PD-1 pathway in tolerance and autoimmunity, Francisco, Sage and Sharpe, 2010.

1.3.3 T cell exhaustion

T cell exhaustion has been initially addressed using a mouse model of chronic lymphocytic choriomeningitis virus (LCMV) infection, where virus-specific cytotoxic T cells fail to eliminate the virus and become progressively dysfunctional and prone to apoptosis (Wherry, Blattman, Murali-Krishna, van der Most, & Ahmed, 2003; Wherry & Kurachi, 2015). In association with their diminishing effector functions, exhausted $CD8^+$ T cells persistently express multiple co-inhibitory receptors such as CTLA-4, PD-1, LAG-3, and TIM-3 (Blackburn et al., 2009). Transcriptional control of exhaustion has been under extensive investigation. Specifically, the transcription factors T-bet and Eomes defined two distinct subpopulations of exhausted $CD8^+$ T cells, including T-$bet^{hi}PD\text{-}1^{int}$ progenitor T cells and $Eomes^{hi}PD\text{-}1^{hi}$ terminally differentiated T cells (Kahan & Zajac, 2019; Paley et al., 2012). The progenitor subset expresses higher levels of transcription factor T cell factor 1 (TCF-1) and retains the self-renewal potential, thus considered 'stem-like' (Im et al., 2016). Importantly, this subset responds to PD-1 blockade more favorably than the terminally differentiated subset (Li, He, Hao, Ni, & Dong, 2018; Paley et al., 2012). On the other hand, mice with disrupted PD-1-mediated inhibition suffered from fatal immunopathology during early systemic virus infection, suggesting that T cell exhaustion may serve as a protective mechanism against excessive immune responses (Frebel et al., 2012).

Using the same mouse model, $CD4^+$ T cell exhaustion has also been characterized. Although some general features of T cell exhaustion are similar in both T cell populations, $CD4^+$ T cell exhaustion is distinct in certain aspects (Crawford et al., 2014). While functional $CD4^+$ T cells were required to maintain intact cytotoxicity of $CD8^+$ T cells against virus-infected cells, exhausted $CD4^+$ T cells gradually lost their ability to produce IL-2 and were skewed to produce IL-10 and/or IL-21 (Brooks, Teyton, Oldstone, & McGavern, 2005; Fröhlich et al., 2009; Fuller & Zajac, 2003). Exhausted $CD4^+$ T cells are not functionally inert but seem to reprogram their differentiation when chronically stimulated. Specifically, these cells appeared to transit into T follicular helper (Tfh) cells in persistent viral infection (Fahey et al., 2011). However, the Tfh master transcription factor Bcl6 was underrepresented in exhausted $CD4^+$ T cells, as transcriptome analysis exhibited substantial heterogeneity in lineage differentiation (Crawford et al., 2014).

In keeping with the observations in mice, T cell exhaustion has also been reported in chronic human viral infections as well as other diseases such as cancer and autoimmune disease (Catakovic, Klieser, Neureiter, & Geisberger, 2017; Day et al., 2006; Dong et al., 2019). While exhaustion of tumor-specific T cells impedes the tumor clearance, T cell exhaustion in autoimmune disease is associated with better prognosis (Catakovic et al., 2017; McKinney, Lee, Jayne, Lyons, & Smith, 2015; Miller et al., 2019).

Taken together, T cells can modulate their response to various chronic stimuli and display a so-called exhausted phenotype. Some researchers deem this phenomenon as functional adaptation, rather than mere loss of functions.

1.3.4 T cell exhaustion during allergen-specific immunotherapy

T cell exhaustion was considered as a potential mechanism leading to tolerance induction following AIT (Wambre, 2015). However, few studies addressed T cell exhaustion in the context of allergy and AIT. It has been shown that allergen-specific $CD4^+$ T cells were terminally differentiated and preferentially deleted during AIT (Wambre et al., 2017; Wambre et al., 2012). However, the contribution of T cell exhaustion to these observations is uncertain. Upon *in vitro* stimulation with common inhalant allergens, $CD4^+$ T cells from allergic patients markedly upregulated PD-1 and CTLA-4. Besides, while PD-1 blockade increased the proliferation of $CD4^+$ T cells in response to allergenic extracts, blocking CTLA-4 signaling reduced the proliferation (Rosskopf, Jahn-Schmid, Schmetterer, Zlabinger, & Steinberger, 2018). Still, it remained largely unknown whether AIT would accentuate the expression of PD-1 and CTLA-4 on proallergic T_H2 cells and whether these cells would reach a state of exhaustion upon the success of AIT.

Development of exhaustion in proallergic T_H2 cells post AIT is proposed and depicted in **Figure 1.4**.

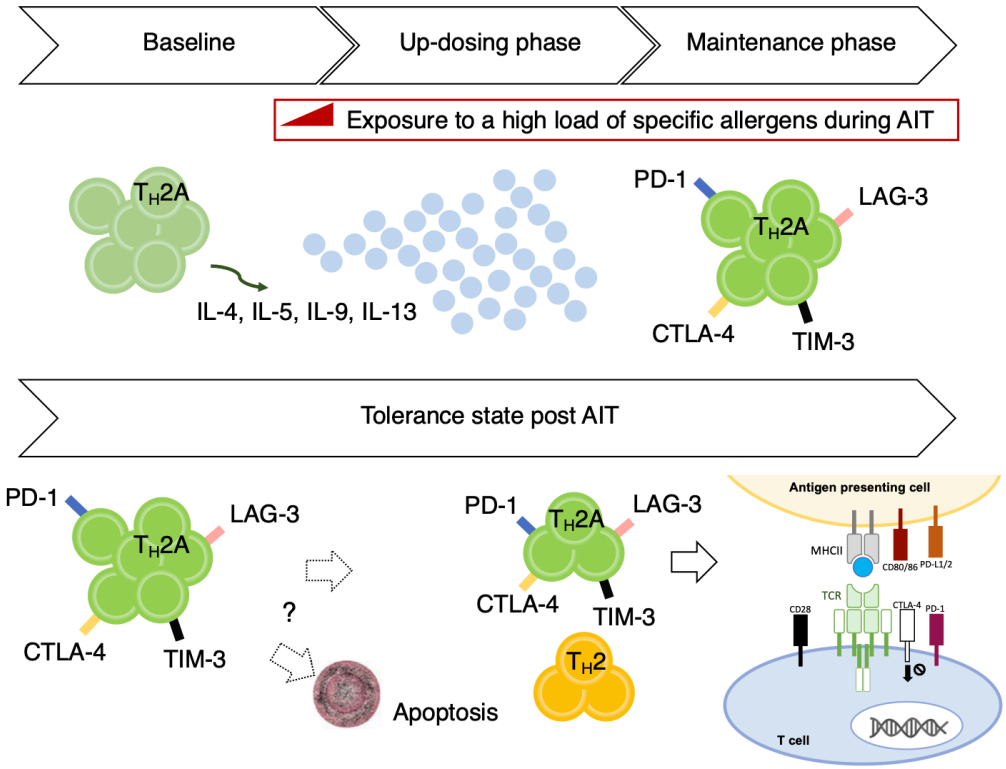

Figure 1.4 A hypothetical scheme of exhaustion of proallergic T_H2 cells post AIT

Proallergic T_H2 cells (T_H2A) may become exhausted due to chronic TCR stimulation during AIT. Upregulation of multiple co-inhibitory receptors may result in diminished effector function. T_H2A cells may become apoptotic or unable to induce allergic inflammation after AIT.

2 Aim of study

Peripheral tolerance to allergen may be induced following successful AIT. It is likely that if AIT protocol is continued beyond the desensitization phase, proallergic T_H2 cells may reach the state of exhaustion given that the allergen dose is persistently high. It is thus of particular interest to know whether T cell exhaustion leads to functional deletion of the T_H2 cells or their attenuated responsiveness to allergens. Since the expression of multiple co-inhibitory receptors is one of the major features for T cell exhaustion, the *ex vivo* expression of these receptors on T_H2 cells is determined by flow cytometry in a mouse model of AIT and two independent allergic patient cohorts.

In parallel, the role of T_H17 and IL-17–secreting regulatory T cells (Tr17) in tolerance induction during AIT is another important topic in the current project. Flow cytometric analysis of their phenotypical change is performed alongside their T_H2 counterparts. Also, *in vitro* generation of Tr17 is pursued in order to better characterize this T cell subset.

3 Materials and Methods

3.1 Materials

3.1.1 Chemicals

Name	Manufacturer
β-mercaptoethanol	Carl Roth, Karlsruhe, Germany
Dimethyl sulfoxide (DMSO) for cell culture	Applicam, Darmstadt, Germany
Ethanol absolute for analysis	Merck, Darmstadt, Germany
Aqua ad injectabilia	Berlin-Chemie, Berlin, Germany
UltraPure DEPC-Treated Water	Thermo Fisher Scientific, Waltham, MA, USA

3.1.2 Reagents and recombinant proteins

Name	Manufacturer
Ionomycin (IM)	Sigma-Aldrich, Merck, Darmstadt, Germany
Phorbol myristate acetate (PMA)	Sigma-Aldrich, Merck, Darmstadt, Germany
Brefeldin A (BFA)	Sigma-Aldrich, Merck, Darmstadt, Germany
Fixable Viability Stain (FVS) 520	BD Biosciences, Franklin Lakes, NJ, USA
LIVE/DEAD™ Fixable Aqua Dead Cell Stain Kit, for 405 nm excitation	Thermo Fisher Scientific, Waltham, MA, USA
Recombinant Phleum P1	BioMay AG, Vienna, Austria
Recombinant Phleum P1	Allergopharma, Merck, Darmstadt, Germany
IL-1β, human, recombinant (E. coli)	PromoCell, Heidelberg, Germany
IL-6, human, recombinant (E. coli)	PromoCell, Heidelberg, Germany
IL-23, human, recombinant (E. coli)	PromoCell, Heidelberg, Germany
TGF-β1, human, recombinant (CHO)	PromoCell, Heidelberg, Germany
Recombinant human IL-2	Miltenyi Biotec, Bergisch Gladbach, Germany
CD4+ T cell isolation kit for human PBMCs	Miltenyi Biotec, Bergisch Gladbach, Germany
CD45RO microbeads	Miltenyi Biotec, Bergisch Gladbach, Germany
Naïve CD4+ T cell isolation kit II, human	Miltenyi Biotec, Bergisch Gladbach, Germany
FITC Annexin V Apoptosis Detection Kit with PI	BioLegend, San Diego, CA, USA
Human TruStain FcX™ (Fc Receptor Blocking Solution)	BioLegend, San Diego, CA, USA
TruStain FcX™ (anti-mouse CD16/32 antibody)	BioLegend, San Diego, CA, USA

Name	Manufacturer
Anti-Mouse Ig, κ/Negative Control Compensation Particles Set	BD Biosciences, Franklin Lakes, NJ, USA
Anti-Rat and Anti-Hamster Ig, κ/Negative Control Compensation Particles Set	BD Biosciences, Franklin Lakes, NJ, USA
Trypan Blue solution, 0.4%	Thermo Fisher Scientific, Waltham, MA, USA
Collagenase V	Sigma-Aldrich, Merck, Darmstadt, Germany
Ovalbumin, grade V	Sigma-Aldrich, Merck, Darmstadt, Germany
RNAlater RNA stabilization reagent	Qiagen, Hilden, Germany
FastStart Universal SYBR Green Master (Rox)	Sigma-Aldrich, Merck, Darmstadt, Germany

3.1.3 Buffers, media and components

Buffer and medium	Manufacturer
Dulbecco's Phosphate-buffered saline (DPBS, 1X), no calcium, no magnesium	Thermo Fisher Scientific, Waltham, MA, USA
Phosphate-buffered saline (10x), RNase-free	Thermo Fisher Scientific, Waltham, MA, USA
RPMI-1640 Medium	Thermo Fisher Scientific, Waltham, MA, USA
Lymphoprep™ density gradient media	Alere Technologies AS, Oslo, Norway
TE Buffer	Thermo Fisher Scientific, Waltham, MA, USA
eBioscience™ | Foxp3/Transcription Factor Staining Buffer Set	Thermo Fisher Scientific, Waltham, MA, USA

Medium component	Manufacturer
Bovine serum albumin (BSA)	Sigma-Aldrich, Merck, Darmstadt, Germany
HyClone™ Fetal bovine serum (FBS), research grade	GE Healthcare Life Science, Chicago, IL, USA
Penicillin-Streptomycin 10,000 U/mL	Thermo Fisher Scientific, Waltham, MA, USA
L-Glutamine, 200 mM	Thermo Fisher Scientific, Waltham, MA, USA
MEM Nonessential amino acids (NEAA), 100X	Thermo Fisher Scientific, Waltham, MA, USA
Sodium Pyruvate, 100 mM	Thermo Fisher Scientific, Waltham, MA, USA

Buffer and medium, house-made	Ingredients
T cell culture medium	RPMI-1640 Medium with 10% FBS, 1% Penicillin-Streptomycin, 2 mM L-Glutamine, 1X NEAA, 1 mM Sodium Pyruvate, sterile filtered
Fluorescence-activated cell sorting (FACS) Buffer	DPBS with 10% FBS, sterile filtered

Buffer and medium, house-made	Ingredients
RNase-free FACS Buffer	RNase-free PBS, 0.5% BSA, sterile filtered
Cell freezing medium	FBS with 10% DMSO, sterile filtered
Magnetic activated cell sorting (MACS) separation buffer	DPBS, 0.5% BSA, 0.5 mM EDTA, sterile filtered

3.1.4 Monoclonal Antibodies (mAb)

Unconjugated mAb		
Specificity	**Clone**	**Manufacturer**
α-human CD3	UCHT1	BD Biosciences, Franklin Lakes, NJ, USA
α-human CD28	CD28.2	BD Biosciences, Franklin Lakes, NJ, USA
α-human IL-12 p70	20C2	BD Biosciences, Franklin Lakes, NJ, USA
α-human IFN-γ	B27	BD Biosciences, Franklin Lakes, NJ, USA
α-human IL-4	8D4-8	BD Biosciences, Franklin Lakes, NJ, USA
α-human PD-1 (Nivolumab)	5C4.B8	Absolute Antibody, Wilton, UK
α-Fluorescein, human IgG4-S228P	4-4-20	Absolute Antibody, Wilton, UK

Anti-human conjugated mAb			
Specificity	**Fluorochrome**	**Clone**	**Manufacturer**
CD3	APC-Cy7	HIT3a	BioLegend, San Diego, CA, USA
CD4	BV421	RPA-T4	BioLegend, San Diego, CA, USA
CD4	BB515	RPA-T4	BD Biosciences, Franklin Lakes, NJ, USA
CD8	AF700	HIT8a	BioLegend, San Diego, CA, USA
CD45RO	BV711	UCHL1	BioLegend, San Diego, CA, USA
CD45RA	BV605	HI100	BioLegend, San Diego, CA, USA
CD45RA	PerCP-Cy5.5	HI100	BioLegend, San Diego, CA, USA
CD45RB	FITC	MEM-55	BioLegend, San Diego, CA, USA
CD27	AF700	O323	BioLegend, San Diego, CA, USA
CD161	BV605	HP-3G10	BioLegend, San Diego, CA, USA
CD294 (CRTH2)	PE	REA598	Miltenyi Biotec, Bergisch Gladbach, Germany
CD294 (CRTH2)	APC	BM16	BioLegend, San Diego, CA, USA
CD154	BV605	24-31	BioLegend, San Diego, CA, USA

Anti-human conjugated mAb			
Specificity	**Fluorochrome**	**Clone**	**Manufacturer**
CD154	PE-CF594	TRAP-1	BD Biosciences, Franklin Lakes, NJ, USA
CD152 (CTLA-4)	PerCP-Cy5.5	BNI3	BioLegend, San Diego, CA, USA
CD152 (CTLA-4)	PE/Cy7	L3D10	BioLegend, San Diego, CA, USA
CD279 (PD-1)	APC	EH12.2H7	BioLegend, San Diego, CA, USA
CD279 (PD-1)	BV650	EH12.2H7	BioLegend, San Diego, CA, USA
CD223 (LAG-3)	BV650	11C3C65	BioLegend, San Diego, CA, USA
CD366 (TIM-3)	PE-Dazzle	F38-2E2	BioLegend, San Diego, CA, USA
CD25	BB515	2A3	BD Biosciences, Franklin Lakes, NJ, USA
CD127 (IL-7Rα)	BV711	A019D5	BioLegend, San Diego, CA, USA
CD49d	PE-Dazzle	9F10	BioLegend, San Diego, CA, USA
CD357 (GITR)	PE	621	BioLegend, San Diego, CA, USA
CD196 (CCR6)	PE-Dazzle	G034E3	BioLegend, San Diego, CA, USA
GATA-3	BV421	16E10A23	BioLegend, San Diego, CA, USA
Foxp3	PerCP-Cy5.5	PCH101	Thermo Fisher Scientific, Waltham, MA, USA
Foxp3	APC	PCH101	Thermo Fisher Scientific, Waltham, MA, USA
IL-4	APC	8D4-8	BD Biosciences, Franklin Lakes, NJ, USA
IL-4	AF488	8D4-8	BD Biosciences, Franklin Lakes, NJ, USA
IL-2	PE-Dazzle	MQ1-17H12	BioLegend, San Diego, CA, USA
IL-2	BV650	MQ1-17H12	BioLegend, San Diego, CA, USA
IL-10	PE	JES3-9D7	BioLegend, San Diego, CA, USA
IL-17A	BV711	BL168	BioLegend, San Diego, CA, USA

Anti-mouse conjugated mAb			
Specificity	**Fluorochrome**	**Clone**	**Manufacturer**
CD3	FITC	145-2C11	BD Biosciences, Franklin Lakes, NJ, USA
CD4	AF700	RM4-5	BD Biosciences, Franklin Lakes, NJ, USA
CD4	BV650	RM4-5	BioLegend, San Diego, CA, USA
CD45	APC-eFluor780	30-F11	Thermo Fisher Scientific, Waltham, MA, USA
CD44	BV605	IM7	BioLegend, San Diego, CA, USA

Anti-mouse conjugated mAb			
Specificity	**Fluorochrome**	**Clone**	**Manufacturer**
IL1RL1 (ST2)	BV421	DIH9	BioLegend, San Diego, CA, USA
CD279 (PD-1)	PE-Cy7	J43	Thermo Fisher Scientific, Waltham, MA, USA
CD223 (LAG-3)	BV650	C9B7W	BioLegend, San Diego, CA, USA
CD152 (CTLA-4)	PE-eFluor610	UC10-4B9	Thermo Fisher Scientific, Waltham, MA, USA
CD19	APC-Cy7	6D5	BioLegend, San Diego, CA, USA
CD1d	AF647	1B1	BioLegend, San Diego, CA, USA
CD5	AF700	53-7.3	BioLegend, San Diego, CA, USA
Ki67	PE-Cy7	B56	BD Biosciences, Franklin Lakes, NJ, USA
CD196 (CCR6)	BV421	29-2L17	BioLegend, San Diego, CA, USA
GATA-3	eFluor660	TWAJ	Thermo Fisher Scientific, Waltham, MA, USA
Foxp3	PerCP-Cy5.5	FJK-16s	Thermo Fisher Scientific, Waltham, MA, USA
RORgt	PE	AFKJS-9	Thermo Fisher Scientific, Waltham, MA, USA
IL-4	PE-CF594	11B11	BD Biosciences, Franklin Lakes, NJ, USA
IL-10	PE	JESS-16E3	BD Biosciences, Franklin Lakes, NJ, USA
IL-17A	AF647	TC11-18H10	BD Biosciences, Franklin Lakes, NJ, USA
IL-17A	BV605	TC11-18H10	BD Biosciences, Franklin Lakes, NJ, USA
CD62L	BV650	MEL-14	BD Biosciences, Franklin Lakes, NJ, USA
CD122	PE-Cy7	TM-b1	Thermo Fisher Scientific, Waltham, MA, USA
KLRG1	BV711	2F1/KLRG1	BioLegend, San Diego, CA, USA
KLRG1	FITC	2F1/KLRG1	BioLegend, San Diego, CA, USA
TCF-1	PE	S33-966	BD Biosciences, Franklin Lakes, NJ, USA
Blimp-1	PE-CF594	6D3	BD Biosciences, Franklin Lakes, NJ, USA
Eomes	PerCP-eFluor710	Dan11mag	Thermo Fisher Scientific, Waltham, MA, USA

Isotype control			
Specificity	**Fluorochrome**	**Clone**	**Manufacturer**
Mouse IgG1, κ	BV421	X40	BD Biosciences, Franklin Lakes, NJ, USA
Mouse IgG1, κ	PE-Dazzle	X40	BD Biosciences, Franklin Lakes, NJ, USA
Mouse IgG1, κ	APC	MOPC-21	BioLegend, San Diego, CA, USA
Mouse IgG1, κ	BV650	MOPC-21	BioLegend, San Diego, CA, USA
Mouse IgG1, κ	BV605	MOPC-21	BioLegend, San Diego, CA, USA
Mouse IgG1, κ	AF700	MOPC-21	BioLegend, San Diego, CA, USA
Mouse IgG1, κ	AF488	MOPC-21	BioLegend, San Diego, CA, USA
Mouse IgG1, κ	FITC	MOPC-21	BioLegend, San Diego, CA, USA
Mouse IgG1, κ	BV711	MOPC-21	BioLegend, San Diego, CA, USA
Mouse IgG1, κ	PE-Cy7	MOPC-21	BD Biosciences, Franklin Lakes, NJ, USA
Mouse IgG2a, κ	APC-Cy7	MOPC-173	BioLegend, San Diego, CA, USA
Mouse IgG2a, κ	PerCP-Cy5.5	eBM2a	Thermo Fisher Scientific, Waltham, MA, USA
Mouse IgG2b, κ	BV711	MPC-11	BioLegend, San Diego, CA, USA
Mouse IgG2b, κ	PE-Dazzle	MPC-11	BioLegend, San Diego, CA, USA
Mouse IgG2b, κ	BV421	MPC-11	BioLegend, San Diego, CA, USA
Rat IgG1, κ	PE	eBRG1	Thermo Fisher Scientific, Waltham, MA, USA
Rat IgG1, κ	BV650	RTK2071	BioLegend, San Diego, CA, USA
Rat IgG1, κ	PE-CF594	R3-34	BD Biosciences, Franklin Lakes, NJ, USA
Rat IgG1, κ	AF647	R3-34	BD Biosciences, Franklin Lakes, NJ, USA
Rat IgG2a, κ	PerCP-Cy5.5	RTK2758	BioLegend, San Diego, CA, USA
Rat IgG2a, κ	APC	RTK2758	BioLegend, San Diego, CA, USA
Rat IgG2a, κ	AF700	R35-95	BD Biosciences, Franklin Lakes, NJ, USA
Rat IgG2a, κ	BV650	R35-95	BD Biosciences, Franklin Lakes, NJ, USA
Rat IgG2a, κ	APC-Cy7	RTK2758	BioLegend, San Diego, CA, USA
Rat IgG2a, κ	BV421	RTK2758	BioLegend, San Diego, CA, USA
Rat IgG2a, κ	PE	eBR2a	Thermo Fisher Scientific, Waltham, MA, USA
Rat IgG2a, κ	PerCP-Cy5.5	eBR2a	Thermo Fisher Scientific, Waltham, MA, USA
Rat IgG2a, κ	PerCP-eFluor710	eBR2a	Thermo Fisher Scientific, Waltham, MA, USA

Isotype control			
Specificity	**Fluorochrome**	**Clone**	**Manufacturer**
Rat IgG2b, κ	PE	R35-38	BD Biosciences, Franklin Lakes, NJ, USA
Rat IgG2b, κ	AF647	RTK4530	BioLegend, San Diego, CA, USA
Rat IgG2b, κ	BV605	RTK4530	BioLegend, San Diego, CA, USA
Rat IgG2b, κ	APC-eFluor780	eB149/10H5	Thermo Fisher Scientific, Waltham, MA, USA
Rat IgG2b, κ	eFluor660	eB149/10H5	Thermo Fisher Scientific, Waltham, MA, USA
REA Control (S)	PE	REA293	Miltenyi Biotec, Bergisch Gladbach, Germany
Hamster IgG	FITC	G235-2356	BD Biosciences, Franklin Lakes, NJ, USA
Hamster IgG	PE-Cy7	eBio299Arm	Thermo Fisher Scientific, Waltham, MA, USA
Hamster IgG	PE-eFluor610	eBio299Arm	Thermo Fisher Scientific, Waltham, MA, USA
Hamster IgG	BV421	HTK888	BioLegend, San Diego, CA, USA
Hamster IgG	BV711	HTK888	BioLegend, San Diego, CA, USA

3.1.5 Animals

Female specific pathogen-free C57BL/6J mice, six weeks of age, were obtained from Charles River (Sulzfeld, Germany) and housed in individually ventilated cages (Green Line, Tecniplast, Italy). The mice were provided with food and water *ad libitum*. The study was conducted under federal guidelines for the use and cares of laboratory animals and was approved by the Government of the District of Upper Bavaria and the Animal Care and Use Committee of the Helmholtz Center Munich (55.2-1-54-2532-50-2017).

3.1.6 Consumables

Name	Manufacturer
96-well plate tissue culture treated, flat/round	Sarstedt, Nümbrecht, Germany
BD Falcon 6-/12-/24-/48-/96-well plate (non-) tissue culture treated, flat	BD Biosciences, Franklin Lakes, NJ, USA
BD Falcon Cell Strainer 70/100 µm	BD Biosciences, Franklin Lakes, NJ, USA
CryoPure Tube 1.8 mL, white	Sarstedt, Nümbrecht, Germany
SafeSeal tube 1.5/2 mL	Sarstedt, Nümbrecht, Germany
Cellstar Tubes 15/50 mL	Greiner Bio-One, Frickenhausen, Germany
Serological Pipettes 5/10/25 mL, graduated	Greiner Bio-One, Frickenhausen, Germany
SurPhob Low Binding Tips 10/200/1250 µL	Biozym Scientific, Hessisch Oldendorf, Germany
SafeSeal SurPhob Tips 10/200/1250 µL	Biozym Scientific, Hessisch Oldendorf, Germany
BRAND Pipette tips, 200 µL	BRAND, Wertheim, Germany
V-bottom Plate for LEGENDplex™ Assay	BioLegend, San Diego, CA, USA
LS Columns	Miltenyi Biotec, Bergisch Gladbach, Germany
gentleMACS C Tubes	Miltenyi Biotec, Bergisch Gladbach, Germany
QIAshredder	Qiagen, Hilden, Germany

3.1.7 Commercial kits

Kit	Manufacturer
RNA 6000 Nano Chip Kit	Agilent Technologies, Santa Clara, CA, USA
RNA 6000 Pico Chip Kit	Agilent Technologies, Santa Clara, CA, USA
RNeasy Micro Kit	Qiagen, Hilden, Germany
RNeasy Mini Kit	Qiagen, Hilden, Germany
RNeasy Midi Kit	Qiagen, Hilden, Germany
Pierce BCA Protein Assay Kit	Thermo Fisher Scientific, Waltham, MA, USA
Precellys lysing kit for tissue homogenizer	Bertin Technologies SAS, Montigny Le Bretonneux, France
Applied Biosystems™ High-Capacity cDNA Reverse Transcription Kit	Thermo Fisher Scientific, Waltham, MA, USA
SurePrint G3 Mouse Gene Expression v2 Microarrays Kit	Agilent Technologies, Santa Clara, CA, USA
SurePrint G3 Human Gene Expression v2 Microarrays Kit	Agilent Technologies, Santa Clara, CA, USA

3.1.8 Commercial assays

Assay	Analyte(s)	Manufacturer
QuantiTect Primer Assays, mouse	TFRC, HPRT, PDCD1, LAG3, CTLA4, RORC, FOXP3, IL24, SCGB1A1	Qiagen, Hilden, Germany
LEGENDplex™ Assays, mouse	IgE panel	BioLegend, San Diego, CA, USA
	Immunoglobulin isotyping panel (6-plex): IgG1, IgG2a, IgG2b, IgG3, IgA, IgM	
	T helper cytokine panel (13-plex): IL-2, IL-4, IL-5, IL-6, IL-9, IL-10, IL-13, IL-17A, IL-17F, IL-21, IL-22, IFN-γ, TNF-α	

3.1.9 Devices

Device	Manufacturer
Axiovert 25/40C Microscope	Zeiss, Oberkochen, Germany
Neubauer improved counting chamber	Marienfeld Superior, Lauda Königshofen, Germany
Heracell™ 150i CO_2 Incubator	Heraeus, Hanau, Germany
Herasafe (KS) Biological Safety Cabinets	Heraeus, Hanau, Germany
autoMACS Pro Separator	Miltenyi Biotec, Bergisch Gladbach, Germany
gentleMACS™ Dissociator	Miltenyi Biotec, Bergisch Gladbach, Germany
BD LSRFortessa™ Flow Cytometer	BD Biosciences, Franklin Lakes, NJ, USA
Megafuge 1.0R Centrifuge	Heraeus, Hanau, Germany
Megafuge 40R Centrifuge	Thermo Fisher Scientific, Waltham, MA, USA
Sigma 1-15 Micorfuge	Sigma Laborzentrifugen, Osterode am Harz, Germany
PerfectSpin 24R Refrigerated Microfuge	PeqLab Biotechnology, Erlangen, Germany
SW21 shaking water bath	Julabo, Seelbach, Germany
Vortex Genie2	Bender + Hobein, Bruchsal, Germany
Agilent 2100 BioAnalyzer	Agilent Technologies, Santa Clara, CA, USA
NanoDrop ND-1000	NanoDrop Technologies Inc., Wilmington, DE, USA
Thermomixer 5437	Eppendorf, Hamburg, Germany
Precellys 24 Tissue Homogenizer	Bertin Technologies SAS, Montigny Le Bretonneux, France
Labcycler Basic	SensoQuest, Göttigen, Germany

Device	Manufacturer
ViiA 7 Real-Time PCR System	Thermo Fisher Scientific, Waltham, MA, USA
Agilent G2545A Hybridization Oven	Agilent Technologies, Santa Clara, CA, USA

3.1.10 Software

Software	Company / Accessibility
Microsoft Office 365	Microsoft, Redmond, WA, USA
FlowJo v10	FlowJo, Ashland, OR, USA
GraphPad Prism 6	GraphPad Software, La Jolla, CA, USA
GeneSpring GX	Agilent Technologies, Santa Clara, CA, USA
Cloud-based LEGENDplex™ Data Analysis Software	BioLegend, San Diego, CA, USA
Gene Set Enrichment Analysis (GSEA) Software	http://www.broadinstitute.org/gsea/index.jsp
R programming software	https://www.r-project.org

3.2 Methods

3.2.1 Study population and blood samples

The cross-sectional study recruited 40 grass-pollen allergic patients with a history of moderate-severe and chronic persistent allergic rhinitis since >2 years during the grass-pollen season, as defined by ARIA (Allergic Rhinitis and its impact on Asthma) criteria, a positive skin prick test wheal >3 mm in diameter and grass-pollen specific IgE-level above 0.70 kU/l. Before recruitment, 20 of them have received AIT treatment. Twenty-seven non-allergic individuals without a clinical history of chronic rhinosinusitis were recruited as controls. The study was approved by the ethics commission of the Technical University of Munich (5534/12). After written and informed patients' consent and in accordance with the Helsinki declaration, peripheral blood was obtained from patients twice, once in (May–July) and once out of grass pollen season (October–January). PBMC samples collected from this study were used for ex vivo phenotyping of T_H2 cells.

PBMC samples collected at predefined time points during a longitudinal prospective study were used for time-course analysis by flow cytometry. The flow cytometric data were furthermore subjected to the unbiased cluster analysis (see section 3.2.11). The design of the study under the name Prospective Allergy and Clinical Immune Function Cohort study (PACIFIC, EudraCT 2015–003545-25) has been described in detail and published previously (Zissler et al., 2018). In brief, after written and informed patients' consent and in accordance with the Helsinki declaration, peripheral blood was obtained from patients at specific time points – at baseline levels, right before and six hours after the first and the last pre-seasonal top dose injection in year one of AIT. Further blood samples were taken twice a year during maintenance phase, once in and once out of grass pollen season, up to three follow-up years. Eight samples were included at each time point for analysis, and the samples used, due to patient dropout, were not linked between time points, rendering the analysis cross-sectional.

Heparinized whole blood was diluted 1:1 in sterile phosphate-buffered saline (PBS). Synthesized polysaccharide medium (Lymphoprep™ density gradient media, Alere Technologies AS, Oslo, Norway) was laid under the diluted blood and then subjected to centrifugation with the setup: 2500 rpm for 15 min without brake. After centrifugation, the mononuclear cell layer between Lymphoprep medium and plasma

was carefully aspirated and collected. Following another washing step with PBS, the pellet was resuspended in 10 ml PBS and a small aliquot (10 µl) was taken for the cell count (section 3.2.2). Last, the cell pellets were resuspended in cell freezing medium (house-made) and cryopreserved in liquid nitrogen for later analysis.

3.2.2 Cell count of viable cells in single cell suspension

Ten microliter of single cell suspension was diluted 1:10 with Trypan blue buffer. Given that Trypan blue is not permeable to intact cell membranes, the dye only stains dead cells. The number of unstained viable cells and stained dead cells was determined using a Neubauer counting chamber (depth 0.1 mm, 0.0025 mm^2; Marienfeld Superior, Lauda Königshofen, Germany) under a microscope. The viability of the cells was calculated as a percentage of unstained cells among all cells.

3.2.3 Culture conditions

For intracellular cytokine staining, the cells were incubated for four hours in culture medium (house-made) containing 10 ng/mL PMA, 1 µg/mL IM, and 5 µg/mL BFA. For anti-PD1 blockade assay, the cells were cultured in culture medium for 24 h with plate-bound anti-CD3 (UCHT1) at 5 µg/ml and soluble anti-CD28 Abs (CD28.2) at 1 µg/ml in the presence of 1 µg/ml Nivolumab (5C4.B8) or mock IgG (4-4-20). BFA was added to the culture medium for the last four hours to block the secretion of the intracellular cytokines.

3.2.4 Flow cytometry

Compensation

As emission spectra of fluorochromes overlap, fluorescence from more than one fluorochrome may be detected. A process of compensation is thus required to correct the spillover from the primary signals in each secondary channel it leaks into. For this, single antibody solution was prepared for each fluorochrome used in the FACS panel as well as the mixture containing negative control beads and beads against the host species of the primary antibody. The compensation bead mixture was incubated with the single antibody solution at room temperature in the dark for 60 min. The samples

were analyzed using a BD LSRFortessa™ Flow Cytometer. The flow cytometric data were analyzed using FlowJo software (v10).

FACS panel controls

FACS panel controls include unstained, single-color, isotype and Fluorescence Minus One (FMO) controls.

1. Unstained control: Unstained cells treated in the same experimental setting were analyzed on the flow cytometer to check if there is any autofluorescence.
2. Single-color staining: Cells were stained with each primary antibody in the panel separately to test the performance of the antibody.
3. Isotype control: Cells were stained with an antibody of the same isotype as each primary antibody in the panel to determine the nonspecific antibody binding.
4. FMO control: Cells were stained with all the fluorochromes in a panel except for one. This allows us to identify any spillover into the unlabeled channel and define the gate properly.
5. Histograms of single-color, isotype and FMO controls were overlaid for an overview of the FACS panel.

Cell surface staining protocol

Because many immune cells express Fc receptors, which may mediate unspecific antibody Fc binding, cells were first incubated at 4°C for 15 min with Fc receptor blocking solution (1:20 in PBS; TruStain FcX, BioLegend, San Diego, CA, USA). Afterwards, the cells were incubated at 4°C for 15 min with fixable viability dye (1:1000 in PBS; LIVE/DEAD™ Fixable Aqua Dead Cell Stain Kit, Thermo Fisher Scientific, Waltham, MA, USA) and then stained at 4°C for 30 min in FACS buffer containing specific antibodies against surface markers.

Intracellular staining protocol

To determine the expression of transcription factors and other intracellular molecules, surface labelled cells were fixed and permeabilized using Foxp3/Transcription Factor Staining Buffer Set (Thermo Fisher Scientific, Waltham, MA, USA) according to manufacturer's instructions. The fixed cells were kept in 1X Perm buffer overnight at 4°C in the dark and stained the next day with specific antibodies against intracellular molecules at room temperature for 30 min. The samples were analyzed using a BD LSRFortessa™ Flow Cytometer. The flow cytometric data were analyzed using FlowJo software (v10).

3.2.5 Ovalbumin immunotherapy model

AG Blank established the protocol for this mouse model (Russkamp et al., 2019). Sonja Heine set up the experiment and took care of the mice.

C57BL/6J mice were assigned to three different groups based on treatment conditions: non-allergic, allergic airway inflammation (AAI), and AAI+AIT (**Figure 3.1**).

For sensitization, mice of the allergic groups received intraperitoneal injections of 30 µg ovalbumin (OVA; Grade V, Sigma-Aldrich, Merck, Darmstadt, Germany) in conjunction with 2 mg aluminum hydroxide (Imject™ Alum, Thermo Fisher Scientific, Waltham, MA, USA) in 200 µl PBS on days 0, 7, 14 and 28. Mice of the non-allergic group received aluminum hydroxide (2 mg/ 200 µl PBS).

After sensitization, the AIT group was treated on days 35, 39, 43, 47, 51 and 55 with subcutaneous injections of OVA (500 µg/ 200 µl PBS), while non-allergic and allergic mice received sham treatment with 200 µl PBS. All animals were exposed to 1% nebulized OVA for 15 min in a challenge chamber on days 34, 41 and 48 during the immunotherapy phase and on days 63, 66 and 69 toward the end of the experiment. All mice were euthanized on day 70.

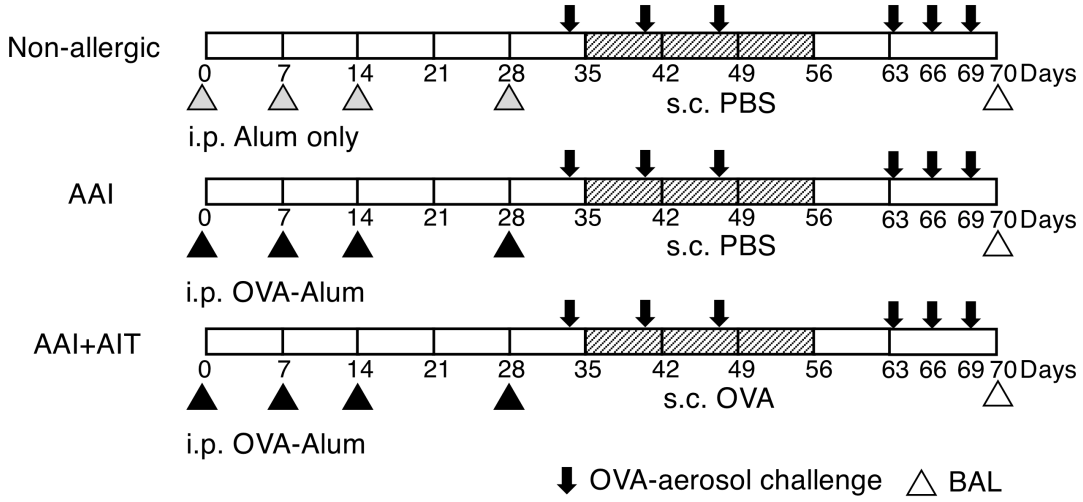

Figure 3.1 Scheme of ovalbumin immunotherapy model.

Shown is a schematic diagram of the mouse model of ovalbumin (OVA)-induced airway inflammation and allergen-specific immunotherapy (AIT). It consists of three groups: non-allergic, AAI and AAI+AIT. For sensitization, the mice were treated with intraperitoneal injections of OVA absorbed onto aluminum (i.p. OVA-Alum, indicated by ▲). One week after sensitization, the mice received either subcutaneous (s.c.) injections of OVA or PBS (gray-shaded blocks) while exposed to OVA aerosols (indicated by downwards pointing arrows). The animals were challenged again with OVA aerosols before bronchoalveolar lavage (BAL, indicated by △). AAI, allergic airway inflammation.

3.2.6 Bronchoalveolar lavage

Prof. Dr. Francesca Alessandrini performed the bronchoalveolar lavage (BAL) with the assistance of Johanna Grosch and Sonja Heine. I performed the experiments after receiving the specimens.

Airways were flushed five times with PBS. Cell-free BAL fluid (BALF) was collected and stored at -80°C for subsequent quantification of cytokines and immunoglobulins. The BAL cells were used for flow cytometric analysis. An aliquot of BAL cell suspension was taken to quantify the number of viable cells on BD Accuri C6 Plus flow cytometer following staining with DAPI (4′,6-diamidino-2-phenylindole) and anti-mouse CD45 antibody (30-F11). For differential cell counts, cytospin smears were prepared using cytocentrifuge technique (600 rpm for 10 minutes), fixed and stained with Diff-Quick (Dade Behring, Marburg, Germany).

3.2.7 Preparation of mouse specimens

Sonja Heine harvested the organs and collected the mouse specimens with the assistance of other lab members in AG Blank. I performed the experiments after receiving the specimens.

Preparation of RBC-free blood samples

The mice were bled on day 70, 24 hours after the last allergen challenge. After centrifugation, plasma was collected and stored at -80°C for subsequent quantification of cytokines and immunoglobulins. In order to lyse red blood cells, the blood cell pellet was resuspended in ACK lysing buffer (house-made) and incubated for two minutes at room temperature. PBS was added to the single cell suspensions to stop the lysing reaction. After centrifugation, the cell pellets were resuspended in cell freezing medium (house-made) and cryopreserved in liquid nitrogen for later analysis.

Organ harvest and lymphocyte preparation

The sacrificed mouse was pinned on a dissection board in a supine position. The skin was then cut with scissors along the midline and along the axis of the four limbs. The skin flaps were deflected laterally and fixed to expose the cervical areas, thoracic cage as well as the abdomen (Van den Broeck, Derore, & Simoens, 2006).

The thoracic cage was cut open to allow access to the mediastinum and the lungs. The lungs were excised and processed in various ways for the subsequent experiments. For transcriptomic analysis, a small piece of lung tissue was stored in RNAlater RNA stabilization reagent (Qiagen, Hilden, Germany). For flow cytometric analysis, the rest of the lungs was digested to isolate intrapulmonary lymphocytes.

Cervical and mediastinal lymph nodes were pinched out with a pair of pointed tweezers and stored in PBS on ice. The lymph nodes were ground through a 100-μm cell strainer using a sterile syringe plunger in a laminar flow hood. The pass-through lymph node cells were washed, resuspended in PBS and kept on ice before subsequent flow cytometric analysis.

Lastly, the abdominal wall was opened with scissors. The spleen was detached carefully from the surrounding soft tissue. The spleen was ground through a 100-μm cell strainer with a sterile syringe plunger in a laminar flow hood. The pass-through

splenocytes were collected as a single cell suspension in a Falcon tube. After centrifugation, the cell pellet was resuspended in ACK lysing buffer to lyse red blood cells. PBS was added to the single cell suspensions in order to stop the lysing reaction. After centrifugation, the cell pellet was resuspended in 10 ml PBS and then subjected to FACS staining protocol. A small aliquot (10 µl) was taken for the cell count (section 3.2.2).

Isolation of intrapulmonary lymphocytes

Lung tissue was cut into small pieces and incubated for 30 min at 37°C with RPMI containing 1 mg/ml collagenase A and 100 µg/ml DNase I (both from Sigma-Aldrich, Merck, Darmstadt, Germany). Digested lung pieces were meshed through a 40-µm cell strainer (EASYstrainer™, Greiner Bio-One, Kremsmünster, Austria). The pass-through cell suspension was collected and subjected to centrifugation. The cell pellet was resuspended with 40% Percoll solution. 80% Percoll solution was laid underneath the cell suspension using a long serological pipet and then centrifuged with the following setup: 1600x*g* for 15 min with brake set to 1. After centrifugation, the interphase lymphocytes were carefully collected, washed, resuspended in PBS and kept on ice before subsequent flow cytometric analysis. An aliquot of the cell suspension was removed to quantify the number of viable cells on BD Accuri C6 Plus flow cytometer following staining with DAPI (4′,6-diamidino-2-phenylindole) and anti-mouse CD45 antibody.

3.2.8 *In vitro* ovalbumin stimulation

Splenocytes were plated at a density of $1x10^6$ cells per milliliter in T cell culture medium (house-made) in a flat bottom 24-well plate. A final concentration of 10 µg/mL OVA was added to the medium. The cells were incubated for 48 hours at 37 °C, 5% CO_2 in a humidified atmosphere. After 48 hours, cell culture supernatants were collected and stored at -80°C for subsequent analysis.

3.2.9 Measurement of T_H cytokines, immunoglobulin isotypes and OVA specific-IgE in BALF and mouse serum

LEGENDplex assays (BioLegend, San Diego, CA, USA) were used to determine the levels of cytokines and various immunoglobulin isotypes in mouse serum and BALF. The samples were diluted, incubated with the capture beads, followed by a biotinylated detection antibody cocktail and streptavidin-phycoerythrin according to the manufacturer's instructions. The samples were analyzed using a BD LSRII Fortessa™ Flow Cytometer. The data were analyzed using a cloud-based LEGENDplex Data Analysis Software (BioLegend, San Diego, CA, USA).

For OVA-specific IgE, mouse serum was incubated with biotinylated anti-mouse IgE antibody (BD Biosciences, Franklin Lakes, NJ, USA), in an OVA-coated microtiter plate. OVA-IgE binding was detected using streptavidin-peroxidase (Calbiochem, Merck, Darmstadt, Germany) and the chromogenic substrate TMB (3,3',5,5'-tetramethylbenzidine; Sigma-Aldrich, Merck, Darmstadt, Germany). The change in color was detected using a plate reader. Mouse anti-ovalbumin IgE (BIOZOL, Eching, Germany) was used to generate a standard curve, allowing the sample concentration to be determined by comparison.

3.2.10 Gene expression analysis

RNA extraction from mouse lung cells

The mouse lungs were stored in RNAlater RNA stabilization reagent (Qiagen, Hilden, Germany) at -80°C until RNA was extracted. For tissue disruption and homogenization, the mouse lung pieces were transferred to a 2-ml microcentrifuge tube containing ceramic beads (Precellys lysing kit for tissue homogenizer) and lysis buffer (Buffer RLT supplemented with 1% β-mercaptoethanol). The microcentrifuge tubes were placed in the Precellys 24 Tissue Homogenizer (Bertin Technologies SAS, Montigny Le Bretonneux, France) with the recommended setup per the manufacturer's manual. After centrifugation to precipitate the debris, the clear lysate was used for RNA extraction using RNeasy Mini kit (Qiagen, Hilden, Germany) according to manufacturer's instructions. The extracted RNA was quantified using ultraviolet–visible spectrophotometry (NanoDrop Technologies Inc., Wilmington, DE, USA). RNA

integrity was determined using RNA 6000 Pico Chip Kit and Agilent 2100 Bioanalyzer (Agilent Technologies, Santa Clara, CA, USA).

Two-step quantitative real-time PCR (qPCR)

The cDNA was first reverse transcribed from the extracted RNA using High-Capacity cDNA Reverse Transcription Kit (Thermo Fisher Scientific, Waltham, MA, USA) according to the manufacturer's protocol. A qPCR reaction was then set up in triplicates using cDNA, primers specific for each target region and SYBR Green that incorporates into double-stranded DNA during amplification (**Table 3.1**) and was performed using the ViiA 7 Real-Time PCR System (Thermo Fisher Scientific, Waltham, MA, USA) following the manufacturer's protocol. As the fluorescence signal increased above background and was detectable by the quantitative thermal cycler, the threshold cycle (C_T) value was determined for the target genes and control genes (*Tfrc, Hprt*, and *Actb*). Using the comparative C_T method, the target gene expression relative to control genes was compared between different groups and presented as fold change in expression (Schmittgen & Livak, 2008).

Table 3.1 Reaction setup for real-time qPCR

Component	**Volume (µl)/reaction**
	384-well block
2x SYBR Green PCR Master Mix	5
10x QuantiTect Primer Assay	1
Template cDNA (diluted)	4
Total volume	10

Whole genome microarray analysis of mouse lung cells

Microarray analysis was performed on 24 independent extracted RNA samples from mouse lung cells. Samples were processed to generate Cy3-incorporated RNA and hybridized with SurePrint G3 Mouse Gene Expression v2 Microarrays (Agilent Technologies, Santa Clara, CA, USA) following the manufacturer's protocol. Quality-control checks and microarray data analysis were performed with GeneSpring GX 14.X (Agilent Technologies, Santa Clara, CA, USA). Data import using a standard

baseline transformation to the median of all values was performed, including log transformation and computation of fold changes. Subsequently, a principle component analysis (PCA) was conducted and revealed a homogenous component distribution. Compromised array signals (array spot is non-uniform if pixel noise of feature exceeds threshold or above saturation threshold) were excluded from further analysis. Differentially expressed genes were considered statistically significant as an absolute log2 fold change greater than 1.5 and a p-value less than 0.05 by using the Moderated T-Test.

Gene ontology (GO) term enrichment analysis was performed using an R package (G. Yu, Wang, Han, & He, 2012). Gene set enrichment analysis (GSEA) was performed using the Broad Institute program (http://www.broadinstitute.org/gsea/index.jsp). GSEA used curated gene sets from the Molecular Signature Database v3.0 (Liberzon et al., 2011) or published gene expression datasets from the Gene Expression Omnibus (GEO) repository at the National Center for Biotechnology Information archive (https://www.ncbi.nlm.nih.gov/geo/). Normalized enrichment score and q value were calculated by permutation testing.

3.2.11 Louvain cluster analysis and differential abundance test

Dr. Maren Büttner performed the analysis with the flow cytometric data and compensation matrix generated from experiments using PACIFIC study samples.

The flow cytometric data (pre-gated in singlet and live populations) were analyzed with scanpy (version 1.5.1) in Python version 3.8. The FlowCytometryTools package (https://github.com/eyurtsev/FlowCytometryTools, github version tag 0.5.0) was used to read the data, which were subsequently converted into the anndata (version 0.7.4) format. The data matrix was compensated using the numpy (version 1.19.1) matrix multiplication function.

The compensated flow cytometric data were normalized using the arcsinh-transformation (with cofactor 150) and the feasibility of the normalization was checked by inspecting the data distribution of each factor in a histogram. Then, the 15 nearest neighbors were computed with the scanpy pp.neighbors function and Louvain clustering with resolution 2.0 was performed.

Finally, hierarchical clustering with the scanpy tl.dendrogram function was performed with default parameters (i.e. the Pearson correlation and the 'complete' linkage method as implemented in the scipy cluster module (scipy version 1.5.2).

Differential Abundance tests were performed for all Louvain clusters and the merged clusters using the Dirichlet Regression model (implemented in the DirichletReg R package, see https://epub.wu.ac.at/4077/) for predefined pairwise comparisons in R (version 3.5.2). All p-values were adjusted using Benjamini-Hochberg multitest correction.

3.2.12 *In vitro* generation of IL-17–secreting Treg cells

In order to gain better insight into Tr17 cells, it was attempted to transdifferentiate Treg and T_H17 cells *in vitro* respectively and aimed to develop a working protocol for *in vitro* generation of Tr17 cells ultimately.

For Treg *in vitro* polarization, naïve $CD4^+$ T cells were sorted from freshly isolated PBMCs using the magnetic activation cell sorting (MACS) approach. The purity of naïve $CD45RA^+CD4^+$ T cells was >98% after the procedure (**Figure 3.2A**). Naïve T cells were stimulated with plate-bound anti-CD3 at 0.1, 0.75, or 2 μg/ml and soluble anti-CD28 antibodies at 0.75 μg/ml. Neutralizing antibodies against IL-12, IFN-γ, and IL-4 were used at 2 μg/ml. TGF-β1 (2 ng/ml) and IL-2 (30 U/ml) were added to facilitate Treg polarization. Cells were stimulated for five days and then detached and transferred to uncoated wells. A higher number of Treg cells were generated *in vitro* with anti-CD3 at 0.1 μg/ml compared with higher concentrations (**Figure 3.2B**). Again, while the percentage of *in vitro*-induced Treg cells peaked on day 12, the absolute cell number was highest by day 7 (**Figure 3.2C**). Lastly, the phenotype of *in vitro*-induced Treg cells was determined using flow cytometry. Similar to their counterparts isolated from peripheral blood, they were characterized by surface expression of CD25 and loss of CD127 and CD49d expression (**Figure 3.2D**).

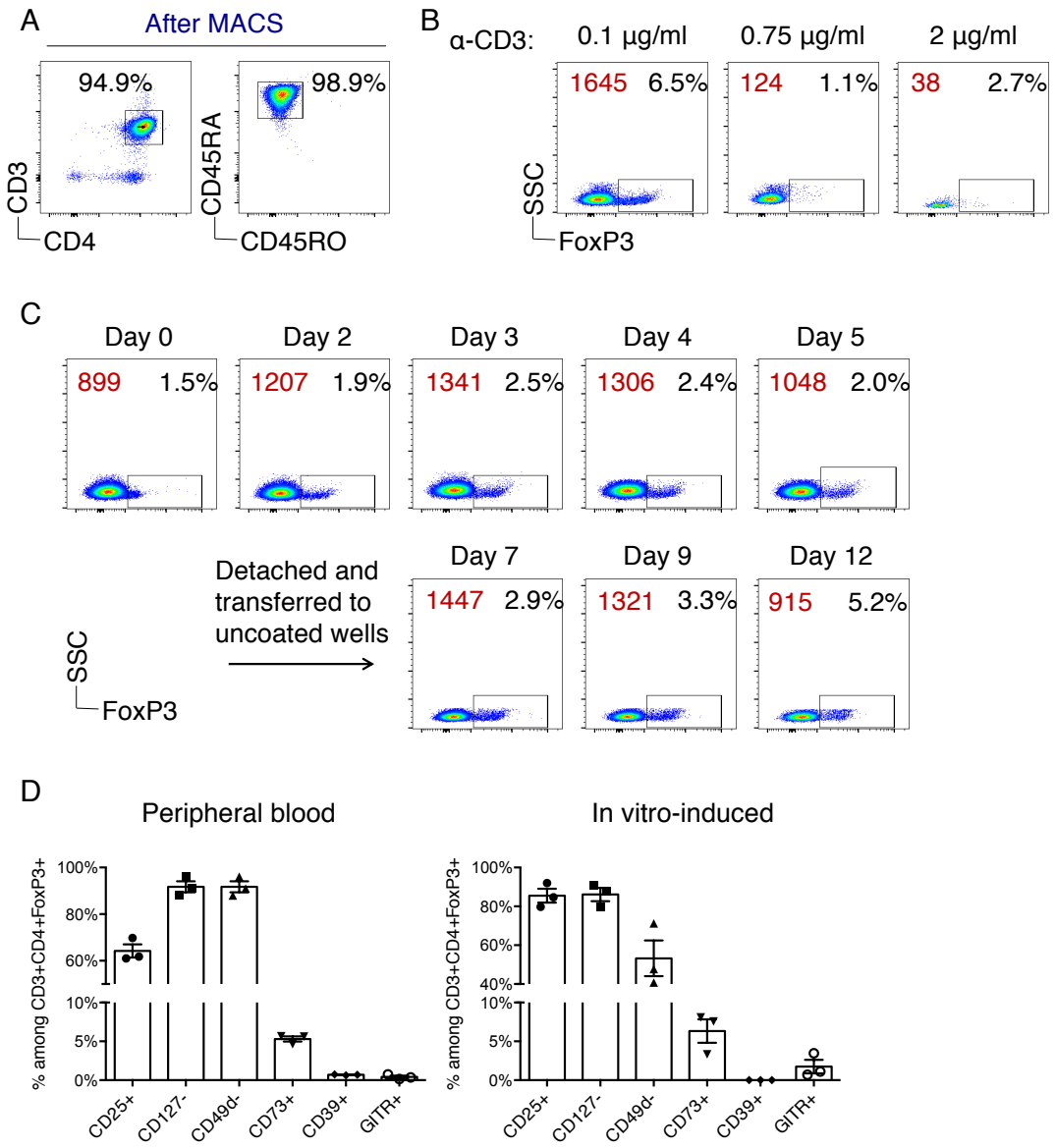

Figure 3.2 *In vitro* polarization of Treg cells from naïve CD4⁺ T cells.

(A) Purity control following naïve T cell enrichment. Non-CD4+ and CD45RO+ cells were depleted from freshly isolated PBMCs using magnetic activation cell sorting (MACS). Naïve CD45RA+CD4+ T cells made up > 98% of non-depleted cells as shown by one representative plot. (B) Comparison of different strength of TCR stimulation for Treg polarization. Naïve T cells were cultured in Treg polarizing conditions for 5 days with three different concentrations of plate-bound α-CD3 as shown here. (C) Frequency of *in vitro*-generated Tregs over time. Naïve T cells were cultured under Treg polarizing condition and harvested at different time points for measurement of Foxp3 expression. The flow cytometric plots shown are gated on singlet viable T helper cells. Numbers within the plots represent percentage (black) and absolute cell number per 100,000 total cells (red). (D) Characteristics of peripheral and i*n vitro*-induced Treg cells. Both shared similar pattern of surface marker expression. Symbols represent three individuals. Graphs show means ± SEM. GITR, glucocorticoid-induced TNFR-related protein.

For T_H17 *in vitro* polarization, four different published protocols were applied in an attempt to reproduce the results and then to develop a working protocol (summarized in supplementary **Table 9.1**). With the protocol A, the MACS-sorted naïve T cells were stimulated with plate-bound anti-CD3 at different concentrations and soluble anti-CD28 in the presence of TGF-β1, IL-1β, IL-6, and IL-23 and neutralizing antibodies against IL-12, IFN-γ, and IL-4. With the protocol B, the MACS-sorted naïve T cells were stimulated in the absence of CD28 costimulation as recent evidence suggests that CD28 suppressed T_H17 differentiation (Revu et al., 2018). With the protocols C and D, naïve Tregs ($CD3^+CD4^+CD45RA^+CD25^+CD127^-$) and $CCR6^+$ Tregs ($CD3^+CD4^+CCR6^+CD25^+CD127^-$) were sorted from fresh PBMCs and stimulated with immobilized anti-CD3 and soluble anti-CD28 in the presence of T_H17 polarizing cytokines. However, a high apoptosis rate of cells cultured under the T_H17 condition was observed, with overall a suboptimal yield of *in vitro*-induced T_H17 cells (supplementary **Figure 9.1A & B**). Meanwhile, in the T_H17 *in vitro* polarization experiments, an elevated frequency of $Foxp3^+$ cells instead of IL-17 producing cells were observed. Given that T_H17 cells have higher metabolic demands and lower oxygen tension favors Foxp3 induction, it might be helpful to culture the cells at lower cell density for the future experiments to optimize the yield of T_H17 cells.

3.2.13 Statistics

GraphPad Prism (GraphPad Software, La Jolla, CA, USA) was used to perform the statistical analysis for the experimental data in the current project for both human and murine studies without assuming Gaussian distribution of the data. Specifically, Kruskal-Wallis test and two-tailed Mann-Whitney *U* test were used to evaluate statistical significance, where appropriate. $P \leq .05$ was considered statistically significant.

4 Results

4.1 Ovalbumin immunotherapy model

4.1.1 Characterization of the effect of AIT on intrapulmonary and systemic allergic inflammation

C57BL/6J mice were assigned based on treatment conditions to three groups: non-allergic, allergic airway inflammation (AAI), and AAI+AIT (**Figure 3.1**). All animals underwent bronchoalveolar lavage (BAL) 24 hours after the last OVA aerosol challenge.

After OVA aerosol challenge, the total BAL cell number increased nearly 40-fold (38±14, $P \leq .001$) in AAI compared to non-allergic mice, while the number decreased 25-fold (25±8, $P \leq .001$) in AAI+AIT compared to AAI (**Figure 4.1A**). While non-allergic mice had a typical BAL cell composition with macrophage predominance, AAI mice displayed a typical lung inflammatory pattern, in which eosinophils were overrepresented (**Figure 4.1B**). An extensive decrease of BAL inflammatory infiltrates was observed in AAI+AIT compared to AAI, in particular of eosinophils (12%±3% vs. 64%±7%, $P \leq .001$), thus returning to a macrophage-predominant composition in AAI+AIT.

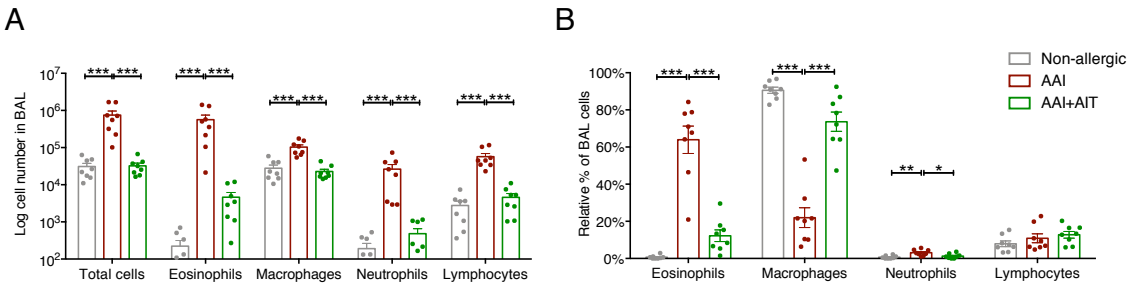

Figure 4.1 Inflammatory cell infiltration into BALF decreased in AAI+AIT mice.

$CD45^+$ cells in BAL fluid (BALF) from non-allergic, AAI and AAI+AIT mice were analyzed using cytospin smears. (A) Cell number of total cells, eosinophils, macrophages, neutrophils and lymphocytes on a logarithmic scale. (B) Percentages of eosinophils, macrophages, neutrophils and lymphocytes within the total BAL cells. Symbols represent individual mice (n = 8 per group). Graphs show means ± SEM. *$P \leq .05$; **$P \leq .01$; ***$P \leq .001$ by Mann-Whitney *U* test.

In addition, the secretion of multiple cytokines into BAL fluid (BALF) significantly increased in AAI compared to non-allergic mice (**Figure 4.2A–C, F–H**). While the average BALF levels of IL-4, IL-6, and TNF-α were reduced by >70% ($P \leq .001$) in AAI+AIT compared to AAI, levels of IL-5, IL-9, and IL-17A were reduced by approximately 30–50% ($P \leq .05$). In contrast, the BALF levels of IFN-γ and IL-2 were comparable across groups (**Figure 4.2E & I**), while IL-13 and IL-10 were barely detectable in most animals, regardless of the treatment conditions (**Figure 4.2D & J**). Similarly, serum levels of IL-4, IL-5, IL-9, IL-6, and IL-17A were significantly higher in AAI compared to non-allergic mice (**Figure 4.2K–M, P & Q**). Serum levels of IL-4 and IL-6 were decreased by more than 50% in AAI+AIT compared to AAI ($P \leq .05$), but levels of IL-5, IL-9, and IL-17A did not significantly decrease after AIT.

To test the allergen-specific response, splenocytes were incubated in T cell culture medium with OVA for 48 hours. Splenocytes of AAI mice produced a significantly greater amount of IL-4 and IL-6 and less IL-10 in response to OVA stimulation compared to non-allergic mice (**Figure 4.2U–W**). Splenocytes of AAI+AIT mice produced comparable amount of IL-4, IL-6, and IL-10 compared to AAI, indicating similar numbers of OVA-specific splenocytes with and without AIT. Other cytokines such as IL-5, IL-17A, TNF-α, and IFN-γ were all below detection limit across groups (supplementary **Table 9.2**).

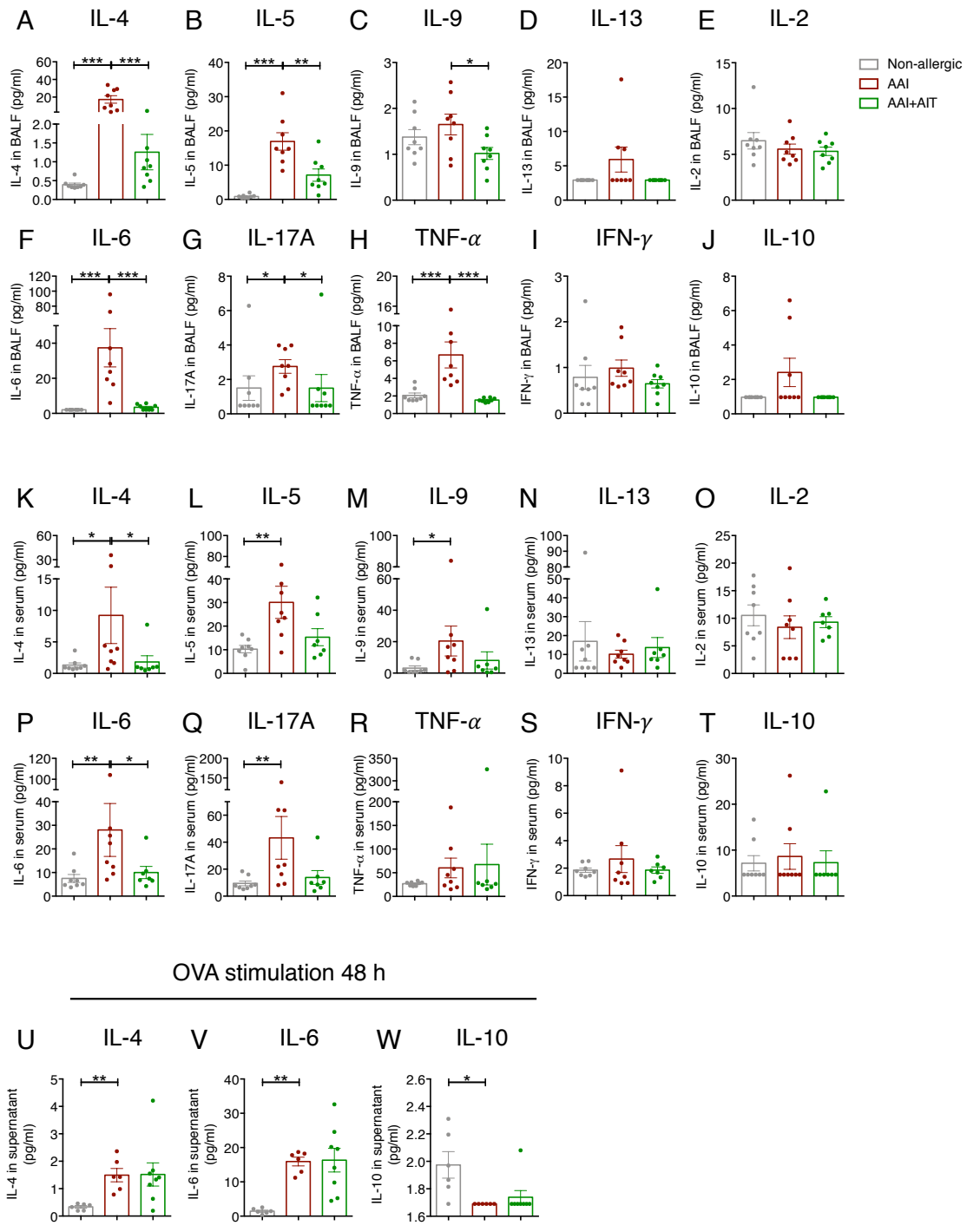

Figure 4.2 Allergic inflammation was alleviated after AIT, both locally and systemically.

Cell-free compartment of BALF and mouse serum from non-allergic, AAI and AAI+AIT mice were analyzed. Cytokine levels in the BALF (A–J) and mouse serum (K–T). Cytokine levels in supernatant were measured after 48 h *in vitro* stimulation of splenocytes with OVA at 10 µg/mL. Shown are IL-4 (U), IL-6 (V), and IL-10 (W). Symbols represent individual mice (n = 8 per group). Graphs show means ± SEM. **P* ≤ .05; ***P* ≤ .01; ****P* ≤ .001 by Mann-Whitney *U* test.

Furthermore, serum levels of total IgG1 and IgE were significantly elevated in AAI compared to non-allergic mice (12±3 and 28±10 fold increase, respectively; both $P \leq .001$; **Figure 4.3A & E**). An additional 3-fold increase of total IgG1 was observed in AAI+AIT compared to AAI but the levels of total IgE were not significantly altered after AIT. OVA-specific IgE was significantly higher in AAI than in non-allergic mice and after AIT returned to control levels (**Figure 4.3F**). Other immunoglobulin isotypes were comparable across groups (**Figure 4.3B–D**).

Overall, AIT attenuated the BAL inflammatory infiltrates and the levels of cytokines involving allergic inflammation, both in the lungs and in the blood.

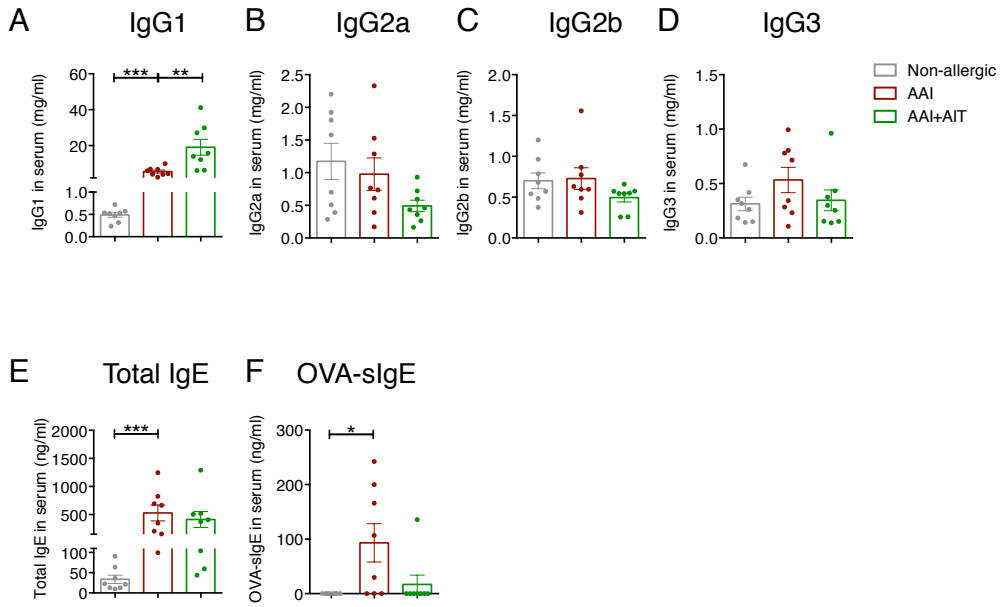

Figure 4.3 AAI+AIT mice had significantly higher levels of IgG1.

Sera from non-allergic, AAI and AAI+AIT mice were collected for analysis. Serum levels of total IgG1 (A), IgG2a (B), IgG2b (C), IgG3 (D) in mg/ml and levels of total IgE (E), and OVA-specific IgE (F) in ng/ml. Symbols represent individual mice (n = 8 per group). Graphs show means ± SEM. **P* ≤ .05; ***P* ≤ .01; ****P* ≤ .001 by Mann-Whitney *U* test.

4.1.2 Analysis of the frequency and phenotype of local and systemic T_H2 cells in AAI and AAI+AIT mice

To assess the dynamic change in frequencies of T_H2 cells following AIT, lymphocytes isolated from spleens, lymph nodes, lungs, BALF, and peripheral blood (PB) were analyzed by flow cytometry (**Figure 4.4A**). T_H2 cells ($CD3^+CD4^+CD44^+GATA3^+$) were overrepresented in the lungs, BALF, and PB of AAI mice (**Figure 4.4B–D**), but not in spleens and lymph nodes (supplementary **Figure 9.2A–C**). The frequency of T_H2 cells was significantly lower in the lungs of AAI+AIT compared to AAI (12%±0.9% vs. 26%±0.9%, $P \leq .001$), whereas T_H2 cells in the BALF and PB remained comparable between the two groups.

Approximately two thirds of T_H2 cells expressed ST2 in AAI, while there were 20–50% fewer in non-allergic mice (**Figure 4.4E–H**), indicating allergen experience and heightened type-2 effector function of T_H2 cells in former group. After AIT, frequencies of $ST2^+$ cells dropped, roughly 10–20% lower than AAI. In non-allergic mice, a greater proportion of local lung and BALF T_H2 cells co-expressed Foxp3 compared to AAI (**Figure 4.4I–L**). In addition, non-regulatory T_H2 cells expressed a significantly higher level of CTLA-4 and PD-1 (**Figure 4.4M & Q**). There were significantly higher frequencies of $CTLA\text{-}4^+$ cells in the lungs and BALF of AAI compared to non-allergic mice, with differences up to 50% (**Figure 4.4N & O**). While in AAI mice more than three quarters of local lung and BALF T_H2 cells expressed PD-1, in non-allergic mice barely one-third T_H2 cells expressed PD-1 (**Figure 4.4R & S**). After AIT, the frequencies of $CTLA\text{-}4^+$ and $PD\text{-}1^+$ cells were markedly reduced. There were 10–30% fewer local lung and BALF T_H2-cells expressing PD-1 and CTLA-4 compared to AAI. Overall, less than one third of peripheral T_H2 cells expressed these markers, with approximately 10% differences between AAI and the other two groups (**Figure 4.4P & T**).

Collectively, these data demonstrate that T_H2 cells in the lungs of AAI mice responded strongly to OVA aerosol challenge and exhibited increased effector functions, yet an exhausted phenotype. After AIT, however, the frequency of intrapulmonary T_H2 cells decreased significantly and these cells expressed a less profound exhausted phenotype.

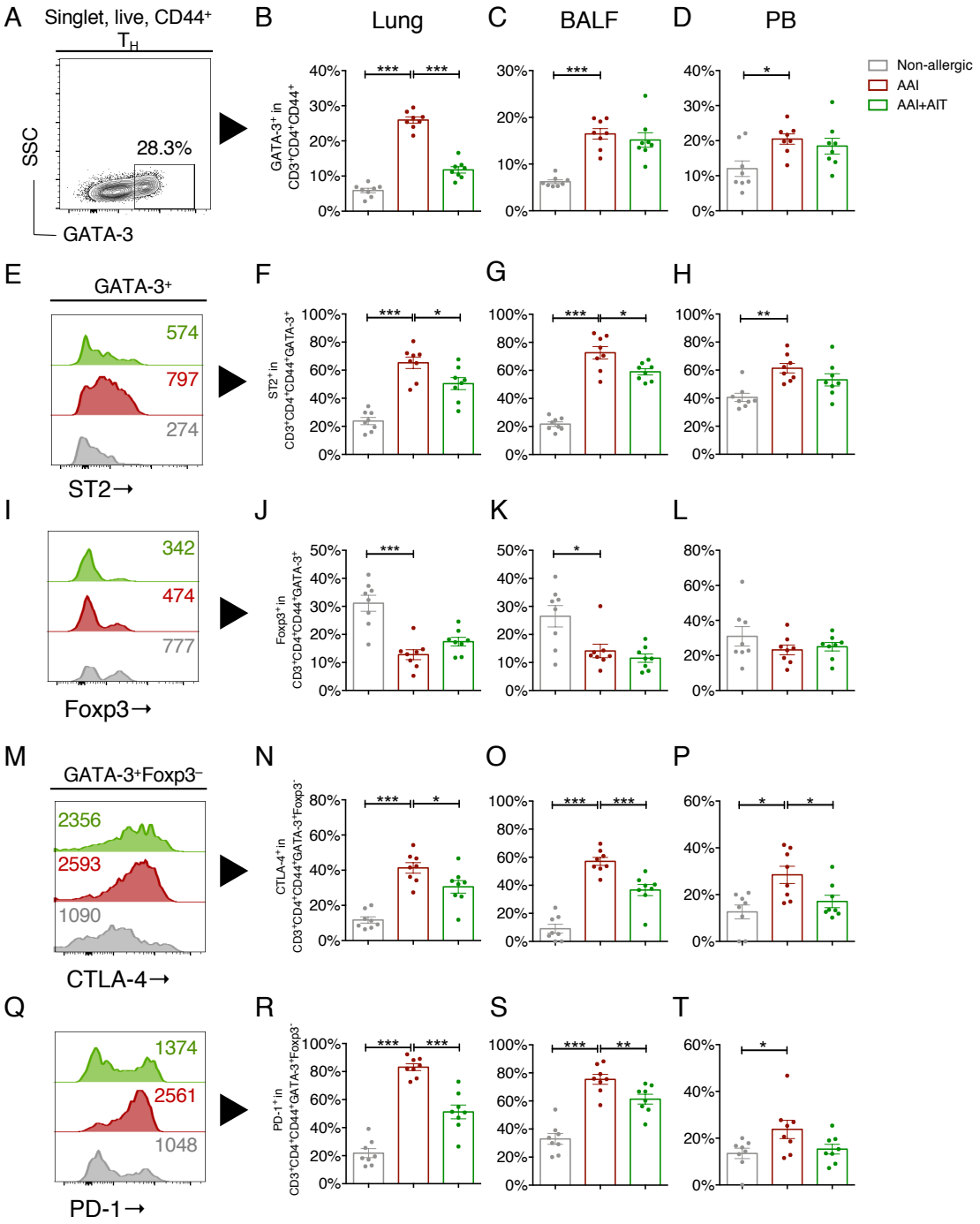

Figure 4.4 Frequency and phenotypes of GATA-3$^+$T$_H$2 cells in AAI mice altered after AIT.

(A) A representative flow cytometry plot shows the gate of GATA-3$^+$ cells among live memory T helper cells. Frequencies of GATA-3$^+$T$_H$2 cells in the lungs (B), BALF (C) and PB (D) of non-allergic, AAI and AAI+AIT mice. Mean fluorescence intensity (MFI) of ST2 (E) and frequency of ST2$^+$ T$_H$2 cells in different organs (F–H). MFI of Foxp3 (I) and frequency of Foxp3$^+$ T$_H$2 cells (J–L). MFI of CTLA-4 (M) and frequency of CTLA-4$^+$ cells (N–P) among nonregulatory T$_H$2 cells. MFI of PD-1 (Q) and frequency of PD-1$^+$ cells (R–T) among nonregulatory T$_H$2 cells. Numbers within representative overlaying histograms denote MFI values. Symbols represent individual mice (n = 8 per group). Graphs show means ± SEM. *P ≤ .05; **P ≤ .01; ***P ≤ .001 by Mann-Whitney U test.

4.1.3 Analysis of the frequency and phenotype of local and systemic T_H17, Tr17, and Treg cells in AAI and AAI+AIT mice

Using RORγt as a surrogate marker for T_H17 cells, analysis revealed that T_H17 cells were overrepresented in the lungs of AAI mice ($P \leq .05$; **Figure 4.5B**) but underrepresented in the spleen compared to non-allergic mice ($P \leq .01$; **Figure 4.5E**). After AIT, the frequency of intrapulmonary T_H17 cells decreased compared to AAI mice (1.1%±0.2% vs. 2%±0.2%, $P \leq .01$) and the frequency of splenic T_H17 cells increased (0.4%±0.04% vs. 0.2%±0.02%, $P \leq .01$). The frequencies of T_H17 cells in the BALF and PB were comparable across different groups (**Figure 4.5C & D**).

Both RORγt$^+$ Tregs (Tr17) and Tregs were also overrepresented in the lungs of AAI compared to non-allergic mice (**Figure 4.5F & J**). AIT significantly reduced the frequencies of intrapulmonary Tr17 and Tregs compared to AAI mice (AAI+AIT vs. AAI: Tr17, 0.2%±0.02% vs. 0.6%±0.09%, $P \leq .001$; Treg, 5.9%±0.3% vs. 9.2%±0.9%, $P \leq .05$). The infiltration of Tr17 and Tregs into the BALF was also significantly higher in AAI compared to non-allergic mice (**Figure 4.5G & K**). Again, AIT significantly reduced the cellular infiltration of both subsets into the BALF (AAI+AIT vs. AAI: Tr17, 0.6%±0.02% vs. 1.4%±0.02%, $P \leq .05$; Treg, 10%±0.6% vs. 20%±2%, $P \leq .001$). There were significantly fewer Tr17 in the spleens of AAI compared to non-allergic mice (0.08%±0.01% vs. 0.19%±0.06%, $P \leq .05$; **Figure 4.5I**), while the frequency of circulating Tr17 was comparable across groups (**Figure 4.5H**). The frequencies of circulating and splenic Tregs were not significantly different between AAI and non-allergic animals, while after AIT the frequency of splenic Tregs increased compared to AAI mice (**Figure 4.5L & M**).

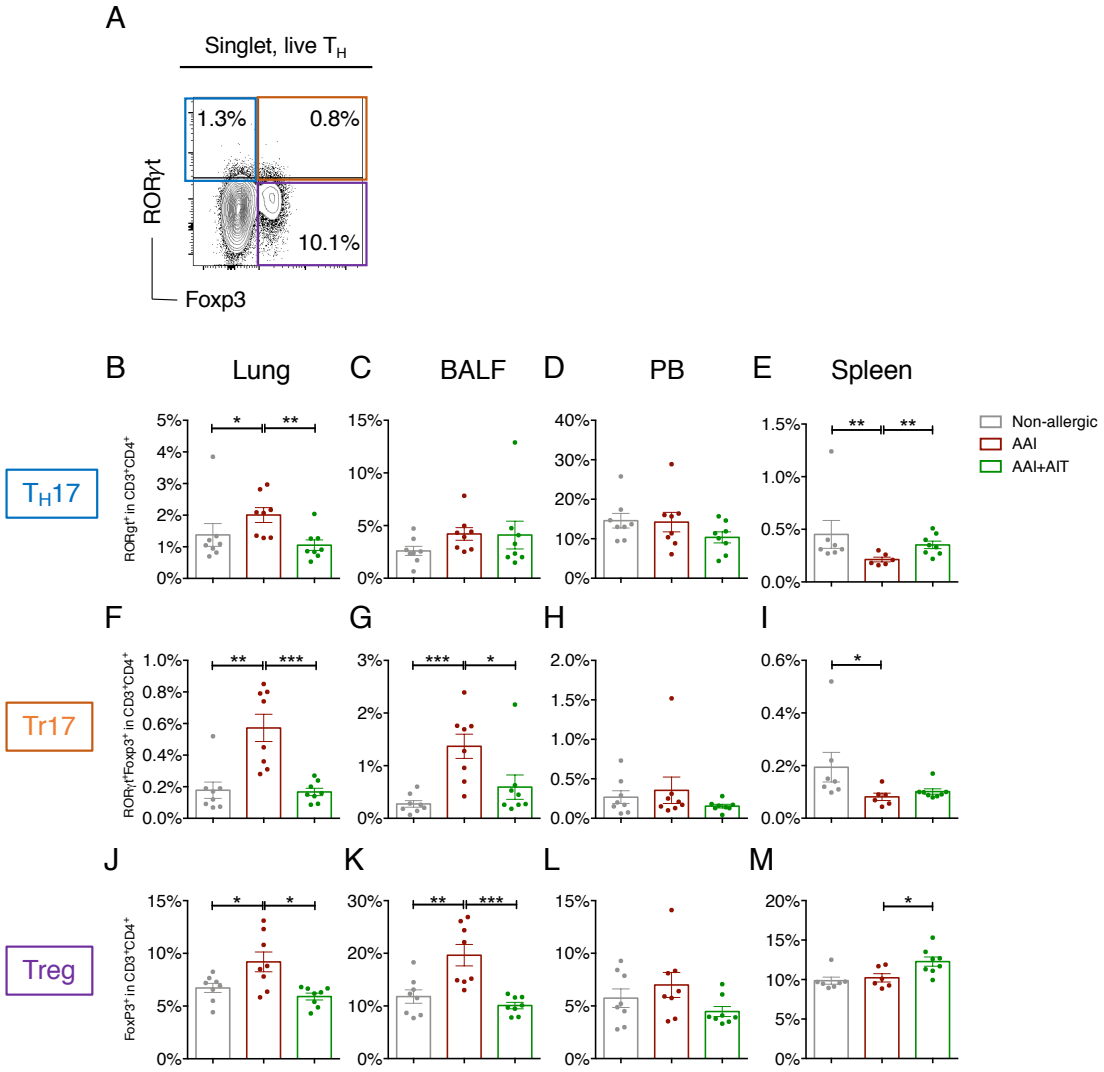

Figure 4.5 Frequencies of T_H17, Tr17, and Treg cells in the lungs of AAI mice decreased following AIT.

(A) A representative flow cytometry plot shows the gate of different T helper subsets among live T helper cells: T helper subsets expressing RORγt (T_H17, blue), Foxp3 (Treg, purple) and both transcription factors (Tr17, orange) in the lungs, BALF, PB, and spleens of non-allergic, AAI and AAI+AIT mice. Frequency of T_H17 cells in the lungs (B), BALF (C), PB (D), and spleens (E). Frequency of Tr17 cells in the lungs (F), BALF (G), PB (H), and spleens (I). Frequency of Tregs in the lungs (J), BALF (K), PB (L), and spleens (M). Symbols represent individual mice (n = 8 per group). Graphs show means ± SEM. **P* ≤ .05; ***P* ≤ .01; ****P* ≤ .001 by Mann-Whitney *U* test.

Since CTLA-4 was constitutively expressed in regulatory T cell lineage, >80% of Tr17 and Tregs were positive for CTLA-4 in all groups (data not shown). Approximately 40% of T_H17 cells expressed CTLA-4 in the lungs and BALF of AAI as opposed to 20% in non-allergic mice ($P \leq .001$; **Figure 4.6A & B**). Following AIT, frequencies of CTLA-4$^+$ T_H17 cells significantly dropped by 15–20% compared to AAI ($P \leq .01$). CTLA-4 expression on circulating and splenic T_H17 cells were comparable across groups (**Figure 4.6C & D**).

Frequencies of PD-1$^+$ cells among local lung and BALF T_H17 cells of AAI were 25–30% higher than those of non-allergic mice, while AIT significantly reduced the frequencies (**Figure 4.6E & F**). In general, PD-1 expression was detected on <10% of splenic T_H17 cells, while the frequencies were significantly higher in AAI than non-allergic mice, with 2% differences (**Figure 4.6H**).

More than one half of local lung Tr17 cells in AAI expressed PD-1, while only less than one forth were PD-1$^+$ in non-allergic and AAI+AIT groups ($P \leq .001$; **Figure 4.6I**). PD-1 expression on Tr17 cells were comparable in BALF, PB and spleens of different groups (**Figure 4.6J–L**).

Although PD-1 expression on intrapulmonary and circulating Tregs of AAI mice was not significantly higher compared to non-allergic mice, its expression was significantly reduced following AIT by approximately 15% ($P \leq .01$) and 5% ($P \leq .05$), respectively (**Figure 4.6M & O**). PD-1 expression on BALF Tregs displayed a different pattern, in which its expression was significantly lower in AAI compared to non-allergic and AAI+AIT mice (**Figure 4.6N**).

Altogether, T_H17, Tr17, and Treg cells all increased in frequency and upregulated PD-1 expression in the lungs of AAI mice, but not in circulation. PD-1 expression on these T cell subsets was significantly lower after AIT.

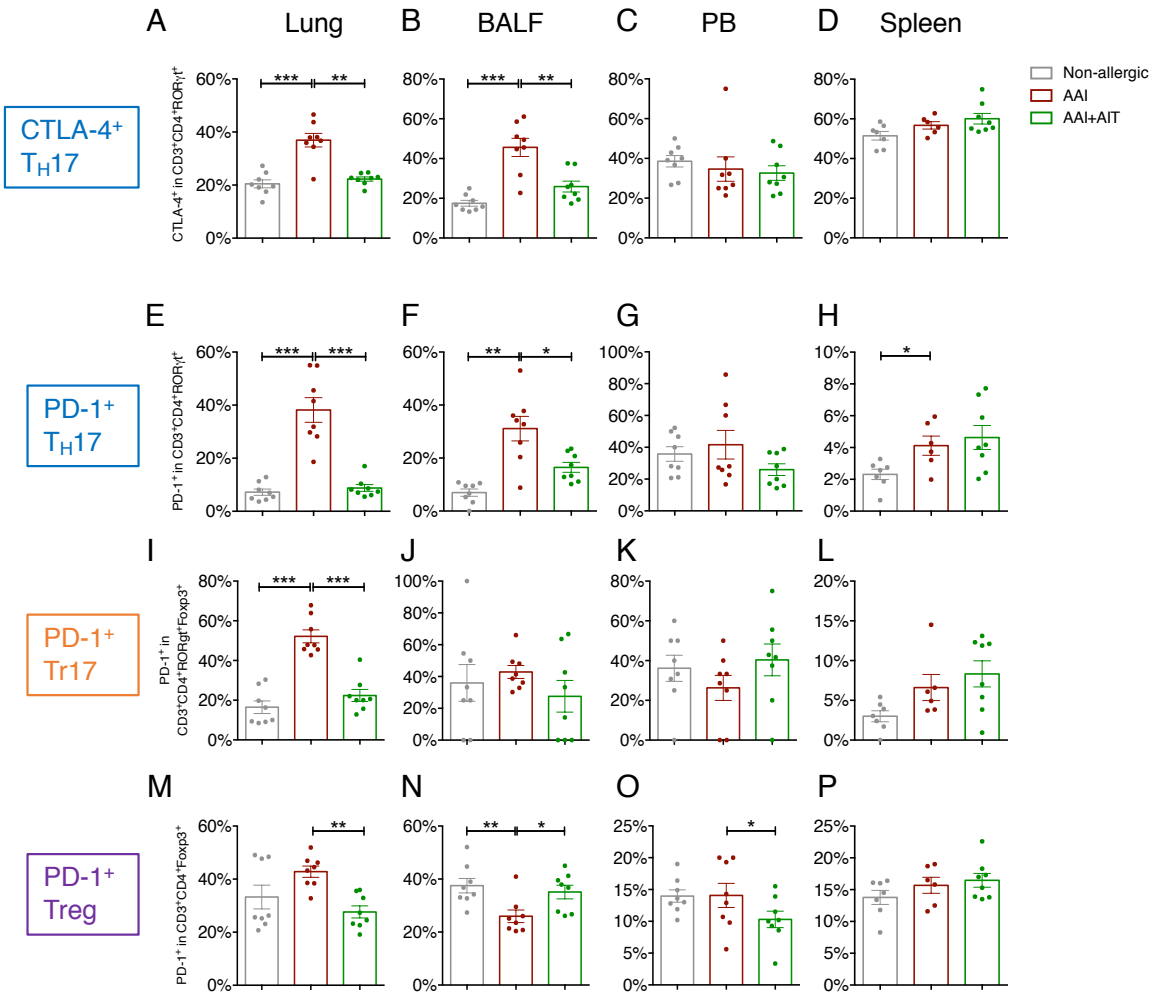

Figure 4.6 Expression of CTLA-4 and PD-1 on T_H17, Tr17, and Treg cells.

Flow cytometric analysis shows the expression of CTLA-4 and PD-1 on different T cell subsets in the lungs, BALF, PB, and spleens of non-allergic, AAI, and AAI+AIT mice. Percentage of CTLA-4$^+$ among T_H17 cells in the lungs (A), BALF (B), PB (C), and spleens (D). Percentage of PD-1$^+$ among T_H17 cells in the lungs (E), BALF (F), PB (G), and spleens (H). Percentage of PD-1$^+$ among Tr17 cells in the lungs (I), BALF (J), PB (K), and spleens (L). Percentage of PD-1$^+$ among Tregs in the lungs (M), BALF (N), PB (O), and spleens (P). Symbols represent individual mice (n = 8 per group). Graphs show means ± SEM. *$P \leq .05$; **$P \leq .01$; ***$P \leq .001$ by Mann-Whitney *U* test.

4.1.4 Microarray analysis of transcriptome of murine lung homogenates

The transcriptome of murine lung homogenates was analyzed using a whole-genome microarray. The data were grouped per treatment condition and a total of 6,500 regulated genes were identified in AAI+AIT compared to AAI mice, including 5,243 upregulated genes and 1,257 downregulated genes ($P \leq .05$; FC ≥ 1.5; **Figure 4.7A**). To gain better insight into the differentially expressed genes (DEGs) between AAI+AIT and AAI mouse lungs, a gene ontology (GO) enrichment analysis of the DEGs was performed (supplementary **Figure 9.3**). GO terms for biological processes were most enriched in association with chemotaxis and cytokine-mediated signaling pathway in AAI. The microarray data were subsequently filtered using the relevant GO terms (0072676, 0048247, and 0005125; **Figure 4.7B & C;** see details of the DEGs in supplementary **Table 9.4** and **Table 9.5**).

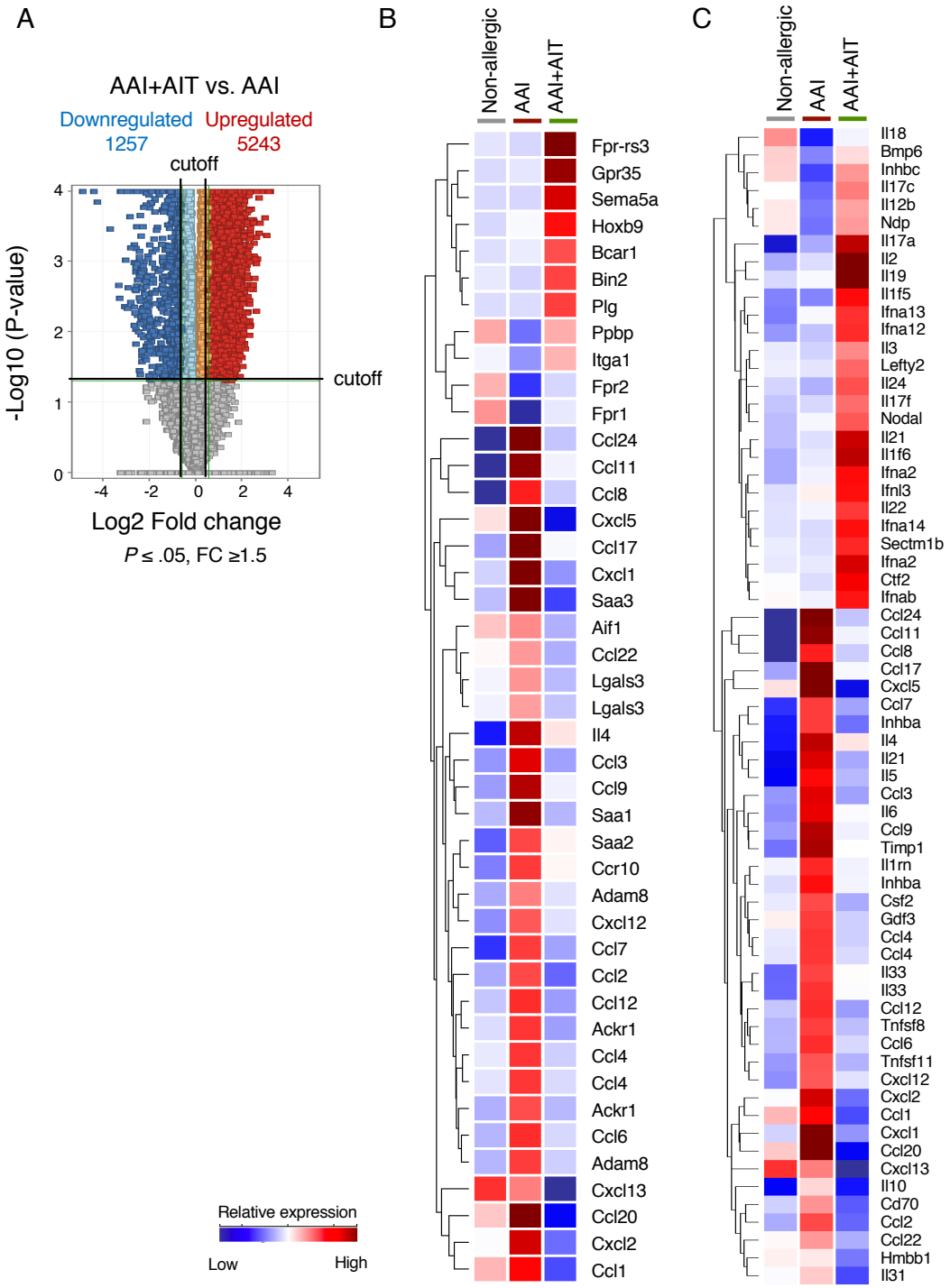

Figure 4.7 Reduced expression of multiple chemoattractant and type-2 cytokine genes in AAI+AIT mouse lungs.

Lung homogenates of non-allergic, AAI and AAI+AIT mice were subjected to RNA whole transcriptome microarray analysis (n = 8 per group). (A) Volcano plot of statistically significant entities ($P \leq .05$; FC ≥ 1.5) comparing AAI+AIT and AAI. Comparisons of differentially expressed genes filtered by different GO terms in AAI+AIT versus AAI. (B) lymphocyte chemotaxis (GO term: 0072676 and 0048247) and (C) cytokine activity (GO term: 0005125). Genes were grouped based on similarity in expression patterns by hierarchical clustering and their relationships were depicted by dendrograms to the left. Each row represents relative intensities of a particular gene across different groups. Colors indicate the abundance of that particular gene across groups.

Diversified chemokine genes were primarily upregulated in AAI mouse lungs, in particular for eosinophils (*Ccl11* and *Ccl24*), $CCR4^+$ T lymphocytes (*Ccl17* and *Ccl2*), and neutrophils (*Cxcl1* and *Cxcl5*). Besides, upregulation of *Saa1/3* genes was also observed in AAI mouse lungs, which encode serum amyloid A. While type-2 cytokine genes were upregulated in AAI mouse lung cells, AIT treatment augmented expression of IL-17 cytokine family members and genes that could skew T_H1/T_H2 balance, such as *Gpr35* and *Sema5a*. Gene set enrichment analysis (GSEA) of the data revealed that AAI mouse lung cells expressed genes associated with glycolysis, oxidative phosphorylation, cell cycle progression, and proliferation as opposed to AAI+AIT mouse lung cells (**Figure 4.8A**). Besides, AAI mouse lung cells expressed a terminally differentiated signature similar to exhausted $CD8^+$ T cells (**Figure 4.8B & C**).

In order to place the data in the context of T cell exhaustion, the microarray data were further probed using a curated gene expression profile of exhausted $CD4^+$ T cells to see whether the cells mirror the previously published phenotype of exhausted $CD4^+$ T cells (supplementary **Table 9.3**). AAI mouse lung cells enhanced the expression of *Ctla4*, *Pdcd1, Tigit, Icos*, *Tnfrsf9* (encodes 4-1BB), and *Tnfrsf4s* (encodes OX40). In contrast, upregulation of *Pilra* and *Cd244*, molecules associated with inhibition of TCR signaling, was observed after AIT (**Figure 4.9A;** supplementary **Table 9.6**)**.** The expression of transcription factors associated with exhaustion, *Eomes* or *Prdm1*, was comparable across groups (**Figure 4.9B**). In consistence with the microarray data, real-time qPCR confirmed that the expression of *Ctla4* and *Pdcd1* was remarkably diminished following AIT (**Figure 4.9C & D**).

The co-expressed genes associated with CTLA-4 and PD-1 were manually curated, based on protein-protein association networks and immune pathways (Gorenshteyn et al., 2015; Szklarczyk et al., 2019). Comparing AAI and non-allergic mice, it showed significant upregulation of CTLA-4 and PD-1 but not their ligands or associated signaling molecules (**Figure 4.9E**). While CTLA-4 was significantly downregulated in the lungs of AAI+AIT compared to AAI, the expression of its ligands CD80/86 was also downregulated (**Figure 4.9F**). Conversely, the expression of PD-1 ligands, PD-L1 (*Cd274*) and PD-L2 (*Pdcd1lg2*), were not significantly altered after AIT. Although the expression of the signaling molecules Lck and Akt1 was not significantly modulated, IL-2 was significantly upregulated comparing AAI+AIT with AAI.

A

Gene Sets	NES	FDR q-val
HALLMARK_OXIDATIVE_PHOSPHORYLATION	-1.9262003	0.016549392
HALLMARK_MTORC1_SIGNALING	-1.896173	0.011547952
HALLMARK_COMPLEMENT	-1.8896416	0.008548358
HALLMARK_COAGULATION	-1.813717	0.020210577
HALLMARK_IL2_STAT5_SIGNALING	-1.808619	0.016902763
HALLMARK_UNFOLDED_PROTEIN_RESPONSE	-1.7465659	0.028542176
HALLMARK_EPITHELIAL_MESENCHYMAL_TRANSITION	-1.7178411	0.03458373
HALLMARK_MYC_TARGETS_V2	-1.6945637	0.038515233
HALLMARK_ADIPOGENESIS	-1.6763971	0.042590573
HALLMARK_MYC_TARGETS_V1	-1.6631454	0.04423425
HALLMARK_GLYCOLYSIS	-1.6321853	0.04795702
HALLMARK_REACTIVE_OXYGEN_SPECIES_PATHWAY	-1.6212206	0.04947643
HALLMARK_PI3K_AKT_MTOR_SIGNALING	-1.6205761	0.0459424

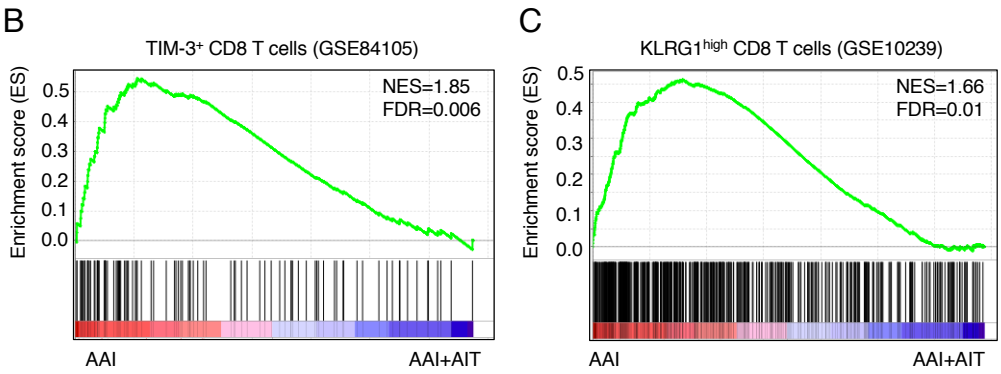

Figure 4.8 GSEA of the data reveals that AAI mouse lung cells expressed a terminally differentiated signature.

(A) Upregulated genes in AAI versus AAI+AIT mouse lung cells (with an FDR of less than 0.05 and the top 200 genes, based on fold change) were analyzed for functional enrichment using hallmark gene sets. GSEA plots comparing gene expression in AAI versus AAI+AIT mouse lung cells using publicly available gene sets of (B) antigen-specific TIM-3^{+} (GSE84105) and (C) KLRG1^{hi} exhausted CD8^{+} T cells (GSE10239) from GEO database. Data are from one experiment (n = 8 mice per group). GSEA, Gene set enrichment analysis; NES, normalized enrichment scores; FDR, false discovery rate.

In summary, AAI mouse lung cells upregulated genes associated with allergic inflammation and eosinophilia, which were significantly reduced following AIT. The AAI mouse lung cells also enhanced the expression of exhaustion-associated markers, CTLA-4 and PD-1, at transcriptional level.

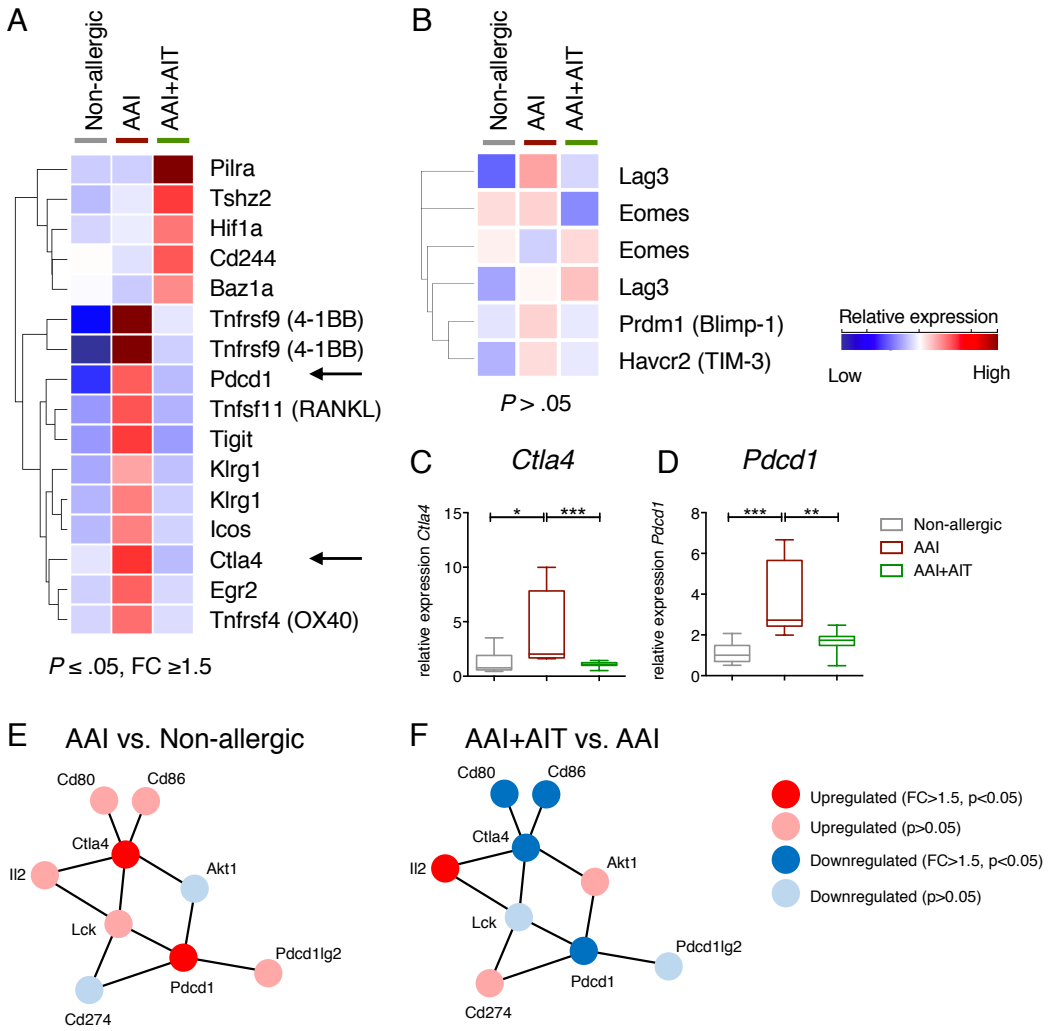

Figure 4.9 Upregulation of *Ctla4* and *Pdcd1* genes was reduced in AAI+AIT mouse lung cells.

Differentially expressed genes of AAI+AIT versus AAI mice was filtered using an entity list curated from exhausted CD4$^+$ T cells. Shown is the statistically significant entities ($P \leq .05$; FC ≥ 1.5) (A) and selection of nonsignificant important entities (B). Real-time qPCR analysis of the indicated genes, *Ctla4* (C) and *Pdcd1* (D). Data are from one experiment (n = 8 mice per group). *$P \leq .05$; **$P \leq .01$; ***$P \leq .001$ by Mann-Whitney *U* test. Co-expressed genes in relation to *Pdcd1* and *Ctla4* were manually curated based on publications and reactome pathways. The upregulation or downregulation of genes was color-coded according to the microarray analysis, comparing AAI versus non-allergic (E) and AAI+AIT versus AAI (F).

4.2 Ex vivo expression of co-inhibitory receptors on human T_H2 cells

In order to validate the previous findings in grass pollen-allergic patients, PBMCs were obtained from healthy controls (HC; n = 27), allergic rhinitis patients with grass-pollen allergy (AR; n = 20) and AIT-treated AR patients (AR+AIT; n = 20; **Table 4.1**). The three groups had comparable distributions of age, sex, and body mass index, while the rate of concurrent asthma was similar among AR patients with and without AIT.

Table 4.1 Demographic data of patient cohorts

	HC (n = 27)	AR (n = 20)	AR+AIT (n = 20)	*P*
Age (years)*	25.5±3.8	25.7±4.8	28.1±7.4	0.46
Female sex (%)	12 (44%)	11 (55%)	13 (65%)	0.38
BMI (kg/m^2)	21.0±2.0	22.6±3.3	21.5±2.0	0.26
Total IgE (IU/L)	n.d.	147.1±48.9	40.8±14.4	
Asthma (%)	0 (0%)	9 (45%)	10 (50%)	

Data shown as means ± SD. HC, healthy control; AR, allergic rhinitis; AIT, allergen-specific immunotherapy; BMI, body mass index

* at informed consent procedure and inclusion into study

Here, the *ex vivo* expression of co-inhibitory receptors CTLA-4, PD-1, LAG-3, and TIM-3 on CRTH2$^+$T$_H$2 cells was compared between the groups using flow cytometry (**Figure 4.10A**). While T$_H$2 cells from AR patients enhanced CTLA-4 expression in season compared to HC (3.6%±0.5% vs. 2.2±0.3%, $P \leq .05$), this expression was revoked by trend upon AIT ($P = 0.07$; **Figure 4.10B**). A significantly higher percentage of PD-1$^+$T$_H$2 cells was found in AR patients, independent of season (**Figure 4.10C**). Besides, the expression of LAG-3 or TIM-3 on T$_H$2 cells was not significantly different across groups (**Figure 4.10D & E**).

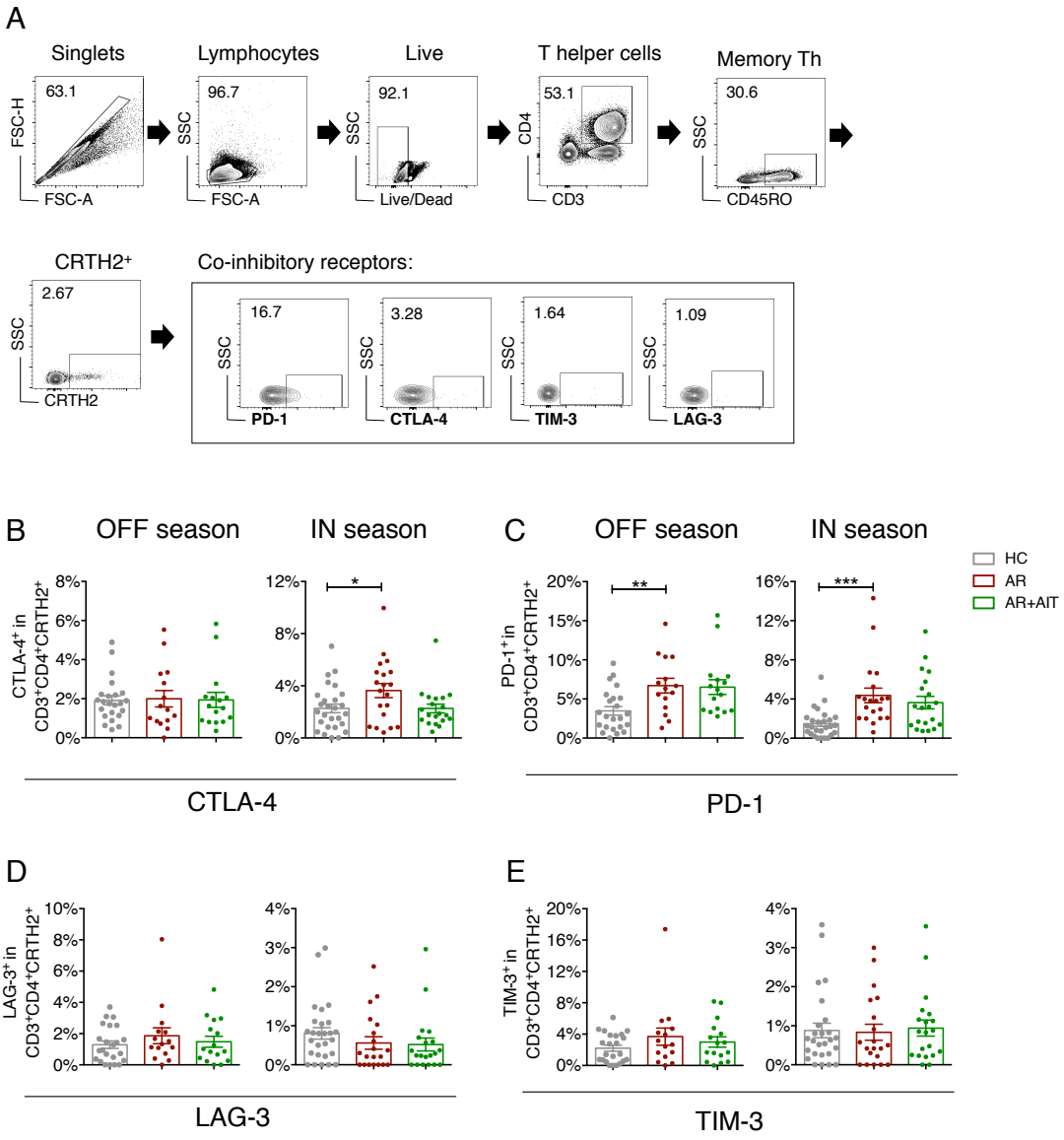

Figure 4.10 PD-1 expression on T_H2 cells in AR patient was independent of season, whereas CTLA-4 expression was associated with pollen flight.

PBMCs collected from healthy controls (HC), patients with allergic rhinitis (AR), and AR patients with AIT (AR+AIT) were analyzed using flow cytometry. (A) Gating strategy. Percentage of CTLA-4$^+$ (B), PD-1$^+$ (C), LAG-3$^+$ (D), TIM-3$^+$ (E) cells among CRTH2$^+$$T_H2$ cells in and out of grass-pollen season. Graphs show means ± SEM. *P ≤ .05; **P ≤ .01; ***P ≤ .001 by Mann-Whitney U test.

The next question was whether the expression of co-inhibitory receptors on T_H2 cells would be different in AR patients with concurrent asthma, denoted as AA patients henceforth. A subgroup analysis was performed accordingly. T_H2 cells expressed significantly higher-level CTLA-4 in AA patients compared to HC during pollen flight, while CTLA-4 expression on T_H2 cells was significantly lower in AA+AIT than AA patients (2.0%±0.3% vs. 3.9%±0.5%, $P \leq .01$; **Figure 4.11D**). This latter effect, however, was not observed in AR patients without concomitant asthma (compare **Figure 4.11A & B**). On the other hand, upregulation of PD-1 on T_H2 cells was observed in AR patients without concomitant asthma in and out of season (**Figure 4.11E & F**) as well as in AA patients during pollen flight (**Figure 4.11H**). PD-1 expression, however, was not changed upon AIT in any of the patient groups. Besides, PD-1 expression also displayed significant seasonal variations, with higher expression out of pollen season compared to in season. Again, no significant difference was detected in the expression of LAG-3 on T_H2 cells (**Figure 4.11I–L**). TIM-3 was significantly higher on T_H2 cells in AA patients out of season compared to HC (4.3%±0.6% vs. 2.2%±0.4%, $P \leq .05$; **Figure 4.11O**), but such upregulation was not observed in AR patients (**Figure 4.11M & N**).

Taken together, in AR patients, upregulation of CTLA-4 on T_H2 cells was associated with allergen exposure and concomitant asthma, while upregulation of PD-1 was persistent throughout the year, albeit with seasonal variations.

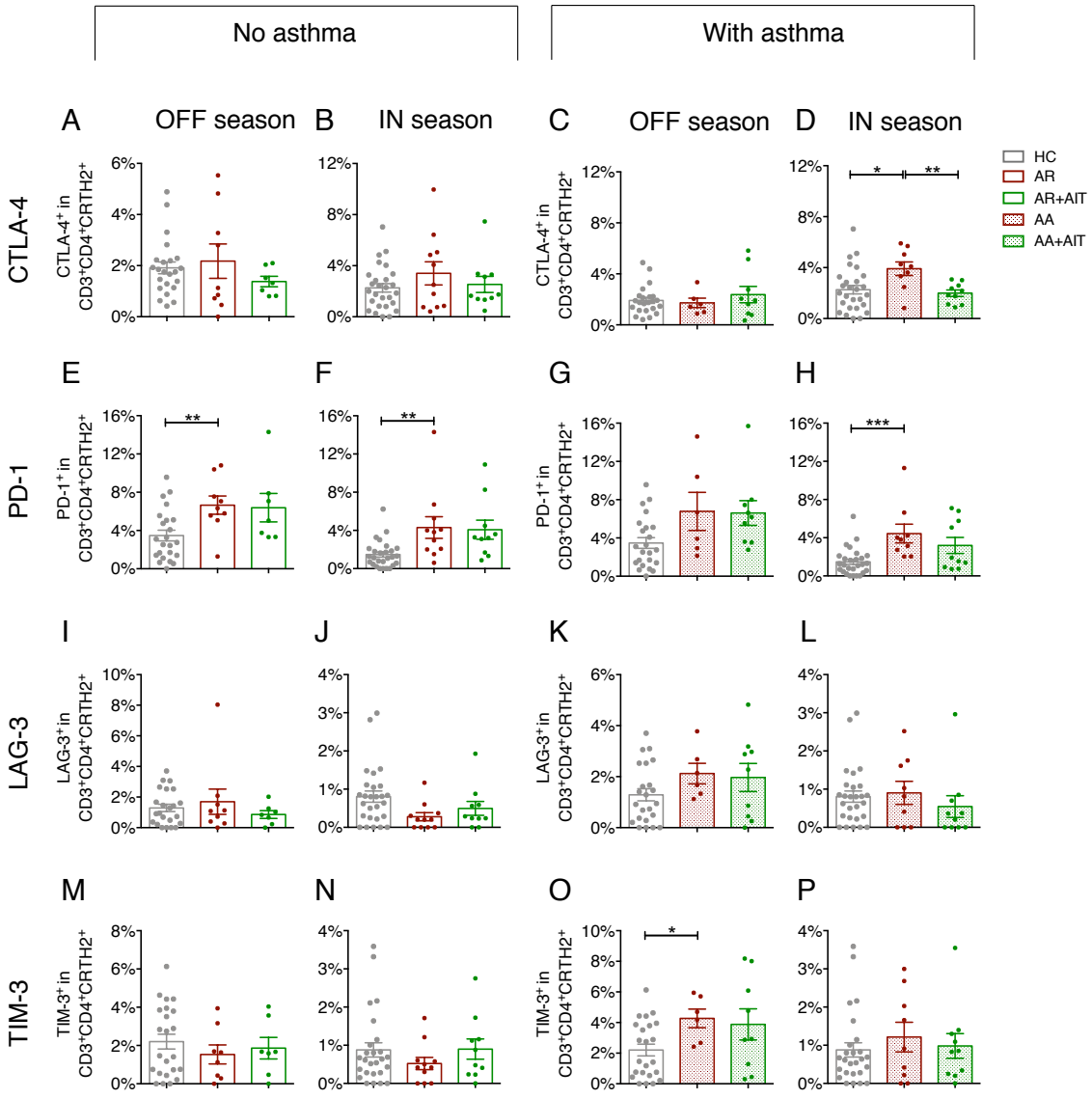

Figure 4.11 CTLA-4 expression was upregulated on T_H2 cells in AA patients during pollen flight but significantly reduced after AIT.

Subgroup analysis according to concomitant asthma was subsequently performed. (A–D) Percentage of CTLA-4$^+$ cells among CRTH2$^+$$T_H2$ cells from AR patients without asthma (A and B) and with asthma (C and D) outside and inside pollen season. (E–H) Percentage of PD-1$^+$ cells in AR patients without asthma (E and F) and with asthma (G and H) outside and inside pollen season. (I–L) Percentage of LAG-3$^+$ cells in AR patients without asthma (I and J) and with asthma (K and L) outside and inside pollen season. (M–P) Percentage of TIM-3$^+$ cells in AR patients without asthma (M and N) and with asthma (O and P) outside and inside pollen season. Graphs show means ± SEM. *P ≤ .05; **P ≤ .01; ***P ≤ .001 by Mann-Whitney U test.

4.3 Time-course analysis of circulating T_H2 and T_H17 cells during AIT

4.3.1 Louvain clustering analysis of T_H2 cells during AIT

In order to examine the treatment effect on exhaustion, flow cytometric analysis was performed using PBMC collected during a longitudinal AIT-treated patient cohort study (**Figure 4.12; Table 4.2**).

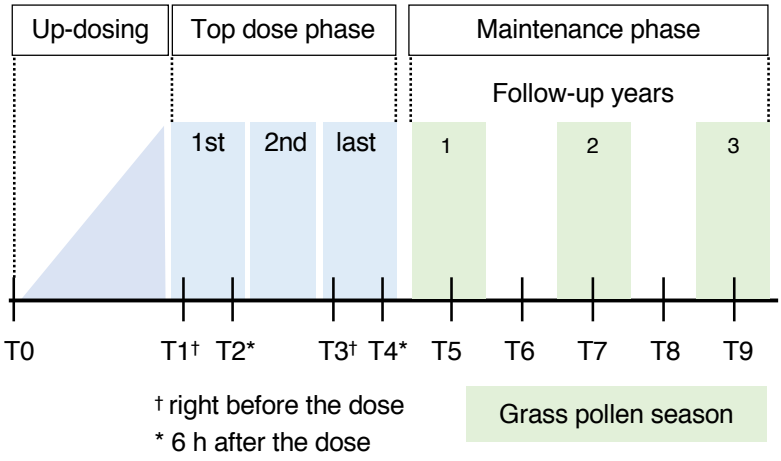

Figure 4.12 Study scheme of PACIFIC study.

PBMCs were collected at the specific time points: baseline levels (T0), right before (T1) and six hours after the first (T2) pre-seasonal top dose injection, and right before (T3) and six hours after the last (T4) pre-seasonal top dose injection in year one of AIT. During maintenance phase, patients were treated with follow-up AIT injections every 4–8 weeks over a period of three years. Further blood samples were taken twice a year, once in and once out of grass pollen season: in (T5) and out of grass pollen season (T6) year one; in (T7) and out of season (T8) year two; in season year three (T9). PBMC samples were analyzed using flow cytometry.

Table 4.2 Characteristics of AIT-treated patient cohort

	Immunotherapy n = 32
Age (years)*	25.6±6.3
Female Sex (%)	16 (50%)
Total IgE	147.1±167.1
Grass pollen allergy:	
specific IgE	32.7±27.9
skin prick test (positive %)	100%
Allergic asthma (%)	14 (44%)

Data shown as means ± SD.
* at informed consent procedure and inclusion into study

The compensated flow cytometric data were subjected to a graph-based Louvain clustering analysis, resulting in 42 clusters (see methods 3.2.11; **Figure 4.13**). The cluster distribution per sample corresponded to the cell-type composition per sample.

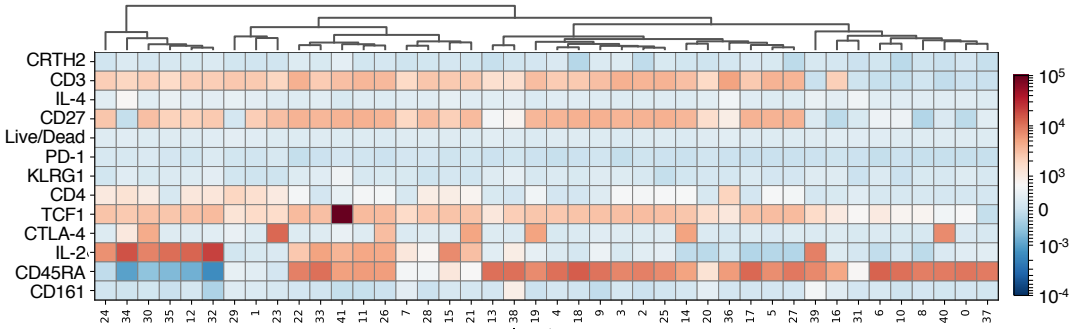

Figure 4.13 A matrix plot depicts the 42 clusters generated by Louvain clustering analysis.

In the matrix plot, each row corresponds to the mean fluorescence intensity for different markers and each column represents one cluster. Hierarchical clustering was performed to determine the relationships between clusters, shown as dendrogram above.

The 42 clusters were merged into ten clusters based on the MFI pattern and the relationships in hierarchical clustering (**Figure 4.14A**). Three mother clusters were further identified by their differential CD45RA expression, and thus could be assigned to “memory”, “intermediate”, and “immature” T cells (**Figure 4.14B & C**).

Both clusters 1 and 10 were assigned to memory T_H2 cells given its expression of CRTH2 and IL-4 and lack of expression of CD45RA (**Figure 4.14C & D**). Cluster 1 expressed CD27 and was identified as central memory T_H2 cells ($CD45RA^-CD27^+CRTH2^+IL\text{-}4^+$). In contrast, given its lack of expression of CD27, cluster 10 represents a subset of highly differentiated T_H2 cells ($CD45RA^-CD27^-CRTH2^+IL\text{-}4^+$; **Figure 4.14E**). With low-intermediate CD161 expression, cluster 10 resembled a previously reported proallergic T_H2 population, known as T_H2A (Wambre et al., 2017; Wambre et al., 2012). The proallergic T_H2 cells expressing intermediate-level TCF-1 and KLRG-1 as well as high-level IL-2 were also positive for exhaustion-associated surface markers CTLA-4 and PD-1. This specific T_H2 population (i.e. cluster 10) was denoted as T_H2A_{EX} henceforth.

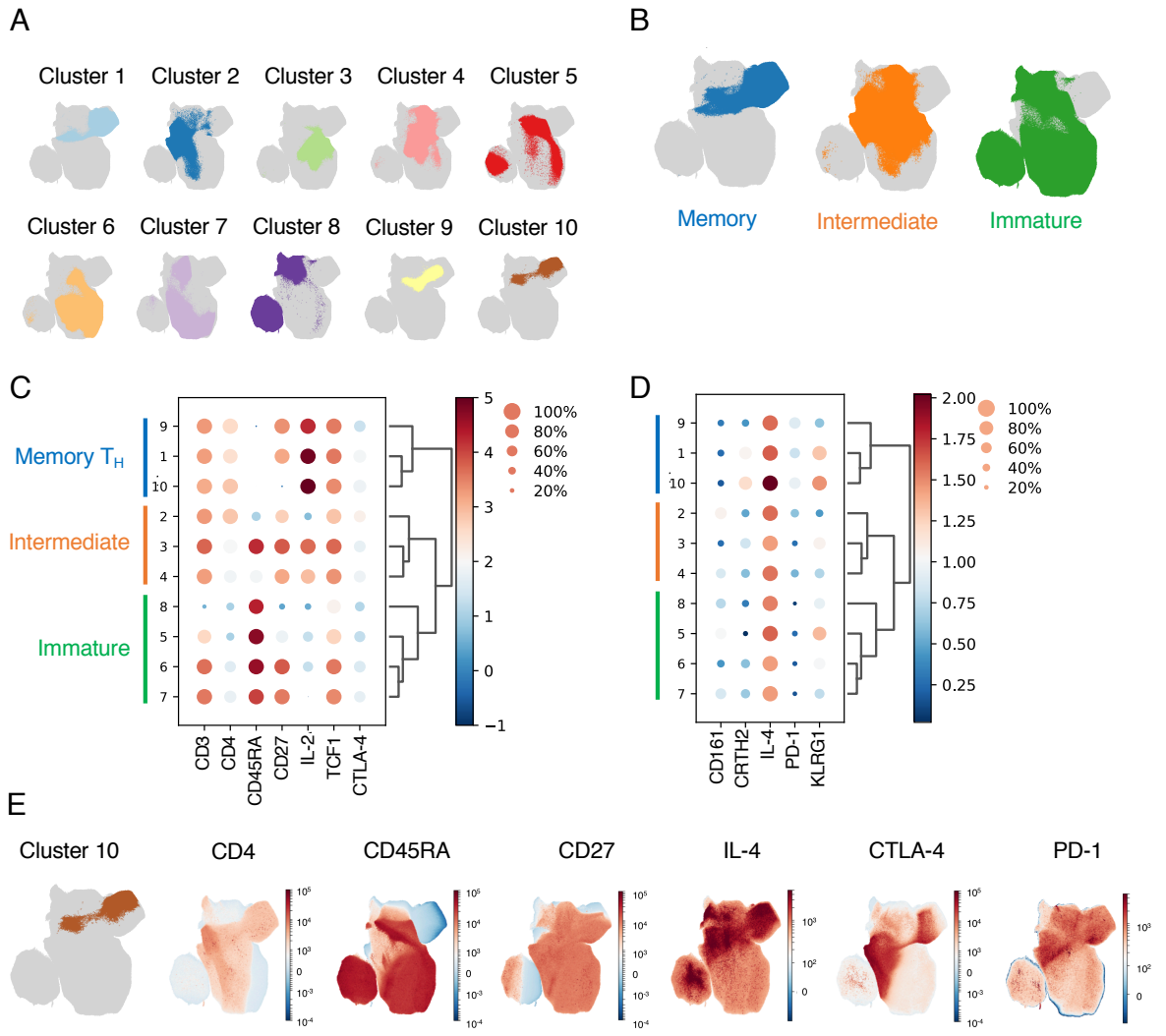

Figure 4.14 The clusters can be categorized into: "memory", "intermediate", and "immature" based on CD45RA expression.

(A) UMAP of ten lymphocyte clusters. (B) UMAP of three mother clusters: "memory", "intermediate", "immature." Dot plots depict the arcsinh-transformation values of MFI for higher-intensity markers in ten clusters (C) with cutoff at one and lower-intensity markers (D) with cutoff at 0.5. (E) UMAP plots of selected fluorescence markers: CD4, CD45RA, CD27, IL-4, CTLA-4, and PD-1, comparing to the UMAP of cluster 10 (left).

The frequency of T_H2A_{EX} cells among viable PBMCs decreased significantly six hours after the last top dose during up-dosing compared to baseline (T4 vs T0; $P \leq .05$; **Figure 4.15A**). Their frequency increased again in the following pollen season (T5), rendering it comparable to baseline levels and remained at this level towards the end of the follow-up (T9; **Figure 4.15B**). While the MFI of IL-4 and PD-1 inside T_H2A_{EX} cells remained relatively stable over the course of AIT, a decrease of the MFI of IL-2 was observed, in correspondence to an increase of CTLA-4 at T9 (**Figure 4.15C**).

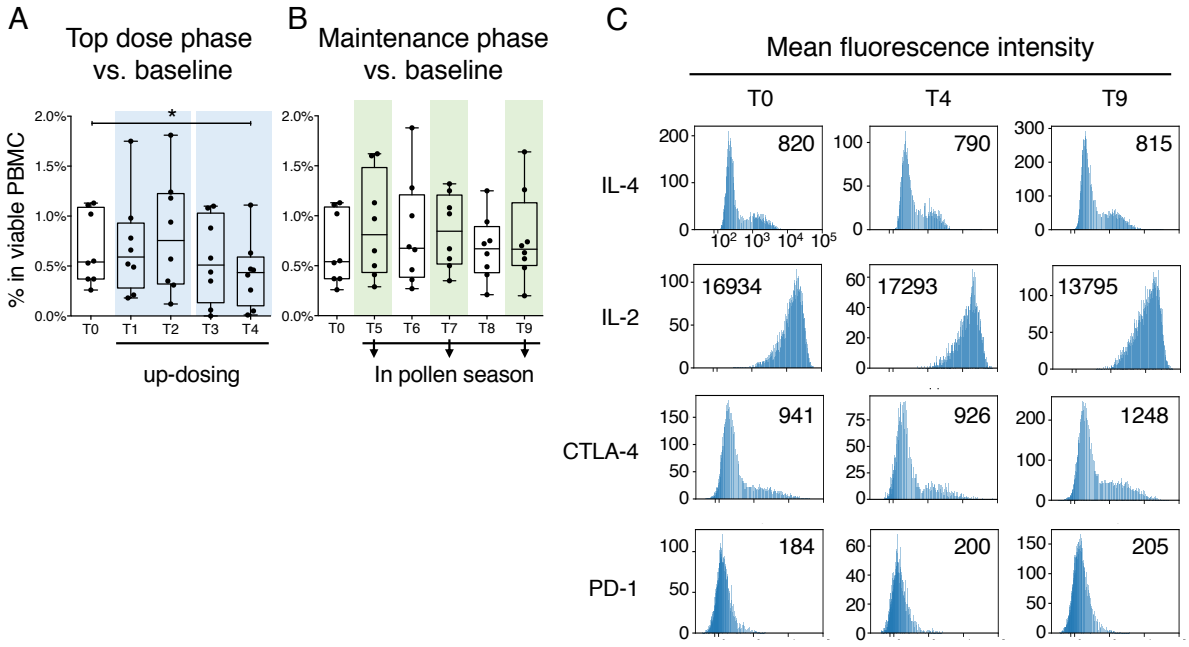

Figure 4.15 T_H2A_{EX} cells persisted throughout the course of AIT.

Box plots depict the dynamic change in frequency of T_H2A_{EX} cells throughout the course of AIT: baseline (T0), right before (T1) and 6h after the first (T2) and right before (T3) and 6h after the last pre-seasonal top dose injection (T4) in year one of AIT, in (T5) and out of grass pollen season (T6) year 1 during maintenance phase, in (T7) and out of season (T8) year 2, and in season year 3 (T9). (A) Top dose phase (T1–T4) versus baseline (T0). (B) Maintenance phase (T5–T9) versus baseline (T0). (**C**) Comparisons of MFI of IL-4, IL-2, CTLA-4, and PD-1 inside T_H2A_{EX} cells at time points: T0, T4, and T9. The numbers within representative histograms denote MFI values. Statistically significant differences are depicted as: $*P \leq .05$

There were two other T helper clusters ($CD3^+CD4^+$), clusters 2 and 9, one non-T cell cluster ($CD3^-$), cluster 8, while the remaining clusters, clusters 3–7, were most likely $CD8^+$ T cells ($CD3^+CD4^-$; **Figure 4.14C**). Cluster 2 and cluster 9 expressed intermediate levels of IL-4 but did not express CRTH2. These two clusters were by definition central memory T cells ($CD45RA^-CD27^+$) but cluster 2 expressed higher-level CTLA-4 and CD161 and low-level IL-2. Similar to cluster 10, cluster 1 and cluster 9 also decreased in frequency during up-dosing, while cluster 2 increased in frequency (**Figure 4.16A–C, & J**).

Overall, while T_H2A_{EX} cells decreased during up-dosing, it stably maintained its exhausted phenotype and persisted long-term during AIT.

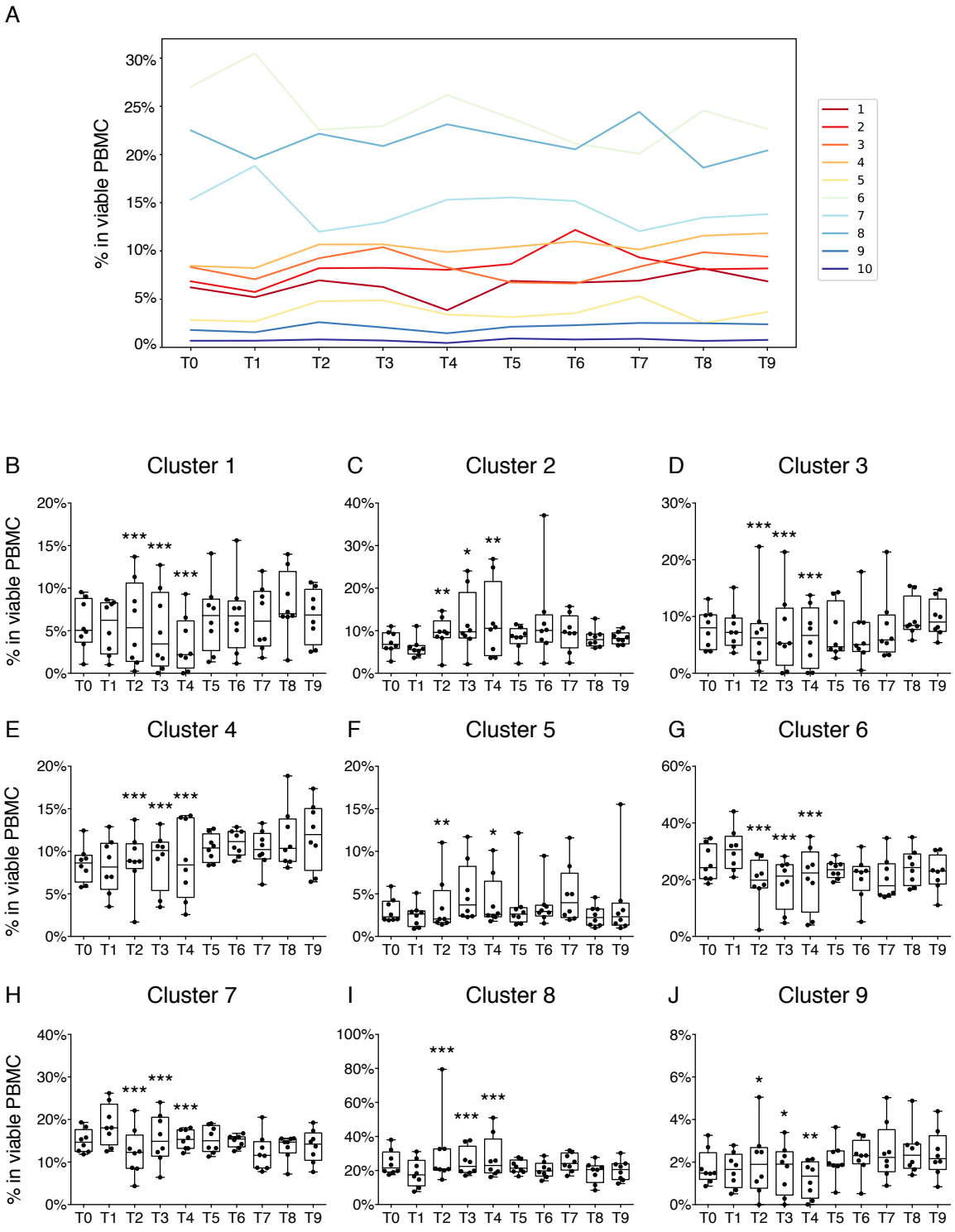

Figure 4.16 The dynamic change in frequencies of different clusters throughout the course of AIT.

(A) A line plot depicts the dynamic change of ten clusters. (B–J) Box plots illustrate the percentage of clusters 1–9 among live PBMCs at different time points: baseline (T0), right before (T1) and 6h after the first (T2) and right before (T3) and 6h after the last pre-seasonal top dose injection (T4) in year one of AIT, in (T5) and out of grass pollen season (T6) year 1 during maintenance phase, in (T7) and out of season (T8) year 2, and in season year 3 (T9). Symbols represent individuals (n = 8). Comparison to the baseline by differential abundance tests using the Dirichlet Regression model. *$P \leq .05$; **$P \leq .01$; ***$P \leq .001$.

4.3.2 Time-course analysis of the IL-2 and TCF-1 expression on circulating T_H2 cells during AIT

Furthermore, the expression of IL-2 and TCF-1 in CTLA-4$^+$ and PD-1$^+$ memory T_H2 cells was determined using flow cytometry in order to assess their survival and self-renewal potential over time. The expression of IL-2 and TCF-1 in PD-1$^+$ and CTLA-4$^+$ memory T_H2 cells was compared to other T cell subsets (**Figure 4.17**).

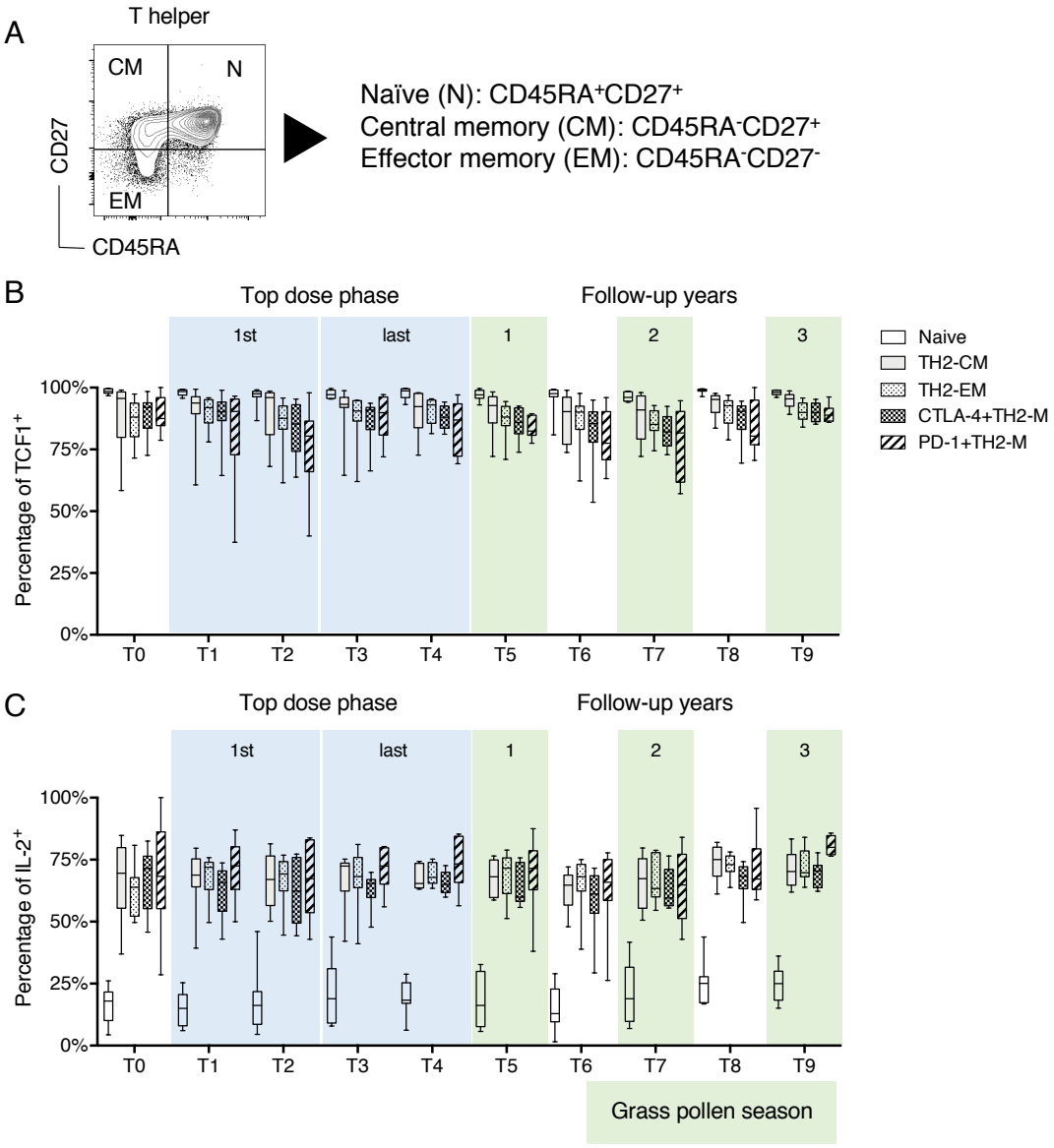

Figure 4.17 PD-1$^+$ and CTLA-4$^+$ memory T_H2 cells were in the late maturation stages.

(A) Differentiation status based on expression of CD45RA and CD27. A representative flow cytometry plot shows naïve (N), central memory (CM) and effector memory (EM) T cell subsets and their expression of CD45RA and CD27. Comparisons of expression of TCF-1 (B) and IL-2 (C) in different T cell subsets at T0–T9 during AIT: baseline (T0), right before (T1) and 6h after the first (T2) and right before (T3) and 6h after the last pre-seasonal top dose injection (T4) in year one of AIT, in (T5) and out of grass pollen season (T6) year 1 during maintenance phase, in (T7) and out of season (T8) year 2, and in season year 3 (T9). **P* ≤ .05; ***P* ≤ .01; ****P* ≤ .001 by Mann-Whitney *U* test.

The expression was significantly lower than that on naive T cells (N, $CD3^+CD4^+CD45RA^+$) and central memory T_H2 cells (T_H2-CM, $CD3^+CD4^+CD45RA^-CD27^+IL\text{-}4^+$), yet comparable to effector memory T_H2 subset (T_H2-EM, $CD3^+CD4^+CD45RA^-CD27^-IL\text{-}4^+$) (**Figure 4.17B**). On the other hand, PD-1^+ and CTLA-4^+ memory T_H2 cells retained their IL-2 producing capacity despite lower TCF-1 expression (**Figure 4.17C**).

By contrast, both TCF-1 and IL-2 expression were significantly lower in the non-T_H2 ($IL\text{-}4^-$) effector memory subset. Taking T9 for example, the average percentage of TCF-1^+ cells were >95% in naïve and T_H2-CM cells, approximately 90% in T_H2-EM, PD-1^+ T_H2-M and CTLA-4^+T_H2-M cells, and barely 75% in non-T_H2-EM cells (**Figure 4.18A & C**). The average percentage of IL-2^+ cells were roughly 70–80% in T_H2-CM, T_H2-EM, CTLA-4^+T_H2-M, and PD-1^+T_H2-M cells, while <50% in non-T_H2-EM cells (**Figure 4.18B & C**).

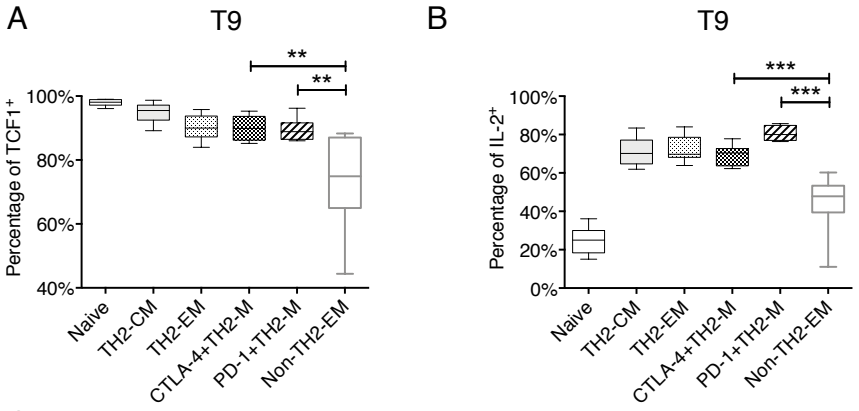

C

	TCF-1^+ (%)	IL-2^+ (%)
N	98.0% ± 0.4%	24.7% ± 2.3%
T_H2-CM	95.0% ± 1.0%	71.5% ± 2.5%
T_H2-EM	90.1% ± 1.3%	72.2% ± 2.2%
CTLA-4^+T_H2-M	90.1% ± 1.2%	69.1% ± 1.8%
PD-1^+T_H2-M	89.5% ± 1.2%	80.7% ± 1.3%
non-T_H2-EM	73.8% ± 4.9%	44.6% ± 4.7%

Figure 4.18 PD-1^+ and CTLA-4^+ memory T_H2 cells retained their IL-2 producing capacity despite lower TCF-1 expression.

Comparisons of expression of TCF-1 (A) and IL-2 (B) in different T cell subsets at T9 (follow-up year 3 in pollen season). (C) Average percentage of TCF-1^+ and IL-2^+ cells in different T cell subsets (means ± SEM).

Taken together, the expression of CTLA-4 and PD-1 on T_H2 cells did not increase significantly during the treatment course of AIT. While the TCF-1 expression declined slightly as T_H2 cells matured, it remained comparatively high, contrasting sharply with the levels of TCF-1 expression in non-T_H2 cells. In general, T_H2 cells retained IL-2 expression irrespective of differentiation state, the levels of which were all higher than non-T_H2 cells.

4.3.3 Time-course analysis of CTLA-4 and PD-1 expression on circulating T_H17 cells during AIT

The frequency of T_H17 cells increased gradually during up-dosing phase and remained significantly higher by the end of the follow-up compared to that at pre-seasonal baseline (T9 vs. T0: 0.9%±0.13% vs. 0.5%±0.06%; $P \leq .05$; **Figure 4.19**).

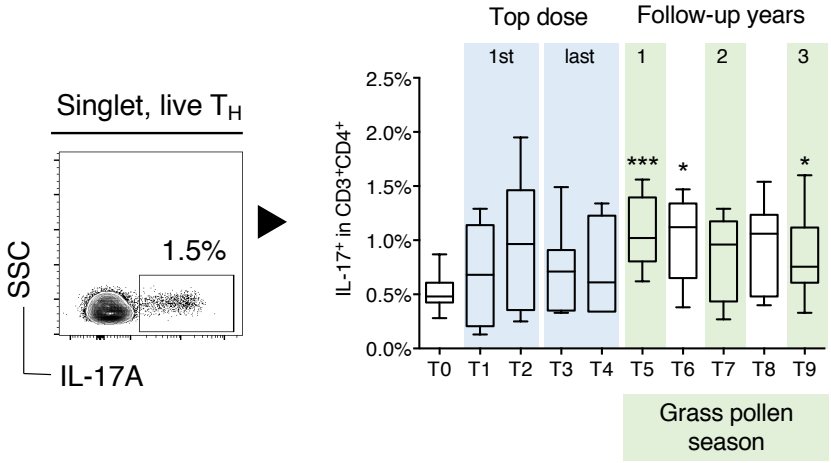

Figure 4.19 Increased frequency of T_H17 in AR patients receiving AIT.

Flow cytometric analysis on the frequency of T_H17 cells. A representative FACS plot shows the gate identifying IL-17A$^+$ cells among live T helper cells. Blue areas indicate top dosing phase of AIT, and green areas indicate grass pollen seasons during follow-up. Study design scheme: baseline (T0), right before (T1) and 6h after the first (T2) and right before (T3) and 6h after the last pre-seasonal top dose injection (T4) in year one of AIT, in (T5) and out of grass pollen season (T6) year 1 during maintenance phase, in (T7) and out of season (T8) year 2, and in season year 3 (T9). Comparisons were performed using unpaired Mann-Whitney test. Statistically significant differences are depicted as *$P \leq .05$.

The expression of CTLA-4 and PD-1 on T_H17 cells (CD3$^+$CD4$^+$IL-17$^+$) at later time points was compared with the expression at the pre-seasonal baseline. CTLA-4 expression was significantly higher at the end of the follow-up (T9 vs. T0: 50.7%±3.2% vs. 37.8%±4.0%; $P \leq .05$; **Figure 4.20A**). In contrast, PD-1 expression on T_H17 cells did not change significantly throughout the course of AIT as opposed to baseline (**Figure 4.20B**).

Next, the expression of IL-2 and TCF-1 in CTLA-4$^+$ and PD-1$^+$ T_H17 cells was analyzed. IL-2 expression was significantly lower in CTLA-4$^+T_H17$ cells at the end of the follow-up (T9 vs. T0: 33.8%±1.7% vs. 43.4%±3.4%; $P \leq .05$; **Figure 4.20C**) and in PD-1$^+T_H17$ out of pollen seasons (T6 and T8) during maintenance phase (T6 vs. T0:

27.3%±3.4% vs. 45.6%±5.3%; $P \leq .05$; T8 vs. T0: 29.2%±4.3% vs. 45.6%±5.3%; $P \leq .05$; **Figure 4.20D**). No significant change of TCF-1 expression in either CTLA-4$^+$ or PD-1$^+$$T_H$17 cells was detected before and after AIT (**Figure 4.20E & F**).

Overall, while the expression of CTLA-4 on T_H17 cells was significantly higher by the end of the follow-up (T9), its IL-2 expression was meanwhile significantly lower compared to that at baseline. In contrast, the expression of PD-1 on T_H17 cells did not change significantly during the course of AIT, but the IL-2 expression in PD-1$^+$$T_H$17 cells was significantly lower outside pollen season during maintenance phase (T6 and T8).

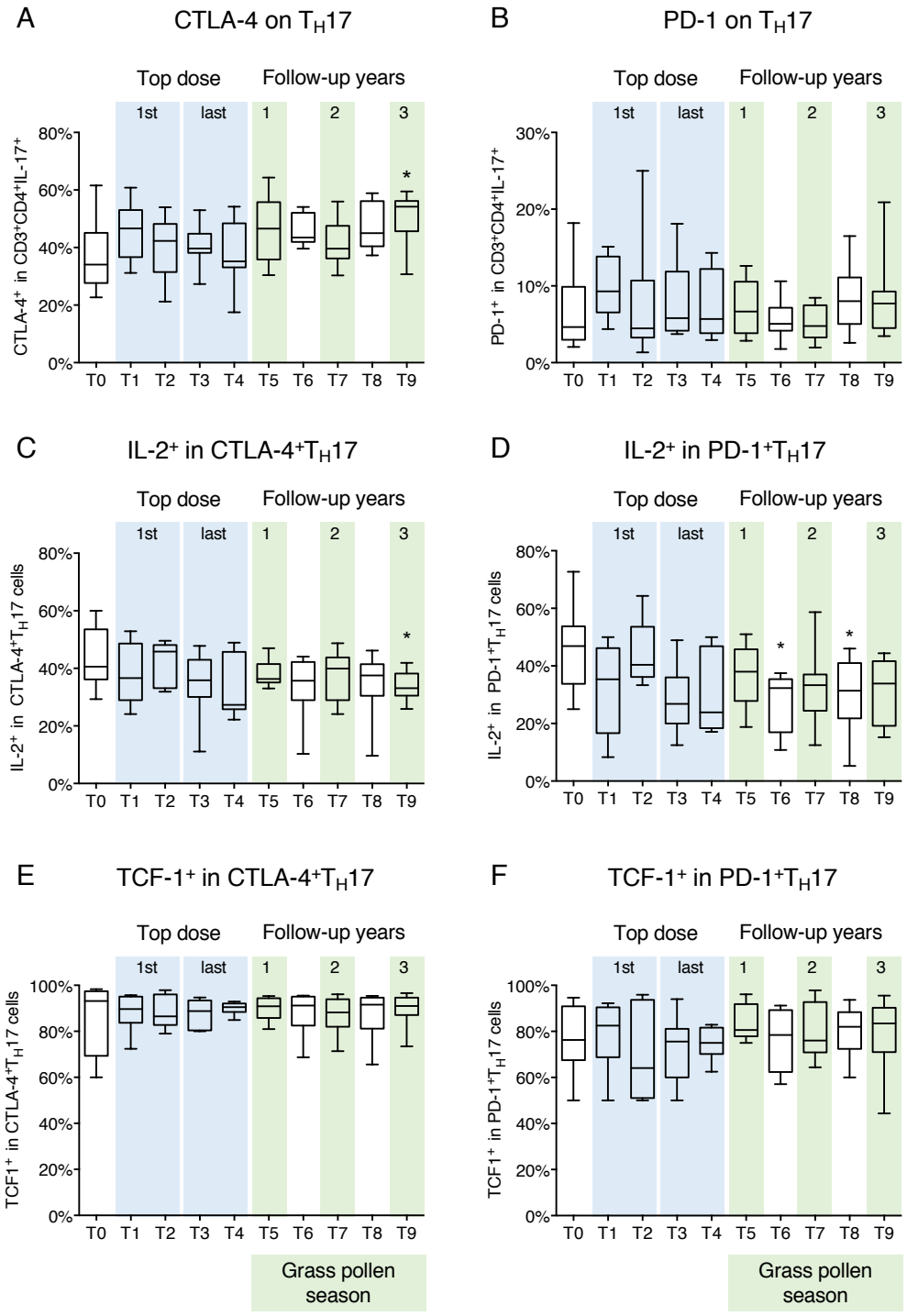

Figure 4.20 Dynamic change of phenotypes of T_H17 in AR patients receiving AIT.

Expression of CTLA-4 (A) and PD-1 (B) on T_H17 cells throughout the course of AIT. IL-2 expression in CTLA-4$^+$$T_H17$ (C) and PD-1$^+$$T_H17$ (D). TCF-1 expression in CTLA-4$^+$$T_H17$ (E) and PD-1$^+$$T_H17$ (F). Blue areas indicate top dosing phase of AIT, and green areas indicate grass pollen seasons during follow-up. Study design scheme: baseline (T0), right before (T1) and 6h after the first (T2) and right before (T3) and 6h after the last pre-seasonal top dose injection (T4) in year one of AIT, in (T5) and out of grass pollen season (T6) year 1 during maintenance phase, in (T7) and out of season (T8) year 2, and in season year 3 (T9). *$P \leq .05$ by Mann-Whitney *U* test.

4.4 *In vitro* PD-1 blockade to rescue exhausted T cells

In order to test whether exhausted T_H2 cells can be reinvigorated, a clinically available anti-PD-1 blocking antibody Nivolumab was applied to the cultured PBMCs and intracellular IL-2 expression was used as readout. PBMCs were obtained from AIT-treated patients with grass pollen allergy at different time points during AIT as described earlier. The PBMCs were stimulated for 24 hours with immobilized anti-CD3 and soluble anti-CD28 Abs in the presence of Nivolumab or mock IgG and analyzed by flow cytometry (**Figure 4.21**). A tendency towards lower-level production of IL-2 in PD-1^+ T helper cells was observed at later time points compared to the pre-seasonal baseline (**Figure 4.21A**). Moreover, although a higher number of PD-1^+ T helper cells produced IL-2 in the presence of Nivolumab compared to mock IgG, the differences were not statistically significant throughout the course of AIT. Similarly, Nivolumab did not potentiate IL-2 production in PD-1^+ T_H2 cells throughout the course of AIT (**Figure 4.21B**).

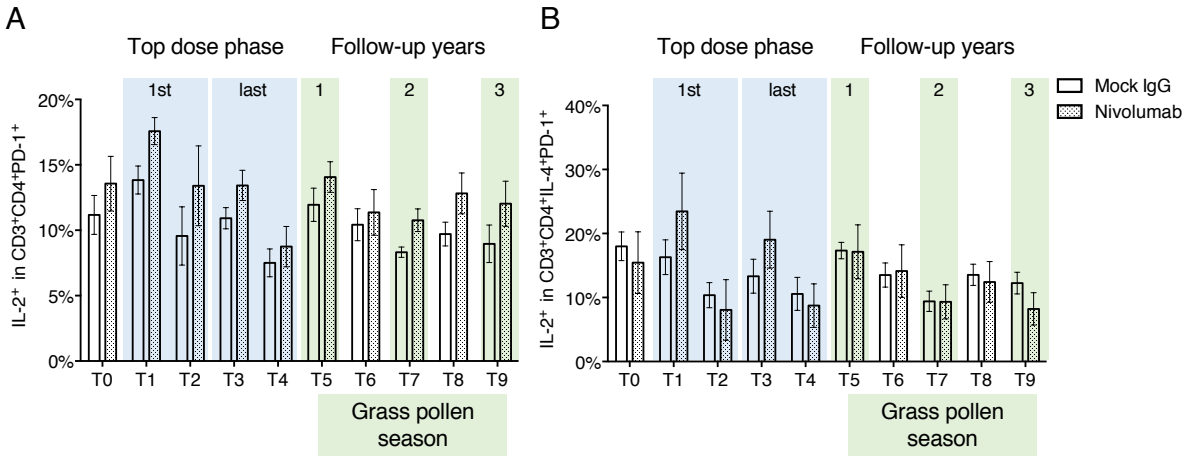

Figure 4.21 Nivolumab failed to potentiate IL-2 production in PD-1^+T_H2 cells.

PBMCs from AIT-treated patients with grass pollen allergy were cultured for 24 h with plate-bound anti-CD3 and soluble anti-CD28 Abs in the presence of Nivolumab (*shaded*) or mock IgG (*unfilled*). (A) IL-2 expression in PD-1^+CD4^+ T cells. (B) IL-2 expression in PD-1^+T_H2 cells. Study design scheme: baseline (T0), right before (T1) and 6h after the first (T2) and right before (T3) and 6h after the last pre-seasonal top dose injection (T4) in year one of AIT, in (T5) and out of grass pollen season (T6) year 1 during maintenance phase, in (T7) and out of season (T8) year 2, and in season year 3 (T9). Data are from 8 donors for each time point. Graphs show means ± SEM.

5 Discussion

5.1 Recurrent allergen exposure drives an exhausted phenotype of T_H2 cells, but AIT does not reinforce exhaustion.

In the present study, a mouse model of allergic airway inflammation and OVA-specific immunotherapy was implemented to test the development of T cell exhaustion of T_H2 cells during AIT. While a myriad of AIT regimens have been reported in different mouse models, subcutaneous immunotherapy with entire OVA, but not immunodominant OVA peptide, was shown effective regardless of the dose used (Aguilar-Pimentel et al., 2017; Fox, Torrero, Evans, & Mitre, 2015; Janssen, van Oosterhout, Nijkamp, van Eden, & Wauben, 2000; Vissers et al., 2004). The effectiveness of AIT in different experimental animal studies was reported using outcomes associated with improved allergic inflammation. This study showed alleviation of intrapulmonary eosinophilia, increase of serum IgG1, and reduction of IL-4 and IL-5, in line with earlier reports (Aguilar-Pimentel et al., 2017; Fox et al., 2015; Janssen et al., 2000; Vissers et al., 2004). In addition, microarray analysis of the murine lung homogenates also provided molecular evidence of alleviated allergic inflammation after AIT. On the other hand, a significant reduction of OVA-specific IgE and an increase of IL-10 after AIT were not observed here. In fact, these two outcomes were not constantly shown in previously published studies (Aguilar-Pimentel et al., 2017; Fox et al., 2015; Janssen et al., 2000; Vissers et al., 2004). Notably, the animals in this study were challenged with OVA aerosols more frequently compared to other mouse models of AIT. This not only recapitulates the recurrent allergen exposure during pollen flight but is also crucial for the development of T cell exhaustion by means of chronic TCR stimulation.

In this mouse study, the expression of the exhaustion-associated surface molecules PD-1 and CTLA-4 was enhanced on T_H2 cells from AAI mice, implying that the exhausted phenotype of T_H2 cells was associated with allergen exposure. In comparison, the expression of PD-1 and CTLA-4 on T_H2 cells from AR patients exhibited a different pattern. While upregulation of PD-1 on T_H2 cells occurred perennially, CTLA-4 was only upregulated during pollen flight. The persistent upregulation of PD-1 is a hallmark of T cell exhaustion and associated with epigenetic imprinting (Alfei & Zehn, 2017; Bally, Austin, & Boss, 2016; Sen et al., 2016). However,

the features of T cell exhaustion have largely been derived from chronic murine LCMV infection or human HIV infection, in which type I interferon could modulate the effects of chronic TCR stimulation (Crawford et al., 2014; Day et al., 2006; Dong et al., 2019; Han, Asoyan, Rabenstein, Nakano, & Obst, 2010; van der Werf, Redpath, Azuma, Yagita, & Taylor, 2013). In a transgenic TCR mouse system in which antigen presentation was controlled inducibly without concurrent infection, PD-1 upregulation on $CD4^+$ T cells was only observed under very high antigen loads, but not under other conditions that induce exhaustion, suggesting against an essential role of PD-1 in enforcing T cell exhaustion (Han et al., 2010). In fact, in contrast to the role of PD-1 in exhaustion, some studies show that PD-1 engagement could enhance T_H2 response and even exacerbate allergic airway inflammation (Akbari et al., 2010; McAlees et al., 2015; Oflazoglu et al., 2004). As reported earlier, PD-1 ligation augmented GATA-3 expression and IL-4 production in murine T cells, while PD-1 deficiency resulted in lower serum levels of IL-4 and IL-13 (McAlees et al., 2015). The administration of PD-L2-Fc was associated with increased serum IgE levels and BAL cell infiltrations in asthmatic mice, whereas greater airway hyperreactivity and inflammation was observed in sensitized PD-L2-KO compared with sensitized wild-type mice (Akbari et al., 2010; Oflazoglu et al., 2004). In contrast to PD-1, CTLA-4 expression on T_H2 cells from AR patients was not sustained but seasonal, indicating a more dynamic regulation of its expression, most probably depending on its reactivity to allergens. Indeed, this result reflects the differences that CTLA-4 functions primarily in the T cell activation phase, whereas PD-1 acts mostly during the effector phase (Fife & Bluestone, 2008; Sugiura et al., 2019). Furthermore, the rapid internalization and recycling of CTLA-4 also contrasts sharply with PD-1 (Khailaie et al., 2018). Altogether, in AAI mice and allergic individuals, upregulation of both markers on T_H2 cells is not synonymous with development of functional deficits. In fact, it has been shown that while exhausted $CD4^+$ T cells lost certain effector functions, they were not functionally inert but could undergo functional adaption such as IL-10 or IL-21 production without skewing to any T helper lineage (Crawford et al., 2014; Fahey et al., 2011; Han et al., 2010; Karmaus et al., 2019; B. Shin et al., 2018).

Again, the expression of PD-1 and CTLA-4 was significantly reduced in AAI+AIT mice. In AR+AIT patients no significant reduction was observed, while in AA+AIT patients only CTLA-4 expression decreased significantly during the pollen flight. These results

show that AIT treatment did not reinforce the exhausted phenotype of T_H2 cells. It is likely that AIT counteracts such upregulation on T_H2 cells. Alternatively, this could reflect a reduced responsiveness of T_H2 cells to the inciting allergens after AIT, as the term 'hypo-sensitization' conveys. Indeed, immunizations with antigens have been shown to reduce the clonal diversity and the average TCR affinity of the responding T cell repertoire (Corse, Gottschalk, & Allison, 2011). Specifically, while highest-affinity T cell clones were lost due to overstimulation, clones with low-affinity TCR that failed to reach the affinity threshold would also be eliminated during an immune response (Amrani et al., 2000; Malherbe, Hausl, Teyton, & McHeyzer-Williams, 2004). In other words, the pool of responding T_H2 cells contracted after AIT, which in turn resulted in lower frequency of PD-1- and CTLA-4-expressing T_H2 cells.

Enhanced expression of CTLA-4 and PD-1 on circulating T_H2 cells was even more profound in AA patients as opposed to AR patients in pollen season, suggesting that, apart from allergen exposure, concurrent asthma could promote the exhausted phenotype as well. Indeed, previous studies reported that PD-1 expression was significantly higher in AA patients compared to healthy controls, whereas there was no consistent correlation with serum levels of IgE or disease severity (Bratke et al., 2017; Mosayebian et al., 2018). Association between CTLA-4 polymorphisms and serum IgE levels, asthma, and lower pulmonary function has also been reported (Munthe-Kaas et al., 2004). In addition, T_H2 cells from AA patients expressed a significantly higher level of TIM-3 outside pollen season compared to controls, while a tendency towards higher TIM-3 expression during pollen flight was observed. Interestingly, unlike CTLA-4 and PD-1, TIM-3 actually strengthens TCR signaling and speculatively helps to drive T cell exhaustion by extending the effector phase of T cell activation, but the exact mechanisms remain unclear (Ferris, Lu, & Kane, 2014). Although upregulation of TIM-3 on T cells has been reported in asthmatic mice and AA patients, its expression was reportedly associated with a T_H1/T_H2 imbalance but not with exhaustion in the context of allergy (Kearley, McMillan, & Lloyd, 2007; Mosayebian et al., 2018; Tang, Wang, An, & Wang, 2015).

In the context of T cell exhaustion, GSEA of the microarray data revealed that genes associated with exhausted $CD8^+$ T cells were enriched in AAI mouse lungs, suggesting that these cells expressed a terminally differentiated signature (B. Shin et al., 2018).

However, the molecular signature of CD4 exhaustion was not as well-characterized as CD8 exhaustion (Crawford et al., 2014). Despite this attempt to probe the microarray data using the curated list of DEG between exhausted and memory $CD4^+$ T cells, there was no compelling evidence of T cell exhaustion at the transcriptional level. While AAI mouse lung cells expressed more *Ctla4* and *Pdcd1*, the cells also upregulated several co-stimulatory molecule genes, suggesting active TCR engagement and associated biological process. On the other hand, AAI+AIT mouse lung cells upregulated *Pilra*, *Hif1a*, and *Cd244*. Paired Ig-like type-2 receptor α inhibitory receptor (encoded by *Pilra*) could dampen the inflammatory response upon engagement (Sun et al., 2014). Hypoxia-inducible factors-1α (encoded by *Hif1a*) is not merely a negative regulator of T cell response, but it also regulates the balance between Treg and T_H17 cells under the condition of low oxygen tension or in the presence of IL-6 (McNamee, Korns Johnson, Homann, & Clambey, 2013). CD244 expression is associated with $CD8^+$ T cell exhaustion, whereas its role in $CD4^+$ T cell exhaustion was not clear (Agresta, Hoebe, & Janssen, 2018). Taken together, although the expression of CTLA-4 and PD-1 was amplified at the transcriptional level in the lungs of AAI mice and GSEA provided ancillary evidence for T cell exhaustion, the bulk microarray analysis of the mixed cell types in the mouse lungs limits the possibility to delve into expression of exhaustion-associated genes specifically in T_H2 cells. Whether T_H2 cells express the exhaustion-associated genes remains to be addressed.

In the unbiased cluster analysis, T_H2A_{EX} cells (i.e. cluster 10) decreased markedly during up-dosing, but were not eliminated by AIT, suggesting that the effect of AIT was probably different between the initial and the late stage of therapy, and that these exhausted T_H2 cells could persist long-term in AIT-treated patients. Specifically, T_H2A_{EX} cells fell into the mature “memory T cell” group and had an effector memory T cell (T_{EM}) phenotype. Previous studies show that T_{EM} cells recirculate between blood and non-lymphoid tissues, such as lung and skin (Islam & Luster, 2012; Masopust, Vezys, Marzo, & Lefrançois, 2001). Therefore, it is likely that the redistribution of these highly differentiated T_H2 cells contributes to their long-term persistence in AIT-treated patients. By contrast, reduced frequency of peripheral T_H2 cells after AIT was reported by several studies (Ihara et al., 2018; Wambre et al., 2017; Wambre et al., 2012). However, as exemplified in this mouse study, AIT significantly reduced the frequency

of intrapulmonary but not circulating T_H2 cells, implying that AIT affects local and systemic T_H2 cells differentially. In fact, fate tracing revealed that T_H2 cells expanded transiently after AIT and persisted in the lungs until subsequent allergen challenge (Mackenzie et al., 2014). This study implicates that AIT had a greater impact on intrapulmonary T_H2 cells, and that AIT did not necessarily drive T_H2 cells to exhaustion over time due to chronic antigen exposure but conditioned them for deletion upon secondary exposure. Future studies are warranted to address mechanisms that can accelerate this process and thereby contribute to shorten treatment duration of AIT, while maintaining long-term treatment efficacy.

T_H2A_{EX} cells also expressed higher levels of KLRG1, a marker associated with late-differentiated effector cells. However, their TCF-1 expression was not significantly reduced as observed in terminally differentiated T cells (Kahan & Zajac, 2019; Paley et al., 2012). Since TCF-1 is associated with self-renewal potential, its expression may partly account for their long-term persistence in AIT-treated patients. Notably, TCF-1 expression in $CD4^+$ T cells was not only associated with the progenitor potential, but also with the fate decisions (Gattinoni, Klebanoff, & Restifo, 2012). For instance, T follicular helper cells express a high level of TCF-1 and sustain greater plasticity, while TCF-1 and β-catenin can jointly promote GATA-3 expression and inhibit IFN-γ expression (Lüthje et al., 2012; B. Shin et al., 2018; Yu et al., 2009). Hence, T_H2 cells appear to have higher stemness by default, rendering them also more resistant to apoptosis.

In addition, T_H2A_{EX} cells, despite expressing both PD-1 and CTLA-4, retained their IL-2 producing capacity throughout the AIT treatment course. However, there appeared to be a reciprocal decrease of IL-2 as CTLA-4 increased in these cells in the third follow-up year. This might be associated with seasonal variations of CTLA-4 upregulation or is suggestive of exhaustion-associated attenuation of IL-2 production late in the course of AIT. The latter speculation implies that T_H2A_{EX} cells might eventually decrease if the maintenance phase of AIT extends further, and that longer duration of AIT treatment might be beneficial. However, the compliance of patients might reduce further in that case. On the other hand, as T_H2A_{EX} cells have been shown to decrease significantly during up-dosing, extension of top dosing phase might help further suppress this T_H2 population early on.

Finally, in an attempt to see whether blockade of PD-1 signaling would enhance the functionality of PD-1$^+$ T_H2 cells, PBMCs collected from AIT-treated patient cohort were stimulated in the presence of Nivolumab compared to mock IgG. However, these data showed that PD-1 blockade could not, or only partially, augment IL-2 production of PD-1$^+$ T_H2 cells, implying that additional inhibitory pathways might be involved in suppressing IL-2 production. In fact, PD-1 expression has been shown to impact T cell functions differentially, as very low levels of expression could already inhibit T cell proliferation and IL-2 production (Wei et al., 2013). While *in vitro* studies demonstrated that interfering with PD-1 signaling could improve cytokine production and cell expansion, it does not exclude that PD-1 blockade selectively stimulated T cells with lower levels of PD-1 expression rather than restored functions to fully exhausted T cells with higher levels of PD-1 expression (Day et al., 2006; Filippis et al., 2017; Kamada et al., 2019; Rosskopf et al., 2018; C. Wang et al., 2014). In other words, PD-1 blockade was effective for a fraction of PD-1$^+$ T_H2 cells that remain functional, whereas overall the beneficial effects were not evident. On the other hand, it has been shown that IL-2 is extremely localized to the immediate environment of cells *in vivo* and acts primarily in a paracrine manner (Long & Adler, 2006; Oyler-Yaniv et al., 2017). Therefore, a low-amplitude increase in IL-2 expression by PD-1 blockade might suffice biologically. Another possible explanation is the suppressive effect of co-existing PD-1$^+$ Tregs. Although the frequency of PD-1$^+$ Tregs could not be discerned in this experiment, their presence might blunt the stimulatory effect of PD-1 blockade on PD-1$^+$ T_H2 cells. Studies show that PD-1 blockade could boost the immunosuppression capacity of PD-1$^+$ Tregs (Kamada et al., 2019; Kumagai et al., 2020). Therefore, the balance between PD-1$^+$ Tregs and PD-1$^+$ T_H2 cells could also affect the overall efficacy of PD-1 blockade. Alternatively, it is likely that PD-1$^+$ T_H2 cells were not terminally exhausted but simply underwent functional adaptation, thus with normal or near-normal IL-2 production capacity and resistance to PD-1 blockade. A proof-of-concept experiment might be performed in the future by administration of anti-PD-1 antibody to the experimental asthmatic mice during immunotherapy to see whether PD-1 blockade would reverse the effect of AIT on T_H2 cells.

5.2 The dynamic change and the development of exhausted phenotypes of T_H17 cells and other T cell subsets

In addition to T_H2 cells, the frequency of T_H17 cells also increased in the lungs of AAI mice, alongside the pulmonary neutrophilia. These findings suggest that the mouse model herein is not only a model of T_H2-dominant eosinophilic asthma, but also one of T_H17-associated neutrophilic asthma. AIT significantly reduced secretion of IL-17A and infiltration of neutrophils into the BALF and the frequency of intrapulmonary T_H17 cells. In fact, extensive evidence demonstrates that IL-17A could induce type-2 immune response and render it more pathological due to neutrophil recruitment and ensuing tissue damage (Kinyanjui, Shan, Nakada, Qureshi, & Fixman, 2013; Kudo et al., 2012; Nakajima et al., 2014; Sutherland et al., 2014; Wakashin et al., 2008). Type-2 cytokines in turn attenuated excessive IL-17A production and the accompanying neutrophilia (Chen et al., 2012; Newcomb et al., 2009; Sutherland et al., 2014). The reverse, however, is also true, as a recent report elaborated that IL-17A suppressed established type-2 immune responses, specifically in the lungs, indicating that both timing and specific tissue are key factors in deciding whether IL-17A is protective (Ajendra et al., 2020). Given that, the increased frequency of T_H17 cells in allergic patients after AIT, as observed in this study and reported in an earlier publication, may plausibly help keep type-2 immunity in check (Zissler et al., 2018). Together, these observations reflect an intricate negative feedback loop between IL-17 and type-2 cytokines, which might be dysregulated in pathological conditions such as allergic asthma.

Furthermore, this mouse study also showed that the expression of CTLA-4 and PD-1 was upregulated on T_H17 cells in the lungs of AAI mice, similar to their T_H2 counterparts. However, it is not clear whether these results can be translated into the exhaustion of T_H17 cells, as there were few studies reporting the expression of either marker on T_H17 cells in different conditions. As reported previously, reduced CTLA-4 expression on T_H17 cells contributed to ongoing inflammation in sarcoidosis, and exhibited a better virus control in HIV infection, indicating a negatively regulatory role of CTLA-4 in T_H17 responses (Broos et al., 2015; Saxena et al., 2018). On the other hand, the suppressive effect of PD-1 on T_H17 cells was described by reports in which PD-1 deficiency resulted in severe experimental autoimmune diseases due to aberrant T_H17 responses (Rui, Honjo, & Chikuma, 2013; Yang et al., 2016). Conversely, PD-1

deficiency reduced inflammation in a murine model of biliary obstruction via attenuation of T_H17 responses (Licata et al., 2013). In patients with pulmonary fibrosis, a higher number of PD-1^+ T_H17 cells were detected compared with healthy controls, while these cells were not functionally deficient but promoted the disease (Celada et al., 2018). In a mouse study of chronic inflammatory conditions, a subset of T_H17 cells transdifferentiated into T_H1-like cells, which expressed lower levels of TCF-1 and their transcriptomes shared considerable similarity with that of the terminally exhausted $CD8^+$ T cells (Karmaus et al., 2019). However, whether the T_H1-like T_H17 cells and the T_H17 cells expressing PD-1 and CTLA-4 in this mouse study are related or not remains to be addressed in future studies.

In comparison to the murine T_H17 cells, the expression of CTLA-4 on T_H17 cells from the AIT-treated patients displayed a tendency towards increase and was indeed significantly higher by the end of the follow-up, while the expression of PD-1 remained stable and comparable to the baseline. In contrast, the IL-2 production capacity of CTLA-4^+ T_H17 cells exhibited a declining tendency over time and was significantly lower towards the end, so was that of PD-1^+ T_H17 cells. However, the relationship between IL-2 and T_H17 cells is complex. While IL-2-STAT5 signaling inhibits T_H17 generation, IL-2 can promote the expansion of differentiated T_H17 cells (Amadi-Obi et al., 2007; Laurence et al., 2007). Hence, the lower IL-2 expression on CTLA-4^+ and PD-1^+ T_H17 cells may restrict their expansion. However, unlike the T_H1-like T_H17 cells mentioned earlier, CTLA-4^+ and PD-1^+ T_H17 cells expressed comparatively high levels of TCF-1 throughout the course of AIT, thus arguing against their state of exhaustion despite the phenotype. Based on the present study, whether they become functionally exhausted during maintenance phase of AIT remains inconclusive. Future studies are certainly warranted to clarify this, considering their intricate relationship with type-2 immunity described earlier.

Despite the increased frequency of T_H17 cells and the elevated levels of IL-6, the frequency of Tregs was not reduced consequently but instead increased significantly in the lungs of AAI mice. The frequency of intrapulmonary Tregs remained significantly lower in AAI+AIT compared with AAI mice. A likely explanation is that the Tregs were functionally impaired and thus unable to suppress the inflammation despite their greater number in AAI mice. This notion was supported by previous reports in mice

and asthmatic patients (Hartl et al., 2007; Joller et al., 2014; Mamessier et al., 2008; Reubsaet et al., 2013; Smyth, Eustace, Kolsum, Blaikely, & Singh, 2010). There, the Tregs were shown to inhibit T_H1/T_H17 responses unchangingly, but exhibited a selective defect in suppressing T_H2 responses (Joller et al., 2014; Reubsaet et al., 2013). These functionally defective Tregs were reported to co-express GATA-3, while it was also shown that GATA-3, albeit not essential for Treg homeostasis, could help stabilize Foxp3 expression during inflammation and keep Tregs accumulating at inflamed sties (Reubsaet et al., 2013; Wohlfert et al., 2011). Overall, the imbalance between T_H2, T_H17, and Treg cells may contribute to the development of allergic diseases and their plasticity makes the intricate interplay even more complex (Du, Zhao, Yan, & Li, 2014; Geginat et al., 2014; Komatsu et al., 2014; Massoud et al., 2016; Peck & Mellins, 2010).

In the unbiased cluster analysis, cluster 2 expressing both CD161 and CTLA-4 but low-level IL-2 increased during AIT up-dosings. Its CD161 expression implied that cluster 2 might be of T_H17 lineage (Cosmi et al., 2008). Since cluster 2 retained CD27 expression, it was not terminally differentiated (Hintzen et al., 1993; Nolte, van Olffen, van Gisbergen, & van Lier, 2009). Cluster 2 might as well be $CD161^+$ Tregs, given that Tregs constitutively express CTLA-4 and CD27 but do not produce IL-2, in line with cluster 2's expression of these markers (Barron et al., 2010; Hintzen et al., 1993; Malek & Bayer, 2004). However, this could not be ascertained in this particular analysis. In contrast, in the mouse study, the frequency of intrapulmonary Tr17 cells was significantly higher in AAI mice and decreased after AIT, exhibiting a similar pattern as the aforementioned murine T_H17 and Tregs. Tr17 cells were likely transitory and proinflammatory in the allergic airway inflammation observed here, but more evidence is needed to support this speculation. Future experiments using a fate-tracing system might help elucidate the role of Th17 cell exhaustion in allergic rhinitis and allergic asthma.

5.3 Conclusion and perspective

Taken together, the expression of PD-1 on T_H2 cells displays a different pattern in allergic individuals as opposed to CTLA-4 in terms of seasonal pollen exposure. Thus, it can be postulated that the upregulation of PD-1 on T_H2 cells is associated with gradual functional adaptation yet less responsiveness to allergens, while upregulation of CTLA-4 remains dynamic and reactive to allergens. Such upregulation is less likely associated with overt functional deficit of T_H2 cells, considering their maintained IL-2 production capacity. In support of this notion, PD-1 expression also links to a heightened T_H2 response under certain circumstances as described earlier (Akbari et al., 2010; McAlees et al., 2015; Oflazoglu et al., 2004). The reduced upregulation of both markers after AIT reflects a decreased size of responding T cell repertoire rather than a mechanism counteracting their expression. The long-term persistence of the highly differentiated T_H2 cells expressing both markers (T_H2A_{EX}) during AIT, on the other hand, could represent a remaining responding T_H2 population. However, their role in allergic reaction and tolerance induction after AIT remains to be addressed.

While the frequency of T_H17 cells increased in AIT-treated allergic patients, there were significantly more T_H17 cells in the lungs of AAI compared to AAI+AIT mice. The former appears to be protective, whereas the latter might be pathological. Timing and location might contribute to this observation and their different roles, let alone the intricate relationship between IL-17A and type-2 cytokines. Similarly, the differences between the local and systemic T_H2 cells observed in the mouse study has not yet been addressed in allergic patients either. Future studies may be needed to assess the frequency of both T helper subsets in the relevant airways such as nasal or bronchial epithelium.

6 Scientific summary

6.1 English version

Alongside clinical improvement, proallergic T_H2 cells are shown to decrease after successful allergen-specific immunotherapy (AIT). Iatrogenic administration of allergens could possibly drive proallergic T_H2 cells to exhaustion because of chronic TCR stimulation. This thesis addresses the hypothesis that immunizations with allergens would lead to exhaustion of T_H2 cells in a mouse model of AIT and two allergic patient cohorts.

These data show that T_H2 cells significantly enhanced CTLA-4 and PD-1 expression upon allergen exposure in OVA-allergic compared to non-allergic mice, at both protein and transcriptional levels. Such enhanced expression was reduced after AIT, in particular on local lung T_H2 cells. Similarly, T_H2 cells from patients with allergic rhinitis also upregulated CTLA-4 and PD-1 and the upregulation was stronger in those with concomitant asthma. In an unbiased Louvain clustering analysis, a highly differentiated T_H2 population expressing both markers persisted long-term during AIT, albeit with a reduction during up-dosing, was discovered.

In conclusion, this study suggests that allergen exposure promotes CTLA-4 and PD-1 expression on T_H2 cells, while AIT does not reinforce the exhausted phenotype. While the persistence of exhausted T_H2 cells during AIT underscores the need of long treatment duration, future studies are warranted to address whether such exhausted T_H2 cells represent the remaining proallergic T_H2 population post AIT, and whether it is possible to eliminate them through personalized modification of the dosing regimens.

6.2 Deutsche Fassung

Neben der Verbesserung des klinischen Bildes zeigt sich, dass proallergische T_H2-Zellen nach erfolgreicher allergenspezifischer Immuntherapie (AIT) abnehmen. Die iatrogene Verabreichung von Allergenen könnte möglicherweise proallergische T_H2-Zellen aufgrund einer chronischen TCR-Stimulation zur Erschöpfung führen. Diese Arbeit befasst sich mit der Hypothese, dass Immunisierungen mit Allergenen zur Erschöpfung von T_H2-Zellen in einem Mausmodell von AIT und zwei allergischen Patientenkohorten führen.

Die Daten dieser Dissertation zeigen, dass T_H2-Zellen die CTLA-4- und PD-1-Expression bei Allergenexposition in OVA-allergischen Mäusen im Vergleich zu nicht allergischen Mäusen sowohl auf Protein- als auch auf Transkriptionsebene signifikant erhöhten. Eine solche verstärkte Expression war nach AIT, insbesondere auf lokalen Lungen-T_H2-Zellen, verringert. In ähnlicher Weise regulierten T_H2-Zellen von Patienten mit allergischer Rhinitis auch CTLA-4 und PD-1 hoch, und die Hochregulation war bei Patienten mit gleichzeitigem Asthma verstärkt. In einer unvoreingenommenen Louvain-Clusteranalyse wurde eine hoch differenzierte T_H2-Population entdeckt, die beide Marker exprimierte und während der AIT langfristig fortbestand, wenn auch mit einer vorrübergehenden Verringerung während der Aufdosierungsphase.

Zusammenfassend legt diese Studie nahe, dass die Allergenexposition die CTLA-4- und PD-1-Expression auf T_H2-Zellen fördert, wobei die AIT den erschöpften Phänotyp nicht verstärkt. Während die Persistenz erschöpfter T_H2-Zellen während der AIT die Notwendigkeit einer langen Behandlungsdauer unterstreicht, sind zukünftige Studien erforderlich, um zu untersuchen, ob solche erschöpften T_H2-Zellen die verbleibende proallergische T_H2-Population nach der AIT darstellen und ob es möglich ist, sie durch personalisierte Änderung der Dosierung zu eliminieren.

7 References

Agresta, L., Hoebe, K. H. N., & Janssen, E. M. (2018). The Emerging Role of CD244 Signaling in Immune Cells of the Tumor Microenvironment. *Front Immunol, 9*, 2809. doi:10.3389/fimmu.2018.02809

Aguilar-Pimentel, A., Graessel, A., Alessandrini, F., Fuchs, H., Gailus-Durner, V., Hrabe de Angelis, M., . . . Schmidt-Weber, C. B. (2017). Improved efficacy of allergen-specific immunotherapy by JAK inhibition in a murine model of allergic asthma. *PLoS One, 12*(6), e0178563. doi:10.1371/journal.pone.0178563

Ajendra, J., Chenery, A. L., Parkinson, J. E., Chan, B. H. K., Pearson, S., Colombo, S. A. P., . . . Allen, J. E. (2020). IL-17A both initiates, via IFNγ suppression, and limits the pulmonary type-2 immune response to nematode infection. *Mucosal Immunol, 13*(6), 958-968. doi:10.1038/s41385-020-0318-2

Akbari, O., Stock, P., Singh, A. K., Lombardi, V., Lee, W. L., Freeman, G. J., . . . Dekruyff, R. H. (2010). PD-L1 and PD-L2 modulate airway inflammation and iNKT-cell-dependent airway hyperreactivity in opposing directions. *Mucosal Immunol, 3*(1), 81-91. doi:10.1038/mi.2009.112

Alfei, F., & Zehn, D. (2017). T Cell Exhaustion: An Epigenetically Imprinted Phenotypic and Functional Makeover. *Trends Mol Med, 23*(9), 769-771. doi:10.1016/j.molmed.2017.07.006

Allen, J. E., Sutherland, T. E., & Ruckerl, D. (2015). IL-17 and neutrophils: unexpected players in the type 2 immune response. *Curr Opin Immunol, 34*, 99-106. doi:10.1016/j.coi.2015.03.001

Amadi-Obi, A., Yu, C. R., Liu, X., Mahdi, R. M., Clarke, G. L., Nussenblatt, R. B., . . . Egwuagu, C. E. (2007). TH17 cells contribute to uveitis and scleritis and are expanded by IL-2 and inhibited by IL-27/STAT1. *Nat Med, 13*(6), 711-718. doi:10.1038/nm1585

Amrani, A., Verdaguer, J., Serra, P., Tafuro, S., Tan, R., & Santamaria, P. (2000). Progression of autoimmune diabetes driven by avidity maturation of a T-cell population. *Nature, 406*(6797), 739-742. doi:10.1038/35021081

Bally, A. P., Austin, J. W., & Boss, J. M. (2016). Genetic and Epigenetic Regulation of PD-1 Expression. *J Immunol, 196*(6), 2431-2437. doi:10.4049/jimmunol.1502643

Barron, L., Dooms, H., Hoyer, K. K., Kuswanto, W., Hofmann, J., O'Gorman, W. E., & Abbas, A. K. (2010). Cutting edge: mechanisms of IL-2-dependent maintenance of functional regulatory T cells. *J Immunol, 185*(11), 6426-6430. doi:10.4049/jimmunol.0903940

Blackburn, S. D., Shin, H., Haining, W. N., Zou, T., Workman, C. J., Polley, A., . . . Wherry, E. J. (2009). Coregulation of CD8+ T cell exhaustion by multiple inhibitory receptors during chronic viral infection. *Nat Immunol, 10*(1), 29-37. doi:10.1038/ni.1679

Bousquet, J., Khaltaev, N., Cruz, A. A., Denburg, J., Fokkens, W. J., Togias, A., . . . Williams, D. (2008). Allergic Rhinitis and its Impact on Asthma (ARIA) 2008*. *Allergy, 63*(s86), 8-160. doi:10.1111/j.1398-9995.2007.01620.x

Bratke, K., Fritz, L., Nokodian, F., Geissler, K., Garbe, K., Lommatzsch, M., & Virchow, J. C. (2017). Differential regulation of PD-1 and its ligands in allergic asthma. *Clin Exp Allergy, 47*(11), 1417-1425. doi:10.1111/cea.13017

Brooks, D. G., Teyton, L., Oldstone, M. B., & McGavern, D. B. (2005). Intrinsic functional dysregulation of CD4 T cells occurs rapidly following persistent viral infection. *J Virol, 79*(16), 10514-10527. doi:10.1128/JVI.79.16.10514-10527.2005

Broos, C. E., van Nimwegen, M., In 't Veen, J. C., Hoogsteden, H. C., Hendriks, R. W., van den Blink, B., & Kool, M. (2015). Decreased Cytotoxic T-Lymphocyte Antigen 4 Expression on Regulatory T Cells and Th17 Cells in Sarcoidosis: Double Trouble? *Am J Respir Crit Care Med, 192*(6), 763-765. doi:10.1164/rccm.201503-0635LE

Brozek, J. L., Bousquet, J., Agache, I., Agarwal, A., Bachert, C., Bosnic-Anticevich, S., . . . Schunemann, H. J. (2017). Allergic Rhinitis and its Impact on Asthma (ARIA) guidelines-2016 revision. *J Allergy Clin Immunol, 140*(4), 950-958. doi:10.1016/j.jaci.2017.03.050

Burks, A. W., Calderon, M. A., Casale, T., Cox, L., Demoly, P., Jutel, M., . . . Akdis, C. A. (2013). Update on allergy immunotherapy: American Academy of Allergy, Asthma & Immunology/European Academy of Allergy and Clinical Immunology/PRACTALL consensus report. *J Allergy Clin Immunol, 131*(5), 1288-1296.e1283. doi:10.1016/j.jaci.2013.01.049

Catakovic, K., Klieser, E., Neureiter, D., & Geisberger, R. (2017). T cell exhaustion: from pathophysiological basics to tumor immunotherapy. *Cell Commun Signal, 15*(1), 1. doi:10.1186/s12964-016-0160-z

Celada, L. J., Kropski, J. A., Herazo-Maya, J. D., Luo, W., Creecy, A., Abad, A. T., . . . Drake, W. P. (2018). PD-1 up-regulation on CD4(+) T cells promotes pulmonary fibrosis through STAT3-mediated IL-17A and TGF-β1 production. *Sci Transl Med, 10*(460). doi:10.1126/scitranslmed.aar8356

Chellappa, S., Hugenschmidt, H., Hagness, M., Line, P. D., Labori, K. J., Wiedswang, G., . . . Aandahl, E. M. (2015). Regulatory T cells that co-express RORγt and FOXP3 are pro-inflammatory and immunosuppressive and expand in human pancreatic cancer. *Oncoimmunology, 5*(4), e1102828. doi:10.1080/2162402x.2015.1102828

Chemnitz, J. M., Parry, R. V., Nichols, K. E., June, C. H., & Riley, J. L. (2004). SHP-1 and SHP-2 associate with immunoreceptor tyrosine-based switch motif of programmed death 1 upon primary human T cell stimulation, but only receptor ligation prevents T cell activation. *J Immunol, 173*(2), 945-954. doi:10.4049/jimmunol.173.2.945

Chen, F., Liu, Z., Wu, W., Rozo, C., Bowdridge, S., Millman, A., . . . Gause, W. C. (2012). An essential role for TH2-type responses in limiting acute tissue damage during experimental helminth infection. *Nat Med, 18*(2), 260-266. doi:10.1038/nm.2628

Ciprandi, G., Caimmi, D., Miraglia Del Giudice, M., La Rosa, M., Salpietro, C., & Marseglia, G. L. (2012). Recent developments in United airways disease. *Allergy Asthma Immunol Res, 4*(4), 171-177. doi:10.4168/aair.2012.4.4.171

Coomes, S. M., Kannan, Y., Pelly, V. S., Entwistle, L. J., Guidi, R., Perez-Lloret, J., . . . Wilson, M. S. (2017). CD4(+) Th2 cells are directly regulated by IL-10 during allergic airway inflammation. *Mucosal Immunol, 10*(1), 150-161. doi:10.1038/mi.2016.47

Corse, E., Gottschalk, R. A., & Allison, J. P. (2011). Strength of TCR-peptide/MHC interactions and in vivo T cell responses. *J Immunol, 186*(9), 5039-5045. doi:10.4049/jimmunol.1003650

Cosmi, L., De Palma, R., Santarlasci, V., Maggi, L., Capone, M., Frosali, F., . . . Annunziato, F. (2008). Human interleukin 17-producing cells originate from a CD161+CD4+ T cell precursor. *J Exp Med, 205*(8), 1903-1916. doi:10.1084/jem.20080397

Cox, L., Nelson, H., Lockey, R., Calabria, C., Chacko, T., Finegold, I., . . . Wallace, D. (2011). Allergen immunotherapy: a practice parameter third update. *J Allergy Clin Immunol, 127*(1 Suppl), S1-55. doi:10.1016/j.jaci.2010.09.034

Crawford, A., Angelosanto, J. M., Kao, C., Doering, T. A., Odorizzi, P. M., Barnett, B. E., & Wherry, E. J. (2014). Molecular and transcriptional basis of CD4(+) T cell dysfunction during chronic infection. *Immunity, 40*(2), 289-302. doi:10.1016/j.immuni.2014.01.005

Day, C. L., Kaufmann, D. E., Kiepiela, P., Brown, J. A., Moodley, E. S., Reddy, S., . . . Walker, B. D. (2006). PD-1 expression on HIV-specific T cells is associated with T-cell exhaustion and disease progression. *Nature, 443*(7109), 350-354. doi:10.1038/nature05115

Deo, S. S., Mistry, K. J., Kakade, A. M., & Niphadkar, P. V. (2010). Role played by Th2 type cytokines in IgE mediated allergy and asthma. *Lung India, 27*(2), 66-71. doi:10.4103/0970-2113.63609

Dhami, S., Kakourou, A., Asamoah, F., Agache, I., Lau, S., Jutel, M., . . . Sheikh, A. (2017). Allergen immunotherapy for allergic asthma: A systematic review and meta-analysis. *Allergy, 72*(12), 1825-1848. doi:10.1111/all.13208

Dong, Y., Li, X., Zhang, L., Zhu, Q., Chen, C., Bao, J., & Chen, Y. (2019). CD4(+) T cell exhaustion revealed by high PD-1 and LAG-3 expression and the loss of helper T cell function in chronic hepatitis B. *BMC Immunol, 20*(1), 27. doi:10.1186/s12865-019-0309-9

Du, R., Zhao, H., Yan, F., & Li, H. (2014). IL-17+Foxp3+ T cells: an intermediate differentiation stage between Th17 cells and regulatory T cells. *J Leukoc Biol, 96*(1), 39-48. doi:10.1189/jlb.1RU0114-010RR

Durham, S. R., Emminger, W., Kapp, A., de Monchy, J. G., Rak, S., Scadding, G. K., . . . Dahl, R. (2012). SQ-standardized sublingual grass immunotherapy: confirmation of disease modification 2 years after 3 years of treatment in a randomized trial. *J Allergy Clin Immunol, 129*(3), 717-725.e715. doi:10.1016/j.jaci.2011.12.973

Fahey, L. M., Wilson, E. B., Elsaesser, H., Fistonich, C. D., McGavern, D. B., & Brooks, D. G. (2011). Viral persistence redirects CD4 T cell differentiation toward T follicular helper cells. *J Exp Med, 208*(5), 987-999. doi:10.1084/jem.20101773

Ferris, R. L., Lu, B., & Kane, L. P. (2014). Too much of a good thing? Tim-3 and TCR signaling in T cell exhaustion. *J Immunol, 193*(4), 1525-1530. doi:10.4049/jimmunol.1400557

Feske, S. (2007). Calcium signalling in lymphocyte activation and disease. *Nature Reviews: Immunology, 7*(9), 690-702. doi:10.1038/nri2152

Fife, B. T., & Bluestone, J. A. (2008). Control of peripheral T-cell tolerance and autoimmunity via the CTLA-4 and PD-1 pathways. *Immunol Rev, 224*, 166-182. doi:10.1111/j.1600-065X.2008.00662.x

Filippis, C., Arens, K., Noubissi Nzeteu, G. A., Reichmann, G., Waibler, Z., Crauwels, P., & van Zandbergen, G. (2017). Nivolumab Enhances In Vitro Effector Functions of PD-1(+) T-Lymphocytes and Leishmania-Infected Human Myeloid Cells in a Host Cell-Dependent Manner. *Front Immunol, 8*, 1880. doi:10.3389/fimmu.2017.01880

Fox, E. M., Torrero, M. N., Evans, H., & Mitre, E. (2015). Immunologic characterization of 3 murine regimens of allergen-specific immunotherapy. *J Allergy Clin Immunol, 135*(5), 1341-1351.e1341-1347. doi:10.1016/j.jaci.2014.07.052

Francis, J. N., James, L. K., Paraskevopoulos, G., Wong, C., Calderon, M. A., Durham, S. R., & Till, S. J. (2008). Grass pollen immunotherapy: IL-10 induction and suppression of late responses precedes IgG4 inhibitory antibody activity. *J Allergy Clin Immunol, 121*(5), 1120-1125.e1122. doi:10.1016/j.jaci.2008.01.072

Francis, J. N., Till, S. J., & Durham, S. R. (2003). Induction of IL-10+CD4+CD25+ T cells by grass pollen immunotherapy. *J Allergy Clin Immunol, 111*(6), 1255-1261. doi:10.1067/mai.2003.1570

Francisco, L. M., Sage, P. T., & Sharpe, A. H. (2010). The PD-1 pathway in tolerance and autoimmunity. *Immunol Rev, 236*, 219-242. doi:10.1111/j.1600-065X.2010.00923.x

Frebel, H., Nindl, V., Schuepbach, R. A., Braunschweiler, T., Richter, K., Vogel, J., . . . Oxenius, A. (2012). Programmed death 1 protects from fatal circulatory failure during systemic virus infection of mice. *J Exp Med, 209*(13), 2485-2499. doi:10.1084/jem.20121015

Fröhlich, A., Kisielow, J., Schmitz, I., Freigang, S., Shamshiev, A. T., Weber, J., . . . Kopf, M. (2009). IL-21R on T cells is critical for sustained functionality and control of chronic viral infection. *Science, 324*(5934), 1576-1580. doi:10.1126/science.1172815

Fuller, M. J., & Zajac, A. J. (2003). Ablation of CD8 and CD4 T cell responses by high viral loads. *J Immunol, 170*(1), 477-486. doi:10.4049/jimmunol.170.1.477

Gagliani, N., Vesely, M. C. A., Iseppon, A., Brockmann, L., Xu, H., Palm, N. W., . . . Flavell, R. A. (2015). Th17 cells transdifferentiate into regulatory T cells during resolution of inflammation. *Nature, 523*(7559), 221-225. doi:10.1038/nature14452

Gattinoni, L., Klebanoff, C. A., & Restifo, N. P. (2012). Paths to stemness: building the ultimate antitumour T cell. *Nat Rev Cancer, 12*(10), 671-684. doi:10.1038/nrc3322

Geginat, J., Paroni, M., Maglie, S., Alfen, J. S., Kastirr, I., Gruarin, P., . . . Abrignani, S. (2014). Plasticity of human CD4 T cell subsets. *Front Immunol, 5*, 630. doi:10.3389/fimmu.2014.00630

Giavina-Bianchi, P., Aun, M. V., Takejima, P., Kalil, J., & Agondi, R. C. (2016). United airway disease: current perspectives. *J Asthma Allergy, 9*, 93-100. doi:10.2147/JAA.S81541

Gorenshteyn, D., Zaslavsky, E., Fribourg, M., Park, Christopher Y., Wong, Aaron K., Tadych, A., . . . Sealfon, Stuart C. (2015). Interactive Big Data Resource to Elucidate Human Immune Pathways and Diseases. *Immunity, 43*(3), 605-614. doi:10.1016/j.immuni.2015.08.014

Gu, Z. W., Wang, Y. X., & Cao, Z. W. (2017). Neutralization of interleukin-17 suppresses allergic rhinitis symptoms by downregulating Th2 and Th17 responses and upregulating the Treg response. *Oncotarget, 8*(14), 22361-22369. doi:10.18632/oncotarget.15652

Han, S., Asoyan, A., Rabenstein, H., Nakano, N., & Obst, R. (2010). Role of antigen persistence and dose for $CD4^+$ T-cell exhaustion and recovery. *Proc Natl Acad Sci U S A, 107*(47), 20453-20458. doi:10.1073/pnas.1008437107

Hartl, D., Koller, B., Mehlhorn, A. T., Reinhardt, D., Nicolai, T., Schendel, D. J., . . . Krauss-Etschmann, S. (2007). Quantitative and functional impairment of pulmonary CD4+CD25hi regulatory T cells in pediatric asthma. *J Allergy Clin Immunol, 119*(5), 1258-1266. doi:10.1016/j.jaci.2007.02.023

Hill, D. A., & Spergel, J. M. (2018). The atopic march: Critical evidence and clinical relevance. *Ann Allergy Asthma Immunol, 120*(2), 131-137. doi:10.1016/j.anai.2017.10.037

Hintzen, R. Q., de Jong, R., Lens, S. M., Brouwer, M., Baars, P., & van Lier, R. A. (1993). Regulation of CD27 expression on subsets of mature T-lymphocytes. *J Immunol, 151*(5), 2426-2435.

Ihara, F., Sakurai, D., Yonekura, S., Iinuma, T., Yagi, R., Sakurai, T., . . . Okamoto, Y. (2018). Identification of specifically reduced Th2 cell subsets in allergic rhinitis patients after sublingual immunotherapy. *Allergy, 73*(9), 1823-1832. doi:10.1111/all.13436

Iinuma, T., Okamoto, Y., Morimoto, Y., Arai, T., Sakurai, T., Yonekura, S., . . . Nakayama, T. (2018). Pathogenicity of memory Th2 cells is linked to stage of allergic rhinitis. *Allergy, 73*(2), 479-489. doi:10.1111/all.13295

Im, S. J., Hashimoto, M., Gerner, M. Y., Lee, J., Kissick, H. T., Burger, M. C., . . . Ahmed, R. (2016). Defining CD8+ T cells that provide the proliferative burst after PD-1 therapy. *Nature, 537*(7620), 417-421. doi:10.1038/nature19330

Isakov, N., & Altman, A. (2012). PKC-theta-mediated signal delivery from the TCR/CD28 surface receptors. *Front Immunol, 3*, 273. doi:10.3389/fimmu.2012.00273

Islam, S. A., & Luster, A. D. (2012). T cell homing to epithelial barriers in allergic disease. *Nat Med, 18*(5), 705-715. doi:10.1038/nm.2760

Jacobsen, L., Wahn, U., & Bilo, M. B. (2012). Allergen-specific immunotherapy provides immediate, long-term and preventive clinical effects in children and adults: the

effects of immunotherapy can be categorised by level of benefit -the centenary of allergen specific subcutaneous immunotherapy. *Clin Transl Allergy, 2*, 8. doi:10.1186/2045-7022-2-8

Janssen, E. M., van Oosterhout, A. J., Nijkamp, F. P., van Eden, W., & Wauben, M. H. (2000). The efficacy of immunotherapy in an experimental murine model of allergic asthma is related to the strength and site of T cell activation during immunotherapy. *J Immunol, 165*(12), 7207-7214. doi:10.4049/jimmunol.165.12.7207

Joller, N., Lozano, E., Burkett, Patrick R., Patel, B., Xiao, S., Zhu, C., . . . Kuchroo, Vijay K. (2014). Treg Cells Expressing the Coinhibitory Molecule TIGIT Selectively Inhibit Proinflammatory Th1 and Th17 Cell Responses. *Immunity, 40*(4), 569-581. doi:10.1016/j.immuni.2014.02.012

Jutel, M., Jaeger, L., Suck, R., Meyer, H., Fiebig, H., & Cromwell, O. (2005). Allergen-specific immunotherapy with recombinant grass pollen allergens. *J Allergy Clin Immunol, 116*(3), 608-613. doi:10.1016/j.jaci.2005.06.004

Kahan, S. M., & Zajac, A. J. (2019). Immune Exhaustion: Past Lessons and New Insights from Lymphocytic Choriomeningitis Virus. *Viruses, 11*(2). doi:10.3390/v11020156

Kamada, T., Togashi, Y., Tay, C., Ha, D., Sasaki, A., Nakamura, Y., . . . Nishikawa, H. (2019). PD-1(+) regulatory T cells amplified by PD-1 blockade promote hyperprogression of cancer. *Proc Natl Acad Sci U S A, 116*(20), 9999-10008. doi:10.1073/pnas.1822001116

Kappen, J. H., Durham, S. R., Veen, H. I., & Shamji, M. H. (2017). Applications and mechanisms of immunotherapy in allergic rhinitis and asthma. *Ther Adv Respir Dis, 11*(1), 73-86. doi:10.1177/1753465816669662

Karmaus, P. W. F., Chen, X., Lim, S. A., Herrada, A. A., Nguyen, T. M., Xu, B., . . . Chi, H. (2019). Metabolic heterogeneity underlies reciprocal fates of TH17 cell stemness and plasticity. *Nature, 565*(7737), 101-105. doi:10.1038/s41586-018-0806-7

Kearley, J., McMillan, S. J., & Lloyd, C. M. (2007). Th2-driven, allergen-induced airway inflammation is reduced after treatment with anti-Tim-3 antibody in vivo. *J Exp Med, 204*(6), 1289-1294. doi:10.1084/jem.20062093

Khailaie, S., Rowshanravan, B., Robert, P. A., Waters, E., Halliday, N., Badillo Herrera, J. D., . . . Meyer-Hermann, M. (2018). Characterization of CTLA4 Trafficking and Implications for Its Function. *Biophys J, 115*(7), 1330-1343. doi:10.1016/j.bpj.2018.08.020

Kim, B. S., Lu, H., Ichiyama, K., Chen, X., Zhang, Y. B., Mistry, N. A., . . . Dong, C. (2017). Generation of RORγt(+) Antigen-Specific T Regulatory 17 Cells from Foxp3(+) Precursors in Autoimmunity. *Cell Rep, 21*(1), 195-207. doi:10.1016/j.celrep.2017.09.021

Kinyanjui, M. W., Shan, J., Nakada, E. M., Qureshi, S. T., & Fixman, E. D. (2013). Dose-dependent effects of IL-17 on IL-13-induced airway inflammatory responses and airway hyperresponsiveness. *J Immunol, 190*(8), 3859-3868. doi:10.4049/jimmunol.1200506

Komatsu, N., Okamoto, K., Sawa, S., Nakashima, T., Oh-hora, M., Kodama, T., . . . Takayanagi, H. (2014). Pathogenic conversion of Foxp3+ T cells into TH17 cells in autoimmune arthritis. *Nat Med, 20*(1), 62-68. doi:10.1038/nm.3432

Kudo, M., Melton, A. C., Chen, C., Engler, M. B., Huang, K. E., Ren, X., . . . Sheppard, D. (2012). IL-17A produced by αβ T cells drives airway hyper-responsiveness in mice and enhances mouse and human airway smooth muscle contraction. *Nat Med, 18*(4), 547-554. doi:10.1038/nm.2684

Kumagai, S., Togashi, Y., Kamada, T., Sugiyama, E., Nishinakamura, H., Takeuchi, Y., . . . Nishikawa, H. (2020). The PD-1 expression balance between effector and regulatory T cells predicts the clinical efficacy of PD-1 blockade therapies. *Nat Immunol, 21*(11), 1346-1358. doi:10.1038/s41590-020-0769-3

Laurence, A., Tato, C. M., Davidson, T. S., Kanno, Y., Chen, Z., Yao, Z., . . . O'Shea, John J. (2007). Interleukin-2 Signaling via STAT5 Constrains T Helper 17 Cell Generation. *Immunity, 26*(3), 371-381. doi:10.1016/j.immuni.2007.02.009

Li, J., He, Y., Hao, J., Ni, L., & Dong, C. (2018). High Levels of Eomes Promote Exhaustion of Anti-tumor CD8(+) T Cells. *Front Immunol, 9*, 2981. doi:10.3389/fimmu.2018.02981

Liberzon, A., Subramanian, A., Pinchback, R., Thorvaldsdóttir, H., Tamayo, P., & Mesirov, J. P. (2011). Molecular signatures database (MSigDB) 3.0. *Bioinformatics, 27*(12), 1739-1740. doi:10.1093/bioinformatics/btr260

Licata, L. A., Nguyen, C. T., Burga, R. A., Falanga, V., Espat, N. J., Ayala, A., . . . Katz, S. C. (2013). Biliary obstruction results in PD-1-dependent liver T cell dysfunction and acute inflammation mediated by Th17 cells and neutrophils. *J Leukoc Biol, 94*(4), 813-823. doi:10.1189/jlb.0313137

Long, M., & Adler, A. J. (2006). Cutting edge: Paracrine, but not autocrine, IL-2 signaling is sustained during early antiviral CD4 T cell response. *J Immunol, 177*(7), 4257-4261. doi:10.4049/jimmunol.177.7.4257

Lüthje, K., Kallies, A., Shimohakamada, Y., Belz, G. T., Light, A., Tarlinton, D. M., & Nutt, S. L. (2012). The development and fate of follicular helper T cells defined by an IL-21 reporter mouse. *Nat Immunol, 13*(5), 491-498. doi:10.1038/ni.2261

Mackenzie, K. J., Nowakowska, D. J., Leech, M. D., McFarlane, A. J., Wilson, C., Fitch, P. M., . . . Anderton, S. M. (2014). Effector and central memory T helper 2 cells respond differently to peptide immunotherapy. *Proc Natl Acad Sci U S A, 111*(8), E784-793. doi:10.1073/pnas.1316178111

Malek, T. R., & Bayer, A. L. (2004). Tolerance, not immunity, crucially depends on IL-2. *Nat Rev Immunol, 4*(9), 665-674. doi:10.1038/nri1435

Malherbe, L., Hausl, C., Teyton, L., & McHeyzer-Williams, M. G. (2004). Clonal Selection of Helper T Cells Is Determined by an Affinity Threshold with No Further Skewing of TCR Binding Properties. *Immunity, 21*(5), 669-679. doi:10.1016/j.immuni.2004.09.008

Mamessier, E., Nieves, A., Lorec, A. M., Dupuy, P., Pinot, D., Pinet, C., . . . Magnan, A. (2008). T-cell activation during exacerbations: a longitudinal study in refractory asthma. *Allergy, 63*(9), 1202-1210. doi:10.1111/j.1398-9995.2008.01687.x

Martinez, F. D., & Vercelli, D. (2013). Asthma. *The Lancet, 382*(9901), 1360-1372. doi:10.1016/s0140-6736(13)61536-6

Masopust, D., Vezys, V., Marzo, A. L., & Lefrançois, L. (2001). Preferential Localization of Effector Memory Cells in Nonlymphoid Tissue. *Science, 291*(5512), 2413. doi:10.1126/science.1058867

Massoud, A. H., Charbonnier, L. M., Lopez, D., Pellegrini, M., Phipatanakul, W., & Chatila, T. A. (2016). An asthma-associated IL4R variant exacerbates airway inflammation by promoting conversion of regulatory T cells to TH17-like cells. *Nat Med, 22*(9), 1013-1022. doi:10.1038/nm.4147

McAlees, J. W., Lajoie, S., Dienger, K., Sproles, A. A., Richgels, P. K., Yang, Y., . . . Lewkowich, I. P. (2015). Differential control of CD4(+) T-cell subsets by the PD-1/PD-L1 axis in a mouse model of allergic asthma. *Eur J Immunol, 45*(4), 1019-1029. doi:10.1002/eji.201444778

McKinney, E. F., Lee, J. C., Jayne, D. R., Lyons, P. A., & Smith, K. G. (2015). T-cell exhaustion, co-stimulation and clinical outcome in autoimmunity and infection. *Nature, 523*(7562), 612-616. doi:10.1038/nature14468

McNamee, E. N., Korns Johnson, D., Homann, D., & Clambey, E. T. (2013). Hypoxia and hypoxia-inducible factors as regulators of T cell development, differentiation, and function. *Immunol Res, 55*(1-3), 58-70. doi:10.1007/s12026-012-8349-8

Meng, Y., Wang, C., & Zhang, L. (2019). Recent developments and highlights in allergic rhinitis. *Allergy, 74*(12), 2320-2328. doi:10.1111/all.14067

Miller, B. C., Sen, D. R., Al Abosy, R., Bi, K., Virkud, Y. V., LaFleur, M. W., . . . Haining, W. N. (2019). Subsets of exhausted CD8(+) T cells differentially mediate tumor control and respond to checkpoint blockade. *Nat Immunol, 20*(3), 326-336. doi:10.1038/s41590-019-0312-6

Mims, J. W. (2014). Epidemiology of allergic rhinitis. *Int Forum Allergy Rhinol, 4 Suppl 2*, S18-20. doi:10.1002/alr.21385

Moote, W., Kim, H., & Ellis, A. K. (2018). Allergen-specific immunotherapy. *Allergy Asthma Clin Immunol, 14*(Suppl 2), 53. doi:10.1186/s13223-018-0282-5

Mosayebian, A., Koohini, Z., Hossein-Nataj, H., Abediankenari, S., Abedi, S., & Asgarian-Omran, H. (2018). Elevated Expression of Tim-3 and PD-1 Immune Checkpoint Receptors on T-CD4+ Lymphocytes of Patients with Asthma. *Iran J Allergy Asthma Immunol, 17*(6), 517-525.

Munthe-Kaas, M. C., Carlsen, K. H., Helms, P. J., Gerritsen, J., Whyte, M., Feijen, M., . . . Undlien, D. E. (2004). CTLA-4 polymorphisms in allergy and asthma and the TH1/ TH2 paradigm. *J Allergy Clin Immunol, 114*(2), 280-287. doi:10.1016/j.jaci.2004.03.050

Nakajima, S., Kitoh, A., Egawa, G., Natsuaki, Y., Nakamizo, S., Moniaga, C. S., . . . Kabashima, K. (2014). IL-17A as an inducer for Th2 immune responses in murine atopic dermatitis models. *J Invest Dermatol, 134*(8), 2122-2130. doi:10.1038/jid.2014.51

Newcomb, D. C., Zhou, W., Moore, M. L., Goleniewska, K., Hershey, G. K., Kolls, J. K., & Peebles, R. S., Jr. (2009). A functional IL-13 receptor is expressed on polarized murine CD4+ Th17 cells and IL-13 signaling attenuates Th17 cytokine production. *J Immunol, 182*(9), 5317-5321. doi:10.4049/jimmunol.0803868

Nolte, M. A., van Olffen, R. W., van Gisbergen, K. P., & van Lier, R. A. (2009). Timing and tuning of CD27-CD70 interactions: the impact of signal strength in setting the balance between adaptive responses and immunopathology. *Immunol Rev, 229*(1), 216-231. doi:10.1111/j.1600-065X.2009.00774.x

North, M. L., Jones, M. J., MacIsaac, J. L., Morin, A. M., Steacy, L. M., Gregor, A., . . . Ellis, A. K. (2018). Blood and nasal epigenetics correlate with allergic rhinitis symptom development in the environmental exposure unit. *Allergy, 73*(1), 196-205. doi:10.1111/all.13263

Oflazoglu, E., Swart, D. A., Anders-Bartholo, P., Jessup, H. K., Norment, A. M., Lawrence, W. A., . . . Fitzpatrick, D. R. (2004). Paradoxical role of programmed death-1 ligand 2 in Th2 immune responses in vitro and in a mouse asthma model in vivo. *Eur J Immunol, 34*(12), 3326-3336. doi:10.1002/eji.200425197

Ogasawara, N., Poposki, J. A., Klingler, A. I., Tan, B. K., Weibman, A. R., Hulse, K. E., . . . Kato, A. (2018). IL-10, TGF-beta, and glucocorticoid prevent the production of type 2 cytokines in human group 2 innate lymphoid cells. *J Allergy Clin Immunol, 141*(3), 1147-1151 e1148. doi:10.1016/j.jaci.2017.09.025

Oyler-Yaniv, A., Oyler-Yaniv, J., Whitlock, B. M., Liu, Z., Germain, R. N., Huse, M., . . . Krichevsky, O. (2017). A Tunable Diffusion-Consumption Mechanism of Cytokine Propagation Enables Plasticity in Cell-to-Cell Communication in the Immune System. *Immunity, 46*(4), 609-620. doi:10.1016/j.immuni.2017.03.011

Paley, M. A., Kroy, D. C., Odorizzi, P. M., Johnnidis, J. B., Dolfi, D. V., Barnett, B. E., . . . Wherry, E. J. (2012). Progenitor and terminal subsets of CD8+ T cells cooperate to contain chronic viral infection. *Science, 338*(6111), 1220-1225. doi:10.1126/science.1229620

Parry, R. V., Chemnitz, J. M., Frauwirth, K. A., Lanfranco, A. R., Braunstein, I., Kobayashi, S. V., . . . Riley, J. L. (2005). CTLA-4 and PD-1 receptors inhibit T-cell activation by distinct mechanisms. *Mol Cell Biol, 25*(21), 9543-9553. doi:10.1128/mcb.25.21.9543-9553.2005

Peck, A., & Mellins, E. D. (2010). Plasticity of T-cell phenotype and function: the T helper type 17 example. *Immunology, 129*(2), 147-153. doi:10.1111/j.1365-2567.2009.03189.x

Pividori, M., Schoettler, N., Nicolae, D. L., Ober, C., & Im, H. K. (2019). Shared and distinct genetic risk factors for childhood-onset and adult-onset asthma: genome-wide and transcriptome-wide studies. *Lancet Respir Med, 7*(6), 509-522. doi:10.1016/s2213-2600(19)30055-4

Qiu, C., Zhong, L., Huang, C., Long, J., Ye, X., Wu, J., . . . Zhang, J. (2020). Cell-bound IgE and plasma IgE as a combined clinical diagnostic indicator for allergic patients. *Sci Rep, 10*(1), 4700. doi:10.1038/s41598-020-61455-8

Qureshi, O. S., Zheng, Y., Nakamura, K., Attridge, K., Manzotti, C., Schmidt, E. M., . . . Sansom, D. M. (2011). Trans-Endocytosis of CD80 and CD86: A Molecular

Basis for the Cell-Extrinsic Function of CTLA-4. *Science, 332*(6029), 600-603. doi:10.1126/science.1202947

Radermecker, C., Sabatel, C., Vanwinge, C., Ruscitti, C., Maréchal, P., Perin, F., . . . Marichal, T. (2019). Locally instructed CXCR4(hi) neutrophils trigger environment-driven allergic asthma through the release of neutrophil extracellular traps. *Nat Immunol, 20*(11), 1444-1455. doi:10.1038/s41590-019-0496-9

Reubsaet, L., Meerding, J., Giezeman, R., de Kleer, I., Arets, B., Prakken, B., . . . van Wijk, F. (2013). Der p 1-induced $CD4^{+}FOXP3^{+}GATA3^{+}$ T cells have suppressive properties and contribute to the polarization of the TH2-associated response. *J Allergy Clin Immunol, 132*(6), 1440-1444. doi:10.1016/j.jaci.2013.06.028

Revu, S., Wu, J., Henkel, M., Rittenhouse, N., Menk, A., Delgoffe, G. M., . . . McGeachy, M. J. (2018). IL-23 and IL-1beta Drive Human Th17 Cell Differentiation and Metabolic Reprogramming in Absence of CD28 Costimulation. *Cell Rep, 22*(10), 2642-2653. doi:10.1016/j.celrep.2018.02.044

Rincon, M., Flavell, R. A., & Davis, R. J. (2001). Signal transduction by MAP kinases in T lymphocytes. *Oncogene, 20*(19), 2490-2497. doi:10.1038/sj.onc.1204382

Romanet-Manent, S., Charpin, D., Magnan, A., Lanteaume, A., Vervloet, D., & Group, E. C. (2002). Allergic vs nonallergic asthma: what makes the difference? *Allergy, 57*(7), 607-613. doi:10.1034/j.1398-9995.2002.23504.x

Rosskopf, S., Jahn-Schmid, B., Schmetterer, K. G., Zlabinger, G. J., & Steinberger, P. (2018). PD-1 has a unique capacity to inhibit allergen-specific human CD4(+) T cell responses. *Sci Rep, 8*(1), 13543. doi:10.1038/s41598-018-31757-z

Rui, Y., Honjo, T., & Chikuma, S. (2013). Programmed cell death 1 inhibits inflammatory helper T-cell development through controlling the innate immune response. *Proc Natl Acad Sci U S A, 110*(40), 16073-16078. doi:10.1073/pnas.1315828110

Russkamp, D., Aguilar-Pimentel, A., Alessandrini, F., Gailus-Durner, V., Fuchs, H., Ohnmacht, C., . . . Blank, S. (2019). IL-4 receptor α blockade prevents sensitization and alters acute and long-lasting effects of allergen-specific immunotherapy of murine allergic asthma. *Allergy, 74*(8), 1549-1560. doi:https://doi.org/10.1111/all.13759

Saito, T. (2013). Mechanisms of T-Lymphocyte Signaling and Activation. In W. H. Paul (Ed.), *Fundamental Immunology* (7 ed., pp. 306-324). Philadelphia: Lippincott Williams & Wilkins.

Saxena, V., Patil, A., Tayde, R., Bichare, S., Chinchkar, V., Bagul, R., . . . Thakar, M. (2018). HIV-specific CD4+Th17 cells from HIV infected long-term non-progressors exhibit lower CTLA-4 expression and reduced apoptosis. *Immunobiology, 223*(11), 658-662. doi:10.1016/j.imbio.2018.07.011

Scadding, G. W., Eifan, A. O., Lao-Araya, M., Penagos, M., Poon, S. Y., Steveling, E., . . . Durham, S. R. (2015). Effect of grass pollen immunotherapy on clinical and local immune response to nasal allergen challenge. *Allergy, 70*(6), 689-696. doi:10.1111/all.12608

Schmittgen, T. D., & Livak, K. J. (2008). Analyzing real-time PCR data by the comparative C(T) method. *Nat Protoc, 3*(6), 1101-1108. doi:10.1038/nprot.2008.73

Schwartz, R. H. (2003). T cell anergy. *Annu Rev Immunol, 21*, 305-334. doi:10.1146/annurev.immunol.21.120601.141110

Sen, D. R., Kaminski, J., Barnitz, R. A., Kurachi, M., Gerdemann, U., Yates, K. B., . . . Haining, W. N. (2016). The epigenetic landscape of T cell exhaustion. *Science, 354*(6316), 1165-1169. doi:10.1126/science.aae0491

Shamji, M. H., & Durham, S. R. (2017). Mechanisms of allergen immunotherapy for inhaled allergens and predictive biomarkers. *J Allergy Clin Immunol, 140*(6), 1485-1498. doi:10.1016/j.jaci.2017.10.010

Shamji, M. H., Kappen, J. H., Akdis, M., Jensen-Jarolim, E., Knol, E. F., Kleine-Tebbe, J., . . . Schmidt-Weber, C. B. (2017). Biomarkers for monitoring clinical efficacy of allergen immunotherapy for allergic rhinoconjunctivitis and allergic asthma: an EAACI Position Paper. *Allergy, 72*(8), 1156-1173. doi:10.1111/all.13138

Sharpe, A. H., & Freeman, G. J. (2002). The B7-CD28 superfamily. *Nat Rev Immunol, 2*(2), 116-126. doi:10.1038/nri727

Shin, B., Kress, R. L., Kramer, P. A., Darley-Usmar, V. M., Bellis, S. L., & Harrington, L. E. (2018). Effector CD4 T cells with progenitor potential mediate chronic intestinal inflammation. *J Exp Med, 215*(7), 1803-1812. doi:10.1084/jem.20172335

Shin, Y. S., Jung, J. W., Park, J. W., Choi, J. H., Kwon, J. W., Lee, S., . . . Clinical, I. (2019). Clinical Efficacy of Allergen-Specific Immunotherapy from Patient and Physician Perspectives. *Yonsei Med J, 60*(5), 446-453. doi:10.3349/ymj.2019.60.5.446

Smyth, L. J., Eustace, A., Kolsum, U., Blaikely, J., & Singh, D. (2010). Increased airway T regulatory cells in asthmatic subjects. *CHEST, 138*(4), 905-912. doi:10.1378/chest.09-3079

Sugiura, D., Maruhashi, T., Okazaki, I. M., Shimizu, K., Maeda, T. K., Takemoto, T., & Okazaki, T. (2019). Restriction of PD-1 function by cis-PD-L1/CD80 interactions is required for optimal T cell responses. *Science, 364*(6440), 558-566. doi:10.1126/science.aav7062

Sun, Y., Caplazi, P., Zhang, J., Mazloom, A., Kummerfeld, S., Quinones, G., . . . Zarrin, A. A. (2014). PILRα negatively regulates mouse inflammatory arthritis. *J Immunol, 193*(2), 860-870. doi:10.4049/jimmunol.1400045

Sutherland, T. E., Logan, N., Rückerl, D., Humbles, A. A., Allan, S. M., Papayannopoulos, V., . . . Allen, J. E. (2014). Chitinase-like proteins promote IL-17-mediated neutrophilia in a tradeoff between nematode killing and host damage. *Nat Immunol, 15*(12), 1116-1125. doi:10.1038/ni.3023

Szklarczyk, D., Gable, A. L., Lyon, D., Junge, A., Wyder, S., Huerta-Cepas, J., . . . Mering, C. V. (2019). STRING v11: protein-protein association networks with increased coverage, supporting functional discovery in genome-wide experimental datasets. *Nucleic Acids Res, 47*(D1), D607-d613. doi:10.1093/nar/gky1131

Tang, F., Wang, F., An, L., & Wang, X. (2015). Upregulation of Tim-3 on CD4(+) T cells is associated with Th1/Th2 imbalance in patients with allergic asthma. *Int J Clin Exp Med, 8*(3), 3809-3816.

Tham, E. H., & Leung, D. Y. (2019). Mechanisms by Which Atopic Dermatitis Predisposes to Food Allergy and the Atopic March. *Allergy Asthma Immunol Res, 11*(1), 4-15. doi:10.4168/aair.2019.11.1.4

Tohidinik, H. R., Mallah, N., & Takkouche, B. (2019). History of allergic rhinitis and risk of asthma; a systematic review and meta-analysis. *World Allergy Organ J, 12*(10), 100069. doi:10.1016/j.waojou.2019.100069

Valmori, D., Raffin, C., Raimbaud, I., & Ayyoub, M. (2010). Human RORgammat+ TH17 cells preferentially differentiate from naive FOXP3+Treg in the presence of lineage-specific polarizing factors. *Proc Natl Acad Sci U S A, 107*(45), 19402-19407. doi:10.1073/pnas.1008247107

van de Veen, W., Stanic, B., Yaman, G., Wawrzyniak, M., Söllner, S., Akdis, D. G., . . . Akdis, M. (2013). IgG4 production is confined to human IL-10-producing regulatory B cells that suppress antigen-specific immune responses. *J Allergy Clin Immunol, 131*(4), 1204-1212. doi:10.1016/j.jaci.2013.01.014

van den Broeck, W., Derore, A., & Simoens, P. (2006). Anatomy and nomenclature of murine lymph nodes: Descriptive study and nomenclatory standardization in BALB/cAnNCrl mice. *Journal of Immunological Methods, 312*(1-2), 12-19. doi:10.1016/j.jim.2006.01.022

van der Werf, N., Redpath, S. A., Azuma, M., Yagita, H., & Taylor, M. D. (2013). Th2 cell-intrinsic hypo-responsiveness determines susceptibility to helminth infection. *PLoS Pathog, 9*(3), e1003215. doi:10.1371/journal.ppat.1003215

Vissers, J. L., van Esch, B. C., Hofman, G. A., Kapsenberg, M. L., Weller, F. R., & van Oosterhout, A. J. (2004). Allergen immunotherapy induces a suppressive memory response mediated by IL-10 in a mouse asthma model. *J Allergy Clin Immunol, 113*(6), 1204-1210. doi:10.1016/j.jaci.2004.02.041

Voo, K. S., Wang, Y. H., Santori, F. R., Boggiano, C., Wang, Y. H., Arima, K., . . . Liu, Y. J. (2009). Identification of IL-17-producing FOXP3+ regulatory T cells in humans. *Proc Natl Acad Sci U S A, 106*(12), 4793-4798. doi:10.1073/pnas.0900408106

Wakashin, H., Hirose, K., Maezawa, Y., Kagami, S., Suto, A., Watanabe, N., . . . Nakajima, H. (2008). IL-23 and Th17 cells enhance Th2-cell-mediated eosinophilic airway inflammation in mice. *Am J Respir Crit Care Med, 178*(10), 1023-1032. doi:10.1164/rccm.200801-086OC

Wambre, E. (2015). Effect of allergen-specific immunotherapy on CD4+ T cells. *Curr Opin Allergy Clin Immunol, 15*(6), 581-587. doi:10.1097/ACI.0000000000000216

Wambre, E., Bajzik, V., DeLong, J. H., O'Brien, K., Nguyen, Q. A., Speake, C., . . . Kwok, W. W. (2017). A phenotypically and functionally distinct human T(H)2 cell subpopulation is associated with allergic disorders. *Sci Transl Med, 9*(401). doi:10.1126/scitranslmed.aam9171

Wambre, E., DeLong, J. H., James, E. A., LaFond, R. E., Robinson, D., & Kwok, W. W. (2012). Differentiation stage determines pathologic and protective allergen-specific CD4+ T-cell outcomes during specific immunotherapy. *J Allergy Clin Immunol, 129*(2), 544-551, 551 e541-547. doi:10.1016/j.jaci.2011.08.034

Wang, C., Thudium, K. B., Han, M., Wang, X. T., Huang, H., Feingersh, D., . . . Korman, A. J. (2014). In vitro characterization of the anti-PD-1 antibody nivolumab, BMS-936558, and in vivo toxicology in non-human primates. *Cancer Immunol Res, 2*(9), 846-856. doi:10.1158/2326-6066.CIR-14-0040

Wang, X. D., Zheng, M., Lou, H. F., Wang, C. S., Zhang, Y., Bo, M. Y., . . . Bachert, C. (2016). An increased prevalence of self-reported allergic rhinitis in major Chinese cities from 2005 to 2011. *Allergy, 71*(8), 1170-1180. doi:10.1111/all.12874

Wei, F., Zhong, S., Ma, Z., Kong, H., Medvec, A., Ahmed, R., . . . Riley, J. L. (2013). Strength of PD-1 signaling differentially affects T-cell effector functions. *Proc Natl Acad Sci U S A, 110*(27), E2480-2489. doi:10.1073/pnas.1305394110

Wherry, E. J., Blattman, J. N., Murali-Krishna, K., van der Most, R., & Ahmed, R. (2003). Viral persistence alters CD8 T-cell immunodominance and tissue distribution and results in distinct stages of functional impairment. *J Virol, 77*(8), 4911-4927. doi:10.1128/jvi.77.8.4911-4927.2003

Wherry, E. J., & Kurachi, M. (2015). Molecular and cellular insights into T cell exhaustion. *Nat Rev Immunol, 15*(8), 486-499. doi:10.1038/nri3862

Wohlfert, E. A., Grainger, J. R., Bouladoux, N., Konkel, J. E., Oldenhove, G., Ribeiro, C. H., . . . Belkaid, Y. (2011). GATA3 controls Foxp3$^+$ regulatory T cell fate during inflammation in mice. *J Clin Invest, 121*(11), 4503-4515. doi:10.1172/jci57456

Yang, L., Qiao, G., Hassan, Y., Li, Z., Zhang, X., Kong, H., . . . Zhang, J. (2016). Program Death-1 Suppresses Autoimmune Arthritis by Inhibiting Th17 Response. *Arch Immunol Ther Exp (Warsz), 64*(5), 417-423. doi:10.1007/s00005-016-0404-z

Yokosuka, T., Kobayashi, W., Takamatsu, M., Sakata-Sogawa, K., Zeng, H., Hashimoto-Tane, A., . . . Saito, T. (2010). Spatiotemporal basis of CTLA-4 costimulatory molecule-mediated negative regulation of T cell activation. *Immunity, 33*(3), 326-339. doi:10.1016/j.immuni.2010.09.006

Yu, G., Wang, L.-G., Han, Y., & He, Q.-Y. (2012). clusterProfiler: an R package for comparing biological themes among gene clusters. *Omics : a journal of integrative biology, 16*(5), 284-287. doi:10.1089/omi.2011.0118

Yu, Q., Sharma, A., Oh, S. Y., Moon, H. G., Hossain, M. Z., Salay, T. M., . . . Sen, J. M. (2009). T cell factor 1 initiates the T helper type 2 fate by inducing the transcription factor GATA-3 and repressing interferon-gamma. *Nat Immunol, 10*(9), 992-999. doi:10.1038/ni.1762

Zissler, U. M., Jakwerth, C. A., Guerth, F. M., Pechtold, L., Aguilar-Pimentel, J. A., Dietz, K., . . . Chaker, A. M. (2018). Early IL-10 producing B-cells and coinciding Th/Tr17 shifts during three year grass-pollen AIT. *EBioMedicine, 36*, 475-488. doi:10.1016/j.ebiom.2018.09.016

8 Publications

1. **Wang, S.**, Chaker, A. M., Guerth, F., Oelsner, M., Schmidt-Weber, C. B., Zissler, U. M., Jakwerth, C. A. Upregulation of co-inhibitory receptors on circulating T_H2 cells in patients with AIT-untreated grass pollen allergy. Poster presentation delivered at the Type 2 Immunity Conference, Bruges, Belgium, February 2019

2. **Wang, S.**, Zissler, U. M., Buettner, M., Heine, S., Heldner, A., Kotz, S., Pechtold, L., Kau, J., Plaschke, M., Ullmann, J. T., Guerth, F., Oelsner, M., Alessandrini, F., Blank, S., Chaker, A. M., Schmidt-Weber, C. B., Jakwerth, C. A. An Exhausted Phenotype of T_H2-Cells Is Primed by Allergen Exposure, But Not Reinforced by Allergen-specific Immunotherapy (Submitted to Journal of Allergy, currently under review)

9 Supplementary data

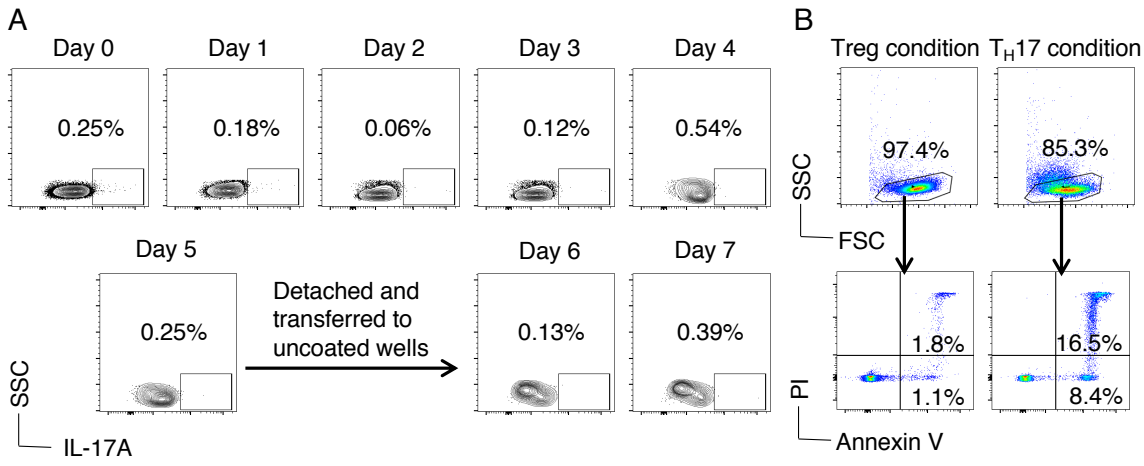

Figure 9.1 Suboptimal yield and high apoptosis rate of in vitro-induced T_H17

MACS-sorted naïve T cells were stimulated in vitro under T_H17 condition. (A) Few cells polarized under T_H17 condition produced IL-17A. Shown is one representative experiment for T_H17 polarization. (B) Cells treated under T_H17 condition had a higher apoptosis rate as opposed to those treated under Treg condition. Numbers shown in the plots are percentage of the gated populations. PI, propidium iodine.

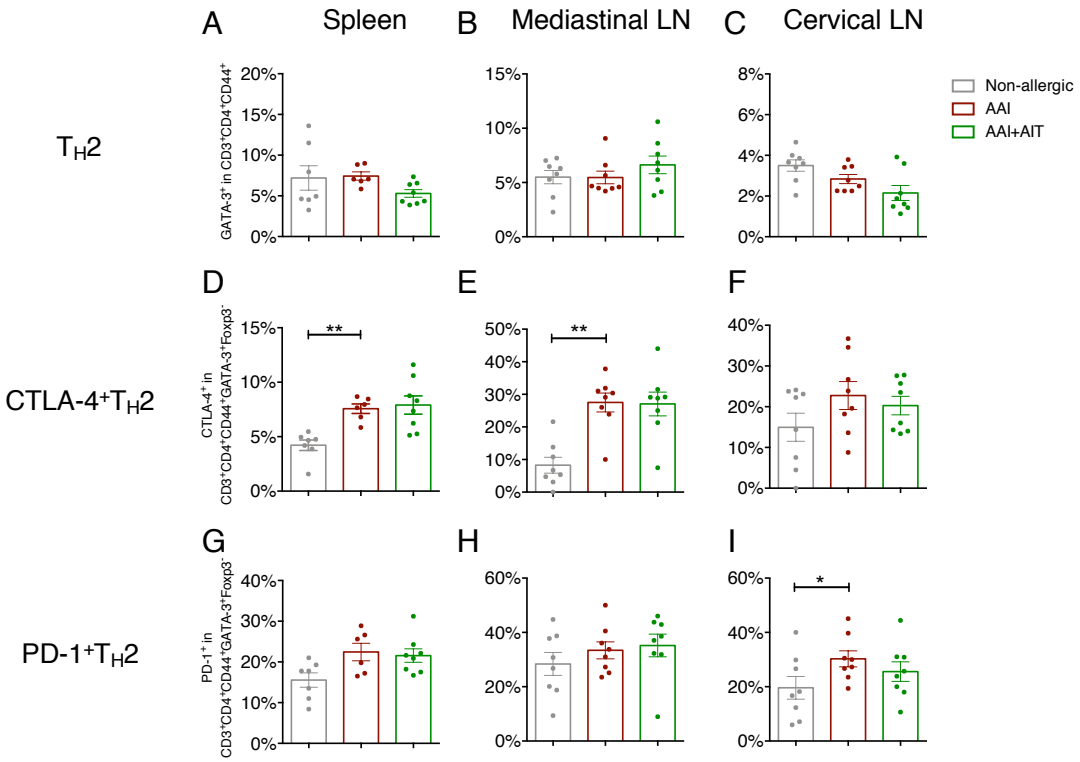

Figure 9.2 Frequency and phenotype of GATA-3^{+}T$_{H}$2 cells in spleens and lymph nodes of mice.

Flow cytometric analysis shows the frequency of GATA-3^{+}T$_{H}$2 cells (A–C) and their expression of CTLA-4 (D–F) and PD-1 (G–I) in spleens and mediastinal and cervical lymph nodes (LN) of non-allergic, AAI and AAI+AIT mice. Symbols represent individual mice (n = 8 per group). Graphs show means ± SEM; unpaired Mann-Whitney test: *$P \leq .05$; **$P \leq .01$.

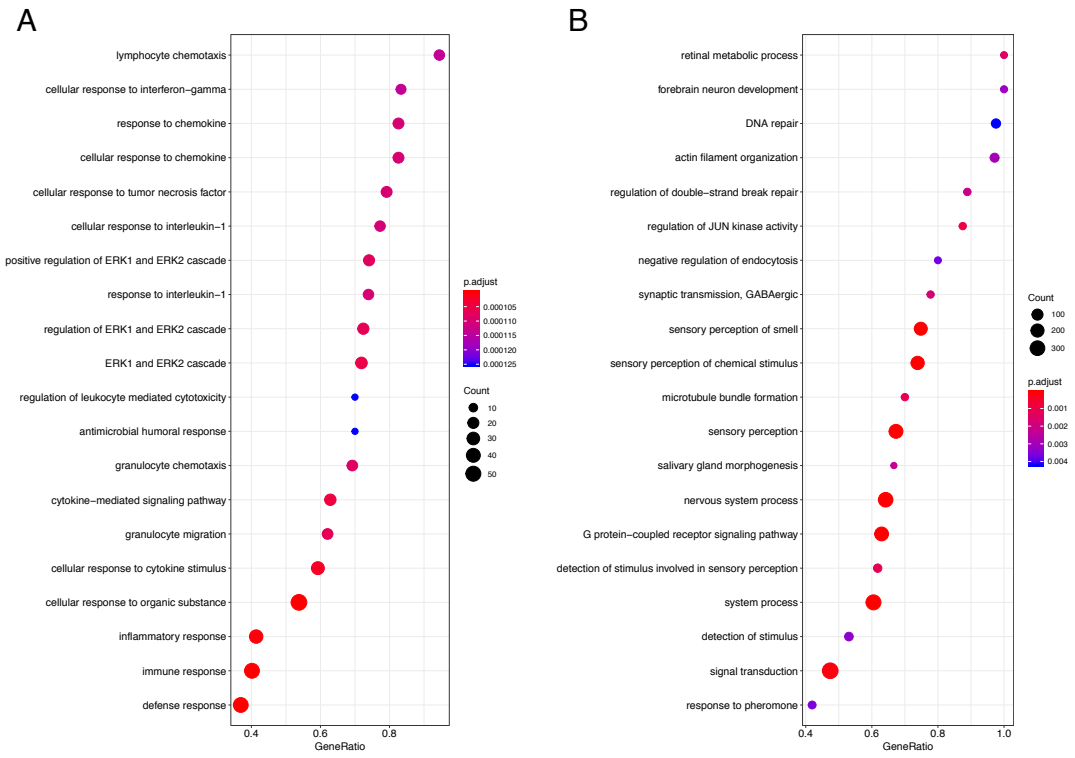

Figure 9.3 GO term enrichment analysis for biological process.

Differentially expressed gene data between AAI+AIT and AAI mouse lung cells were subjected to GO term enrichment analysis. Top 20 GO terms for biological process enriched in AAI (A) and AAI+AIT (B).

Table 9.1 Protocols for in vitro generation of T_H17 cells

		A	B	C	D
Culture medium		RPMI	RPMI w/ 10% FCS	IMDM	RPMI w/ 10% human serum
T cell stimulation	α-CD3, plate-bound	0.02 μg/ml	5 μg/ml	T cell activation/ expansion kit: α-CD2, α-CD3 & α-CD28 coated beads	2 μg/ml
	α-CD28	6 μg/ml	with 2.5 μg/ml or w/o α-CD28		1 μg/ml
Cell type		naïve CD4	naïve CD4	naïve Treg and Tconv	$CCR6^+$ Treg
Cell density (per 96-well)		5 $x10^4$ cells	2.5$x10^5$ cells	3$x10^4$ cells	5 $x10^4$ cells
Cytokine	IL-2	X	X	100 U/ml	40 U/ml
	IL-6	10 ng/ml	X	+/-	20 ng/ml
	IL-1β	10 ng/ml	50 ng/ml	10 ng/ml	10 ng/ml
	IL-23	10 ng/ml	50 ng/ml	100 ng/ml	20 ng/ml
	TGF-β	1 ng/ml	5 ng/ml	10 ng/ml	-
Neutralizing Ab	α-IL-4	2 μg/ml	X	X	5 μg/ml
	α-IL-12	2 μg/ml	X	X	X
	α-INF-γ	2 μg/ml	X	X	5 μg/ml
Timing		96 h, transfer to uncoated wells, for additional 48 h	7 d	5 d or 12 d	15-18 d
Readout		FACS	FACS	FACS	ELISA
Re-stimulation		PMA 500 ng/ml, IM 1 μg/ml, BFA 10 μg/ml 5 h	PMA 50 ng/ml, IM 500 ng/ml, Golgiplug 4 h	PMA 100 ng/ml, IM 1 μg/ml, BFA 10 μg/ml 4 h	α-CD3 2 μg/ml, α-CD28 1 μg/ml 24 h

Tconv, conventional T cells; PMA, phorbol myristate acetate; IM, ionomycin; BFA, brefeldin-A

Reference: (A) Kastirr et al. J Immunol 2015; (B) Revu et al. Cell Reports 2018; (C) Valmori et al. PNAS 2010; (D) Voo et al. Proc Natl Acad Sci USA 2009

Table 9.2 Cytokines in supernatant after 48 h *in vitro* OVA stimulation

	Well	IL-5	TNF-α	IFN-γ	IL-2	IL-9	IL-17A
Non-allergic	cytokine_mouse02_1.fcs	<1.63	<1.25	0.35	<0.84	<0.322	<1.09
	cytokine_mouse02_2.fcs	<1.63	<1.25	0.56	<0.84	0.473	1.28
	cytokine_mouse03_1.fcs	<1.63	<1.25	0.69	<0.84	0.368	<1.09
	cytokine_mouse03_2.fcs	<1.63	<1.25	<0.30	<0.84	0.473	<1.09
	cytokine_mouse04_1.fcs	<1.63	<1.25	<0.30	<0.84	0.473	<1.09
	cytokine_mouse04_2.fcs	<1.63	<1.25	<0.30	<0.84	<0.322	<1.09
	cytokine_mouse06_1.fcs	<1.63	<1.25	<0.30	<0.84	0.343	<1.09
	cytokine_mouse06_2.fcs	<1.63	<1.25	<0.30	<0.84	<0.322	<1.09
	cytokine_mouse07_1.fcs	<1.63	<1.25	0.41	<0.84	<0.322	<1.09
	cytokine_mouse07_2.fcs	<1.63	<1.25	<0.30	<0.84	<0.322	<1.09
	cytokine_mouse08_1.fcs	<1.63	<1.25	<0.30	<0.84	<0.322	<1.09
	cytokine_mouse08_2.fcs	<1.63	<1.25	<0.30	<0.84	<0.322	<1.09
AAI	cytokine_mouse09_1.fcs	<1.63	<1.25	<0.30	<0.84	<0.322	<1.09
	cytokine_mouse09_2.fcs	<1.63	<1.25	<0.30	<0.84	0.473	<1.09
	cytokine_mouse10_1.fcs	<1.63	<1.25	<0.30	<0.84	<0.322	<1.09
	cytokine_mouse10_2.fcs	<1.63	<1.25	<0.30	<0.84	<0.322	<1.09
	cytokine_mouse11_1.fcs	<1.63	<1.25	0.31	<0.84	<0.322	<1.09
	cytokine_mouse11_2.fcs	<1.63	<1.25	<0.30	<0.84	<0.322	<1.09
	cytokine_mouse12_1.fcs	<1.63	<1.25	<0.30	<0.84	<0.322	<1.09
	cytokine_mouse12_2.fcs	<1.63	<1.25	<0.30	<0.84	<0.322	<1.09
	cytokine_mouse13_1.fcs	<1.63	<1.25	<0.30	<0.84	<0.322	<1.09
	cytokine_mouse13_2.fcs	<1.63	<1.25	<0.30	<0.84	<0.322	<1.09
	cytokine_mouse16_1.fcs	<1.63	<1.25	<0.30	<0.84	<0.322	<1.09
	cytokine_mouse16_2.fcs	<1.63	<1.25	<0.30	<0.84	<0.322	<1.09
AAI+AIT	cytokine_mouse17_1.fcs	<1.63	<1.25	<0.30	<0.84	<0.322	<1.09
	cytokine_mouse17_2.fcs	<1.63	<1.25	<0.30	<0.84	<0.322	<1.09
	cytokine_mouse18_1.fcs	<1.63	<1.25	<0.30	<0.84	<0.322	<1.09
	cytokine_mouse18_2.fcs	<1.63	<1.25	<0.30	<0.84	<0.322	<1.09
	cytokine_mouse19_1.fcs	<1.63	<1.25	<0.30	<0.84	<0.322	<1.09
	cytokine_mouse19_2.fcs	<1.63	<1.25	<0.30	<0.84	<0.322	<1.09
	cytokine_mouse20_1.fcs	<1.63	<1.25	<0.30	<0.84	<0.322	<1.09
	cytokine_mouse20_2.fcs	<1.63	<1.25	0.43	<0.84	<0.322	<1.09
	cytokine_mouse21_1.fcs	<1.63	<1.25	<0.30	<0.84	<0.322	<1.09
	cytokine_mouse21_2.fcs	<1.63	<1.25	0.35	<0.84	<0.322	<1.09
	cytokine_mouse22_1.fcs	<1.63	<1.25	0.45	<0.84	<0.322	<1.09
	cytokine_mouse22_2.fcs	<1.63	<1.25	<0.30	<0.84	<0.322	<1.09
	cytokine_mouse23_1.fcs	<1.63	<1.25	<0.30	<0.84	<0.322	<1.09
	cytokine_mouse23_2.fcs	<1.63	<1.25	<0.30	<0.84	<0.322	<1.09
	cytokine_mouse24_1.fcs	<1.63	<1.25	<0.30	<0.84	<0.322	<1.09
	cytokine_mouse24_2.fcs	<1.63	1.82	0.35	<0.84	0.368	1.78

Cytokines were measured in pg/ml; each sample was measured twice (technical replicates).

Table 9.3 List of genes that were differentially expressed between exhausted and memory T cells (Crawford et al., 2014).

Ctla4	*Pilra*	*Tnfsf4*	*Maf*	*Mcm6*	*Taf1a*	*Jun*	*Fosb*
Lilrb4	*Sirpb1*	*Tnfsf11*	*Prdm1*	*Tshz2*	*Arid3b*	*Arntl*	*Cebpa*
Pdcd1	*Cd160*	*Treml2*	*Pawr*	*Sap30*	*Txnip*	*Zfp1*	*Maf*
Lag3	*Btla*	*Tnfrsf9*	*Jazf1*	*Baz1a*	*Zfp652*	*Zfp81*	*Fosl2*
Cd274	*Lair1*	*Cd40ig*	*Nab1*	*Nfat5*	*Spic*	*Mef2d*	*Stat4*
Cd200	*Tnfrsf4*	*CD28*	*Nfatc1*	*Mdfic*	*Klf6*	*Zbtb20*	*Egr2*
Havcr2	*Icos*	*Ikzf2*	*Zbtb32*	*Pbx3*	*Vgll4*	*Hif1a*	*Bcl6*
Cd244	*Tnfsf9*	*Eomes*	*Klf4*	*Plag1*	*Junb*	*Etv6*	

Table 9.4 Significant entities of genes filtered by GO term: 0072676 and 004824

ProbeName	GeneSymbol	Description	*P*	FC (abs)	Regulation
A_55_P2739607	Bcar1	Mus musculus breast cancer anti-estrogen resistance 1 (Bcar1), transcript variant 2, mRNA [NM_009954]	7.50E-04	1.6917508	up
A_55_P2039681	Gpr35	Mus musculus G protein-coupled receptor 35 (Gpr35), transcript variant 1, mRNA [NM_022320]	4.26E-05	2.8183925	up
A_51_P458584	Fpr-rs3	Mus musculus formyl peptide receptor, related sequence 3 (Fpr-rs3), mRNA [NM_008040]	1.19E-04	4.5865965	up
A_51_P428372	Ppbp	Mus musculus pro-platelet basic protein (Ppbp), mRNA [NM_023785]	0.001356008	1.8507907	up
A_51_P288138	Fpr2	Mus musculus formyl peptide receptor 2 (Fpr2), mRNA [NM_008039]	0.0237685	1.5507616	up
A_55_P2717129	Bin2	bridging integrator 2 [Source:MGI Symbol;Acc:MGI:3611448] [ENSMUST00000183193]	0.001128301	1.8719321	up
A_51_P312485	Fpr1	Mus musculus formyl peptide receptor 1 (Fpr1), mRNA [NM_013521]	1.37E-04	2.5840476	up
A_55_P2738827	Itga1		1.66E-05	1.6260186	up
A_66_P140937	Hoxb9	Mus musculus homeobox B9 (Hoxb9), mRNA [NM_008270]	0.035362974	1.9729214	up
A_66_P125784	Plg	Mus musculus plasminogen (Plg), mRNA [NM_008877]	0.00264109	1.8488367	up
A_55_P2729378	Sema5a	Q6P1C9_MOUSE (Q6P1C9) Sema5a protein, partial (95%) [TC1599505]	0.015485268	2.4898396	up
A_55_P2171116	Lgals3	Mus musculus lectin, galactose binding, soluble 3 (Lgals3), transcript variant 1, mRNA [NM_001145953]	1.26E-05	1.6047273	down
A_51_P166886	Saa2	Mus musculus serum amyloid A 2 (Saa2), mRNA [NM_011314]	0.022200095	1.6082252	down
A_51_P101929	Lgals3	Mus musculus lectin, galactose binding, soluble 3 (Lgals3), transcript variant 2, mRNA [NM_010705]	4.49E-06	1.5282675	down
A_51_P327996	Ccl22	Mus musculus chemokine (C-C motif) ligand 22 (Ccl22), mRNA [NM_009137]	0.002465375	1.6434481	down
A_51_P185660	Ccl9	Mus musculus chemokine (C-C motif) ligand 9 (Ccl9), mRNA [NM_011338]	5.23E-06	2.554627	down
A_51_P400543	Aif1	Mus musculus allograft inflammatory factor 1 (Aif1), mRNA [NM_019467]	1.06E-04	1.6994497	down
A_51_P509573	Ccl4	Mus musculus chemokine (C-C motif) ligand 4 (Ccl4), mRNA [NM_013652]	0.005759234	1.9741256	down
A_52_P318673	Saa1	Mus musculus serum amyloid A 1 (Saa1), mRNA [NM_009117]	7.56E-05	3.286053	down
A_51_P460954	Ccl6	Mus musculus chemokine (C-C motif) ligand 6 (Ccl6), mRNA [NM_009139]	3.73E-07	1.9679912	down
A_55_P2105878	Ccr10	Mus musculus chemokine (C-C motif) receptor 10 (Ccr10), mRNA [NM_007721]	0.014573993	1.6671506	down
A_51_P140710	Ccl3	Mus musculus chemokine (C-C motif) ligand 3 (Ccl3), mRNA [NM_011337]	3.64E-05	2.7900608	down
A_51_P436652	Ccl7	Mus musculus chemokine (C-C motif) ligand 7 (Ccl7), mRNA [NM_013654]	1.24E-04	2.1809807	down

ProbeName	GeneSymbol	Description	*P*	FC (abs)	Regulation
A_55_P2025765	Adam8	Mus musculus a disintegrin and metallopeptidase domain 8 (Adam8), transcript variant 1, mRNA [NM_007403]	5.12E-05	1.9376212	down
A_55_P2869822	Ccl11	Mus musculus chemokine (C-C motif) ligand 11 (Ccl11), mRNA [NM_011330]	3.55E-06	2.7997506	down
A_55_P2736435	Adam8	Mus musculus a disintegrin and metallopeptidase domain 8 (Adam8), transcript variant 1, mRNA [NM_007403]	1.52E-04	1.5322936	down
A_55_P2811679	Cxcl1	Mus musculus chemokine (C-X-C motif) ligand 1 (Cxcl1), mRNA [NM_008176]	1.20E-06	4.9006886	down
A_55_P2744077	Ccl4	Mus musculus chemokine (C-C motif) ligand 4 (Ccl4), mRNA [NM_013652]	0.007921795	1.9034137	down
A_55_P1966204	Cxcl12	Mus musculus chemokine (C-X-C motif) ligand 12 (Cxcl12), transcript variant 1, mRNA [NM_021704]	2.80E-05	1.6991965	down
A_51_P114462	Ccl17	Mus musculus chemokine (C-C motif) ligand 17 (Ccl17), mRNA [NM_011332]	2.36E-07	7.441073	down
A_51_P217463	Cxcl2	Mus musculus chemokine (C-X-C motif) ligand 2 (Cxcl2), mRNA [NM_009140]	1.52E-06	3.3652542	down
A_52_P249514	Ccl12	Mus musculus chemokine (C-C motif) ligand 12 (Ccl12), mRNA [NM_011331]	8.82E-06	2.3267226	down
A_52_P18116	Ccl24	Mus musculus chemokine (C-C motif) ligand 24 (Ccl24), mRNA [NM_019577]	1.57E-04	4.420853	down
A_51_P286737	Ccl2	Mus musculus chemokine (C-C motif) ligand 2 (Ccl2), mRNA [NM_011333]	1.88E-05	2.4999163	down
A_51_P408595	Ccl20	Mus musculus chemokine (C-C motif) ligand 20 (Ccl20), transcript variant 1, mRNA [NM_016960]	2.91E-10	6.7121267	down
A_52_P110052	Ackr1	Mus musculus atypical chemokine receptor 1 (Duffy blood group) (Ackr1), mRNA [NM_010045]	1.88E-04	1.9644057	down
A_55_P2904117	Ackr1	Mus musculus atypical chemokine receptor 1 (Duffy blood group) (Ackr1), mRNA [NM_010045]	3.29E-05	2.2581291	down
A_51_P237865	Il4	Mus musculus interleukin 4 (Il4), transcript variant 1, mRNA [NM_021283]	3.36E-04	2.2242913	down
A_66_P106131	Saa3	Mus musculus serum amyloid A 3 (Saa3), mRNA [NM_011315]	9.62E-06	6.951669	down
A_55_P1960386	Ccl1	Mus musculus chemokine (C-C motif) ligand 1 (Ccl1), mRNA [NM_011329]	1.67E-07	3.2391655	down
A_55_P1990032	Cxcl5	Mus musculus chemokine (C-X-C motif) ligand 5 (Cxcl5), mRNA [NM_009141]	4.47E-08	29.790846	down
A_51_P378789	Cxcl13	Mus musculus chemokine (C-X-C motif) ligand 13 (Cxcl13), mRNA [NM_018866]	1.07E-04	4.406385	down
A_51_P464703	Ccl8	Mus musculus chemokine (C-C motif) ligand 8 (Ccl8), mRNA [NM_021443]	3.81E-05	2.1218212	down

Table 9.5 Significant entities of genes filtered by GO term: 0005125

ProbeName	GeneSymbol	Description	*P*	FC (abs)	Regulation
A_55_P2741233	Il12b	Mus musculus interleukin 12b (Il12b), mRNA [NM_001303244]	1.73E-04	1.8477591	up
A_52_P656790	Ctf2	Mus musculus cardiotrophin 2 (Ctf2), mRNA [NM_198858]	0.005114046	2.241319	up
A_55_P2935935	Il2	Mus musculus interleukin 2 (Il2), mRNA [NM_008366]	1.84E-05	3.7589598	up
A_51_P112796	Il1f5	Mus musculus interleukin 1 family, member 5 (delta) (Il1f5), transcript variant 2, mRNA [NM_019451]	1.74E-04	2.7156081	up
A_55_P2744827	Il21	Mus musculus interleukin 21 (Il21), transcript variant 1, mRNA [NM_001291041]	3.37E-04	2.5235662	up
A_52_P87757	Il24	Mus musculus interleukin 24 (Il24), mRNA [NM_053095]	0.013938826	1.9922079	up
A_55_P2720030	Il1f6	Mus musculus interleukin 1 family, member 6 (Il1f6), mRNA [NM_019450]	0.002836923	2.5477848	up
A_55_P2166020	Ifna13	Mus musculus interferon alpha 13 (Ifna13), mRNA [NM_177347]	0.014385053	1.778753	up
A_51_P519301	Il17f	Mus musculus interleukin 17F (Il17f), mRNA [NM_145856]	0.011406475	1.6541293	up
A_55_P2732528	Il18	Mus musculus interleukin 18 (Il18), mRNA [NM_008360]	9.58E-05	1.8074615	up
A_55_P1985985	Il3	Mus musculus interleukin 3 (Il3), mRNA [NM_010556]	0.017051853	1.561119	up
A_55_P2199202	Il22	Mus musculus interleukin 22 (Il22), mRNA [NM_016971]	0.002910094	1.7656146	up
A_52_P482280	Ifna2	interferon alpha 2 [Source:MGI Symbol;Acc:MGI:107666] [ENSMUST00000105147]	0.023194369	2.0098205	up
A_55_P1996365	Ifna14	Mus musculus interferon alpha 14 (Ifna14), mRNA [NM_206975]	0.002628428	2.120864	up
A_55_P2030171	Ifna2	Mus musculus interferon alpha 2 (Ifna2), mRNA [NM_010503]	5.03E-06	2.3674192	up
A_51_P387681	Ifnab	GB	0.012984594	1.9567547	up
A_51_P317887	Sectm1b	Mus musculus secreted and transmembrane 1B (Sectm1b), mRNA [NM_026907]	6.69E-05	1.968251	up
A_51_P350005	Il17c	Mus musculus interleukin 17C (Il17c), mRNA [NM_145834]	7.56E-04	2.139632	up
A_52_P576049	Inhbc	Mus musculus inhibin beta-C (Inhbc), mRNA [NM_010565]	0.00268494	2.2109673	up
A_66_P136102	Lefty2	Mus musculus left-right determination factor 2 (Lefty2), mRNA [NM_177099]	0.002167371	1.6284444	up
A_66_P127574	Ifna12	Mus musculus interferon alpha 12 (Ifna12), mRNA [NM_177361]	0.01615672	2.1017344	up
A_55_P1994117	Ifnl3	Mus musculus interferon lambda 3 (Ifnl3), mRNA [NM_177396]	0.005939508	1.8560853	up
A_51_P429903	Ndp	Mus musculus Norrie disease (pseudoglioma) (human) (Ndp), mRNA [NM_010883]	1.52E-05	1.9270904	up
A_55_P2156697	Il17a	Mus musculus interleukin 17A (Il17a), mRNA [NM_010552]	8.47E-05	2.995631	up

ProbeName	GeneSymbol	Description	*P*	FC (abs)	Regulation
A_52_P413646	Bmp6	Mus musculus bone morphogenetic protein 6 (Bmp6), mRNA [NM_007556]	4.05E-05	1.5316795	up
A_52_P633560	Nodal	Mus musculus nodal (Nodal), mRNA [NM_013611]	1.85E-04	1.6147039	up
A_55_P2001489	Il19	Mus musculus interleukin 19 (Il19), mRNA [NM_001009940]	4.06E-05	4.0247793	up
A_55_P1964960	Il33	Mus musculus interleukin 33 (Il33), transcript variant 1, mRNA [NM_001164724]	7.17E-05	1.656724	down
A_55_P2131483	Hmgb1	Mus musculus high mobility group box 1 (Hmgb1), transcript variant 1, mRNA [NM_001313894]	7.29E-08	1.5352703	down
A_51_P171075	Csf2	Mus musculus colony stimulating factor 2 (granulocyte-macrophage) (Csf2), mRNA [NM_009969]	4.23E-06	2.047887	down
A_51_P327996	Ccl22	Mus musculus chemokine (C-C motif) ligand 22 (Ccl22), mRNA [NM_009137]	0.002465375	1.6434481	down
A_51_P185660	Ccl9	Mus musculus chemokine (C-C motif) ligand 9 (Ccl9), mRNA [NM_011338]	5.23E-06	2.554627	down
A_51_P509573	Ccl4	Mus musculus chemokine (C-C motif) ligand 4 (Ccl4), mRNA [NM_013652]	0.005759234	1.9741256	down
A_66_P107818	Gdf3	Mus musculus growth differentiation factor 3 (Gdf3), mRNA [NM_008108]	0.007402576	1.9400156	down
A_52_P431159	Il1rn	Mus musculus interleukin 1 receptor antagonist (Il1rn), transcript variant 2, mRNA [NM_001039701]	9.78E-04	1.868729	down
A_51_P484371	Tnfsf8	Mus musculus tumor necrosis factor (ligand) superfamily, member 8 (Tnfsf8), mRNA [NM_009403]	1.92E-04	2.0129375	down
A_51_P460954	Ccl6	Mus musculus chemokine (C-C motif) ligand 6 (Ccl6), mRNA [NM_009139]	3.73E-07	1.9679912	down
A_52_P87713	Timp1	Mus musculus tissue inhibitor of metalloproteinase 1 (Timp1), transcript variant 1, mRNA [NM_001044384]	1.09E-05	2.511524	down
A_51_P140710	Ccl3	Mus musculus chemokine (C-C motif) ligand 3 (Ccl3), mRNA [NM_011337]	3.64E-05	2.7900608	down
A_51_P436652	Ccl7	Mus musculus chemokine (C-C motif) ligand 7 (Ccl7), mRNA [NM_013654]	1.24E-04	2.1809807	down
A_51_P303791	Inhba	Mus musculus inhibin beta-A (Inhba), mRNA [NM_008380]	6.95E-04	2.5073574	down
A_55_P2869822	Ccl11	Mus musculus chemokine (C-C motif) ligand 11 (Ccl11), mRNA [NM_011330]	3.55E-06	2.7997506	down
A_55_P2039359	Tnfsf11	Mus musculus tumor necrosis factor (ligand) superfamily, member 11 (Tnfsf11), mRNA [NM_011613]	1.69E-04	1.9583496	down
A_55_P2811679	Cxcl1	Mus musculus chemokine (C-X-C motif) ligand 1 (Cxcl1), mRNA [NM_008176]	1.20E-06	4.9006886	down
A_51_P430766	Il10	Mus musculus interleukin 10 (Il10), mRNA [NM_010548]	0.007507978	2.119456	down
A_55_P2614900	Il33	Mus musculus interleukin 33 (Il33), transcript variant 1, mRNA [NM_001164724]	3.69E-05	1.7525749	down
A_55_P2744077	Ccl4	Mus musculus chemokine (C-C motif) ligand 4 (Ccl4), mRNA [NM_013652]	0.007921795	1.9034137	down
A_55_P1966204	Cxcl12	Mus musculus chemokine (C-X-C motif) ligand 12 (Cxcl12), transcript variant 1, mRNA [NM_021704]	2.80E-05	1.6991965	down

ProbeName	GeneSymbol	Description	*P*	FC (abs)	Regulation
A_51_P114462	Ccl17	Mus musculus chemokine (C-C motif) ligand 17 (Ccl17), mRNA [NM_011332]	2.36E-07	7.441073	down
A_51_P217463	Cxcl2	Mus musculus chemokine (C-X-C motif) ligand 2 (Cxcl2), mRNA [NM_009140]	1.52E-06	3.3652542	down
A_51_P239750	Inhba	Mus musculus inhibin beta-A (Inhba), mRNA [NM_008380]	2.82E-05	1.9964522	down
A_52_P249514	Ccl12	Mus musculus chemokine (C-C motif) ligand 12 (Ccl12), mRNA [NM_011331]	8.82E-06	2.3267226	down
A_52_P18116	Ccl24	Mus musculus chemokine (C-C motif) ligand 24 (Ccl24), mRNA [NM_019577]	1.57E-04	4.420853	down
A_55_P2029319	Cd70	Mus musculus CD70 antigen (Cd70), mRNA [NM_011617]	9.04E-04	2.096882	down
A_51_P286737	Ccl2	Mus musculus chemokine (C-C motif) ligand 2 (Ccl2), mRNA [NM_011333]	1.88E-05	2.4999163	down
A_51_P408595	Ccl20	Mus musculus chemokine (C-C motif) ligand 20 (Ccl20), transcript variant 1, mRNA [NM_016960]	2.91E-10	6.7121267	down
A_55_P1997756	Il6	Mus musculus interleukin 6 (Il6), transcript variant 1, mRNA [NM_031168]	9.88E-04	2.1384084	down
A_51_P237865	Il4	Mus musculus interleukin 4 (Il4), transcript variant 1, mRNA [NM_021283]	3.36E-04	2.2242913	down
A_52_P153179	Il31	Mus musculus interleukin 31 (Il31), mRNA [NM_029594]	0.01264545	1.8996928	down
A_55_P2106121	Il21	Mus musculus interleukin 21 (Il21), transcript variant 1, mRNA [NM_001291041]	0.002453658	2.772329	down
A_55_P1960386	Ccl1	Mus musculus chemokine (C-C motif) ligand 1 (Ccl1), mRNA [NM_011329]	1.67E-07	3.2391655	down
A_51_P185415	Il5	Mus musculus interleukin 5 (Il5), mRNA [NM_010558]	0.001098734	2.364928	down
A_55_P1990032	Cxcl5	Mus musculus chemokine (C-X-C motif) ligand 5 (Cxcl5), mRNA [NM_009141]	4.47E-08	29.790846	down
A_51_P378789	Cxcl13	Mus musculus chemokine (C-X-C motif) ligand 13 (Cxcl13), mRNA [NM_018866]	1.07E-04	4.406385	down
A_51_P464703	Ccl8	Mus musculus chemokine (C-C motif) ligand 8 (Ccl8), mRNA [NM_021443]	3.81E-05	2.1218212	down

Table 9.6 Significant entities of genes filtered by curated gene list

ProbeName	GeneSymbol	Description	*P*	FC (abs)	Regulation
A_55_P2149011	Hif1a	hypoxia inducible factor 1, alpha subunit [Source:MGI Symbol;Acc:MGI:106918] [ENSMUST00000110464]	0.00300952	1.5157217	up
A_55_P2090612	Pilra	paired immunoglobin-like type 2 receptor alpha [Source:MGI Symbol;Acc:MGI:2450529] [ENSMUST00000110980]	1.35E-04	3.4829297	up
A_55_P1977812	Cd244	Mus musculus CD244 natural killer cell receptor 2B4 (Cd244), mRNA [NM_018729]	1.93E-06	1.7166915	up
A_55_P2883248	Baz1a	bromodomain adjacent to zinc finger domain 1A [Source:MGI Symbol;Acc:MGI:1309478] [ENSMUST00000173176]	0.0301197	1.5790795	up
A_55_P2770047	Tshz2	PREDICTED: Mus musculus teashirt zinc finger family member 2 (Tshz2), transcript variant X2, mRNA [XM_006499424]	4.82E-07	1.8169348	up
A_55_P1988844	Klrg1	Mus musculus killer cell lectin-like receptor subfamily G, member 1 (Klrg1), mRNA [NM_016970]	4.10E-05	1.6108124	down
A_52_P682768	Icos	Mus musculus inducible T cell co-stimulator (Icos), mRNA [NM_017480]	8.70E-05	1.5901304	down
A_55_P2147712	Ctla4	Mus musculus cytotoxic T-lymphocyte-associated protein 4 (Ctla4), transcript variant 1, mRNA [NM_009843]	1.94E-04	2.0983176	down
A_55_P2039359	Tnfsf11	Mus musculus tumor necrosis factor (ligand) superfamily, member 11 (Tnfsf11), mRNA [NM_011613]	1.69E-04	1.9583496	down
A_51_P173043	Egr2	Mus musculus early growth response 2 (Egr2), transcript variant 1, mRNA [NM_010118]	2.89E-07	1.7080414	down
A_55_P2026903	Tigit	Mus musculus T cell immunoreceptor with Ig and ITIM domains (Tigit), mRNA [NM_001146325]	1.83E-05	2.227425	down
A_55_P2082180	Tnfrsf9	Mus musculus tumor necrosis factor receptor superfamily, member 9 (Tnfrsf9), transcript variant 1, mRNA [NM_011612]	5.07E-06	3.6775577	down
A_51_P256983	Klrg1	Mus musculus killer cell lectin-like receptor subfamily G, member 1 (Klrg1), mRNA [NM_016970]	2.39E-04	1.5172349	down
A_55_P2831060	Tnfrsf9	Mus musculus tumor necrosis factor receptor superfamily, member 9 (Tnfrsf9), transcript variant 1, mRNA [NM_011612]	4.12E-06	4.8933034	down
A_55_P2125491	Tnfrsf4	Mus musculus tumor necrosis factor receptor superfamily, member 4 (Tnfrsf4), mRNA [NM_011659]	2.82E-05	1.6231472	down
A_51_P285736	Pdcd1	Mus musculus programmed cell death 1 (Pdcd1), mRNA [NM_008798]	0.006098429	1.8720162	down

Acknowledgments

First, I would like to thank my supervisor Prof. Dr. Carsten Schmidt-Weber for broadening my vision of science and providing coherent answers to my questions. I gained much better insights into my studies and learned how to be more persuasive in a scientific way in the process.

Next, I want to thank my thesis advisors Prof. Dr. Dietmar Zehn, PD Dr. Caspar Ohnmacht, and Dr. Ulrich Zissler for their insightful comments and constructive advice on the project.

I owe particular thanks to Dr. Constanze Jakwerth, whose penetrating questions taught me to question more deeply and helped my project to move forward. Her advice on how to organize the experiments in the project made everything more efficient. In addition, her suggestions on the analysis were of tremendous help, rendering the thesis better structured and the overall presentation of the data more appealing to the eye.

Also, I want to offer my enduring gratitude to Dr. Adam Chaker, who provided precious clinical samples and made the project possible. Personally, I learned a lot from his scientific and medical expertise, which is inspiring for my career as a scientist and a physician.

Equally important is the support for mouse work from PD Dr. Simon Blank and his lab members, Sonja, Alex, Benjamin and Johanna. I cannot express my gratitude enough for their help, in particular Sonja, who helped set up the experiments and collect all the required mouse specimens. I also want to thank Prof. Dr. Francesca Alessandrini for her performing the bronchoalveolar lavage and the cytospin smears, and more importantly for her advice on the submitted manuscript.

My sincere thanks also goes to Dr. Maren Büttner, for her meticulous work on the unbiased clustering analysis, which provides a new dimension for the data and thus brings the work to a different level.

Trying to accomplish a doctoral research is never an easy task. Nevertheless, working in ZAUM is pleasant, simply because the staff, the lab members and my fellow students at ZAUM are incredibly nice: Pascal, Toni, Fiona, Sina, Fabiana, Julia, Sonja, Myriam, Joana, Jeroen, Jose, Gudrun, Elke, Christine, Cordula, Steffi, Manja, Jenny,

Jana, Kerstin, Caro, Sophia, Alex, David, Evelyn, Anna-Lena, and Frau Pilz. They helped me to solve a wide variety of technical problems, shared with me some home baked goodies, bore with my far-from-perfect German, and the list could go on and on. Above all, I can't express my gratitude enough especially to the best TA, Ferdi and Madlen. Both have saved my day for countless times.

Last but not least, I want to thank my friends, Shannon, Calum, Felix, Mitko, Jonatan, Hazav, Pieter, and Karel, who encouraged me to continue my work when I felt particularly downbeat. Their support lends me a lot of strength, especially amid pandemic.

最後，要謝謝遠在台灣的親愛的爸媽、家人們一直以來的包容與支持。唸博士班稱不上什麼遠大的志向，更多的是任性的追求。點點滴滴、著實不容易啊。